UNIVERSITÀ DEGLI STUDI
DI GENOVA

Doctoral Program in Neuroscience

Curriculum in Neuroscience and Brain Technologies

XXXV cycle

# PRRT2-$Na^+$ CHANNELS INTERACTION: PATHOGENETIC BASIS OF PRRT2-ASSOCIATED PAROXYSMAL DISORDERS AND NEW THERAPEUTIC STRATEGIES

Author: Francesca Franchi
Supervisors: Prof. Fabio Benfenati
Prof. Pierluigi Valente

# TABLE OF CONTENTS

# ABSTRACT

Proline-Rich Transmembrane protein 2 (PRRT2) is a neuron-specific protein whose mutations are involved in pleiotropic paroxysmal syndromes including epilepsy, kinesigenic dyskinesia, episodic ataxia and migraine. PRRT2 is a type-2 membrane protein with a transmembrane domain and a long proline-rich N-terminal cytoplasmic region. According to several data, PRRT2 regulates membrane exposure and the biophysical properties of voltage-dependent Na+ channels (Nav) 1.2 and 1.6 that negatively modulate intrinsic excitability. Nav channels form complexes with β-subunits that facilitate the membrane targeting and the activation of the α-subunits. The objective of this thesis is to characterize the molecular and functional PRRT2-Nav interaction clarify: (i) whether PRRT2 and β-subunits interact or compete for common binding sites on the α-subunit, generating Nav complexes with distinct functional properties, (ii) based on its membrane topology, study the structure-function PRRT2 relationships regarding the interaction with Nav, (iii) focus on some point PRRT2 mutations involved in the binding to the Nav directly implicated in PRRT2-related pathologies. Since PRRT2 and β-subunits have opposite effects on Nav channels, it is unclear whether PRRT2 and β-subunits interact or compete for common binding sites on the α-subunit, leading to Nav complexes with different functional features. Using a heterologous expression system, we observed that β-subunits and PRRT2 do not interact with each other acting as independent non-competitive modulators of Nav1.2 channel trafficking and biophysical properties. The data indicate that β4-subunit and PRRT2 form a push-pull system that finely tunes the membrane expression and function of Nav channels and the intrinsic neuronal excitability. In addition, we observed that the unstructured N-terminal cytoplasmic region mimicked full-length PRRT2 by binding to the Nav1.2 more efficiently than the isolated transmembrane domain. Only the C-terminal intramembrane domain was able to modulate Nav properties, maintaining the striking specificity for Nav1.2 vs Nav1.1 channels. These results identify PRRT2 as a multi-domain protein in which the N-terminal cytoplasmic region acts as a binding antenna for $Na^+$ channels, while the transmembrane domain mechanistically regulates channel exposure on the membrane and its biophysical properties. Since the majority of the PRRT2 pathogenic mutations cause the loss of protein expression making in vitro studies difficult or impossible, a restricted number of missense mutations maintains the protein expression and the trafficking to the membrane allowing their characterization. Hence, their expression and function were studied in the same system used for the previous points. Two residues were identified, V286M and A320, that, if mutated, cause Nav binding alteration, and therefore that can be involved in the direct modulation of PRRT2 functions.

# 1. INTRODUCTION

## 1.1. Paroxysmal Disorders

Paroxysms (from Greek παροξυσμός, *paroxysmos* or *paroxyno*, meaning to sharpen or irritate) are a sudden recurrence or intensification of symptoms. Paroxysmal disorders (PDs) are a clinical and genetically heterogeneous group of disorders characterized by signs or symptoms that occur unexpectedly, resulting in spasms, convulsions, or other abrupt onset of physical dysfunctions. In neurology, the term is typically associated with seizure, migraine, or movement disorders and may include almost any bodily system. The signs and symptoms of a paroxysmal disorder depend entirely on the particular disorder. Some of these dysfunctions are treated with simple bedside maneuvers, whilst others require further examinations and specific pharmacological treatment [1]. Shuzo Kure, a prominent Japanese psychiatrist, provided the first detailed description of a case of paroxysmal movement disorder in 1892. He reported a case of paroxysmal movement disorder in a Japanese 23-year-old man who showed short, recurrent episodes of irregular, purposeless, and frequently bizarre involuntary movements from age 10. [2]. The movement-induced paroxysmal attacks were recognized as salient clinical features of what was later termed paroxysmal kinesigenic dyskinesia (PKD) [3].

Several classification schemes of paroxysmal movement disorders were proposed, especially based on the duration and aetiology of the attacks. More recently, a descriptive classification of paroxysmal movement disorders based on attack triggers was proposed [3]. According with this classification, paroxysmal movement disorders have been divided into four types:

(I) PKD, in which the attacks are triggered by sudden movements;

(II) Paroxysmal exercise-induced dyskinesias (PED) brought about by sustained and prolonged exercise;

(III) Paroxysmal non-kinesigenic dyskinesia (PNKD) in which triggers might be quite heterogeneous or non-identifiable;

(IV) Paroxysmal hypnogenic dyskinesia (PHD) in which attacks occur during sleep.

The main primary forms of paroxysmal movement disorders together with other PDs (e.g. several forms of epilepsy and heachache disorders) can be related to the following few genes: Myofibrillogenesis regulator 1 (*MR-1*) [2], Solute carrier family 2 facilitated glucose

transporter member 1 (*SLC2A1*) [3] and Proline-Rich Transmembrane Protein 2 (*PRRT2*) [4](Figure 1).

Human *MR-1* is a functional gene considered the main cause of PNKD and for this reason, it is also known as PNKD. *MR-1* is localized on human chromosome 2q35 and has three isomeric forms: MR-1L, MR-1M and MR-1S, formed by alternative splicing [5]. It is known that mutations in the N-terminal region of MR-1L and MR-1S are the main causes of PNKD [6]. The *MR-1L* isoform is specifically expressed in the brain and is localized to the neuronal membrane, while the *MR-1S* isoform is ubiquitously expressed with a diffuse cytoplasmic and nuclear localization [7]. It has been shown by bioinformatics analysis that the MR-1 gene is homologous to the hydroxyacylglutathione hydrolase gene (*HAGH*) that acts in a biochemical pathway to detoxify methylglyoxal, a by-product contained in coffee and alcoholic beverages [7]. The results of this study suggest a mechanism whereby alcohol, coffee and stress may act as precipitants of attacks in PNKD. Patients with MR1 mutations do not have epilepsy. However, a substantial proportion of patients with MR1 mutations can have migraine, thus linking this gene to another episodic neurological disorder [8].

*SLC2A1*, also known as *GLUT1* (Glucose Transporter 1), encodes for the GLUT1 protein, the most important energy carrier of the brain that is expressed in the endothelial cells of the blood-brain barrier level and assures the energy-independent, facilitative transport of glucose to the brain [9]. Several evidence emerged about the link between mutations of *SLC2A1* and PED both in isolation and in association with epilepsy [5], [10].

*PRRT2,* at now, is the major gene responsible for PKD [11]. *PRRT2* was identified as the causative gene for a wide spectrum of paroxysmal disorders including benign familial infantile epilepsy (BFIE), infantile convulsions (IC) and hemiplegic migraine (HM) [12], [13] (Figure 2). The broad spectrum of clinical manifestations suggests that there is a marked pleiotropy and variable penetrance of *PRRT2* mutations [14].

Historically, PDs were mainly considered as disorders representing ion channel dysfunction (channelopathies) [6] [7] [8]. In fact, the discovery of the molecular defects led to recognition of the role of the mutations of different types of ion channels in the onset of episodic brain diseases. These disorders include not only muscle diseases, but also numerous forms of epilepsy, movement disorders, headache, and cardiac dysrhythmias [8]. However, the discovery of the genes responsible for several forms of PDs disproved this ion channel

theory. In fact, in addition to mutations in ion channels, also mutations in the genes encoding for proteins involved in neuronal transmission and in the transporter proteins were found to be associated with several PDs (respectively identified as “synaptopathies” and “transportopathies”)[8], [15].

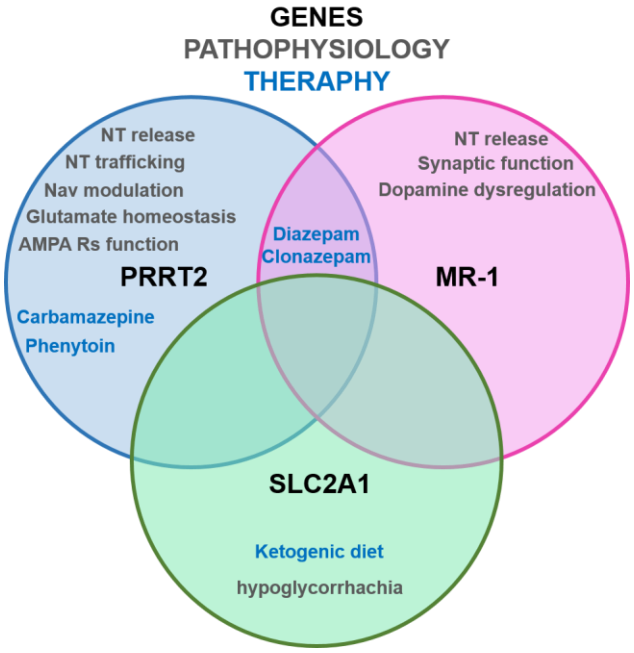


**Figure 1.** Venn diagrams of the three major genes mutated in the PDs with main pathophysiological mechanisms and current therapies (Paroxysmal Movement Disorders, Seth et al. 2020, *modified*).

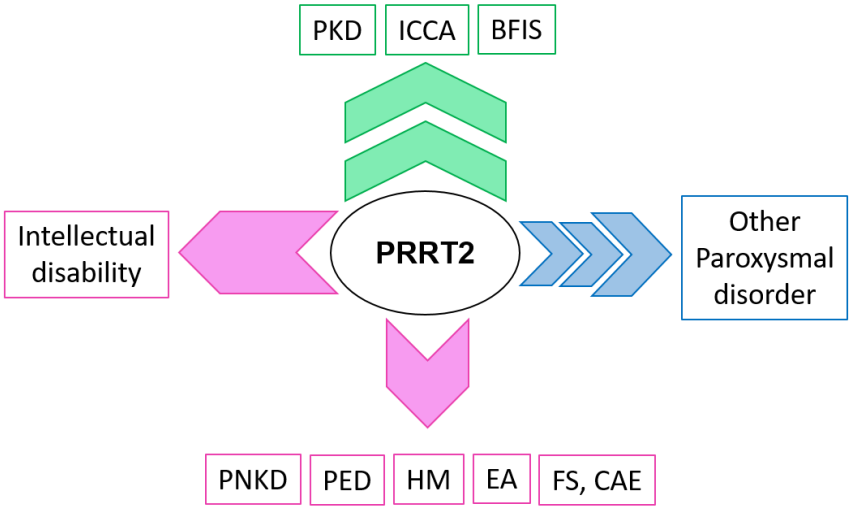


**Figure 2.** Clinical spectrum of PRRT2-related disorders. The green arrows point to the predominant phenotypes caused by PRRT2 mutations, PKD, ICCA (infantile convulsions with choreoathetosis syndrome), BFIS. The pink arrows point to rare phenotypes, PNKD, PED, HM, EA (episodic ataxia), FS (febrile seizures), CAE (childhood-absence epilepsy). The blue arrows indicate putative PRRT2 mutation-related phenotypes. (Méneret et al., 2013, *modified*).

## 1.2. Gene, protein structure and membrane topology of PRRT2

In the adult human brain, the PRRT2 protein is highly expressed in cerebellar, occipital, frontal and temporal cortices, putamen and hippocampus. To a lesser extent, PRRT2 is also expressed in other brain regions, such as the substantia nigra, thalamus, inferior olivary nucleus, and intralobular white matter [16] [17]. Furthermore, Chen and colleagues examined the PRRT2's expression pattern in the developing murine nervous system. They found a marked increase expression during early postnatal stages, declining during adulthood [12]. In human, longitudinal analysis of mRNA levels during brain development showed a rapid increase of PRRT2 expression in the striatum, neocortex, hippocampus, and thalamus until around 100 days post-conception. When a plateau is reached, the levels even start to decline in thalamic regions. Age-dependent expression changes can explain the age-dependence of different disease manifestations linked to PRRT2 mutations (Figure 3).

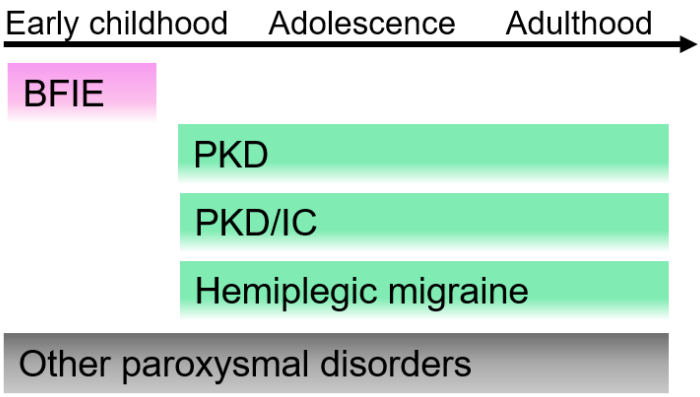


**Figure 3.** Natural history of PRRT2-associated diseases. In the majority of the cases BFIE, PKD and PKD/IC represent the core of PRRT2-associated diseases, while HM usually emerges as novel associated disease. PRRT2-associated BFIE manifests with non-febrile seizures in the first year of life with an average age of onset around 6 months. In PKD, there is a peak in early adolescence and PKD attacks may decrease in frequency during adulthood and remit completely in mid- or late adulthood. Other movement, seizure or headache disorders may also manifest in patients with PRRT2 mutation (Ebrahimi-Fakhari et al., 2015, *modified*).

The PRRT2 gene is located on the short arm of chromosome 16 (16p11.2) and consists of four exons. While exon 1 of the gene is non-coding, the exons 2-4 encode for a 340-amino acid protein containing two predicted transmembrane domains [12]. Among mammals, sequence conservation is very high (~80%), maintaining some still appreciable similarity (~30%) in lower vertebrates (e.g., zebrafish) [18].

PRRT2 was initially described as a protein belonging to the Dispanin family [19]. Dispanins or Interferon-induced transmembrane proteins (IFITM) are a group of transmembrane proteins characterized by a topology containing two transmembrane alpha-helix regions within the membrane [19], [20] . Exons 2-4 encode for a long N-terminal domain (1-268) containing a proline-rich region (PRD), two putative transmembrane helices, TM1 (269-289) and TM2 (318-338), separated by an intracellular loop (CYT, 290-317), and a C-terminal dipeptide (339-340) [21]. However, the predictions were not confirmed and the correct topology of PRRT2 protein was subsequently demonstrated using a combination of different experimental approaches, including live immunolabeling, immunogold electron microscopy, surface biotinylation and computational modeling [19].

Molecular dynamics simulations ascertained that the helix of TM1 flexes in correspondence with a five-amino acid hinge that includes two proline residues, forming a helix-loop-helix structure. The M1 helix is beaked in two halves, called M1a/ M1b that are stably folded at

the cytoplasmic side of the plasma membrane. Consequently, only M2 is a true transmembrane helix. Due to its single transmembrane domain, PRRT2 exposes the long N-terminal domain and the short M1-M2 loop to the cytoplasm and maintains a C-terminal anchor. This configuration is in line with the model of a type II transmembrane protein in which only the second hydrophobic segment completely spans the plasma membrane, the first one it is associated with the internal half of the plasma membrane via a helix-loop-helix structure, and the N-terminal is located intracellularly [18], [19] (Figure 4).

PRRT2 shares (67% sequence similarity) the proline-rich N-terminal domain with the product of the *SynDIG4* gene (synapse differentiation-induced gene 1) also known as PRRT1 (Proline Rich Transmembrane protein 1), a type II transmembrane protein that interacts with AMPARs in brain and heterologous cells and regulates synaptic strength [22].

SynDIG4/PRRT1 was identified in several independent proteomic studies as a candidate AMPAR-associated protein [23][24], [25] [26], as well as a component of the postsynaptic density [27], [28]. SynDIG4/PRRT1 is not enriched at synapses but was found to colocalize with the AMPAR subunit GluA1 at extrasynaptic sites in rat cortical neurons [28].

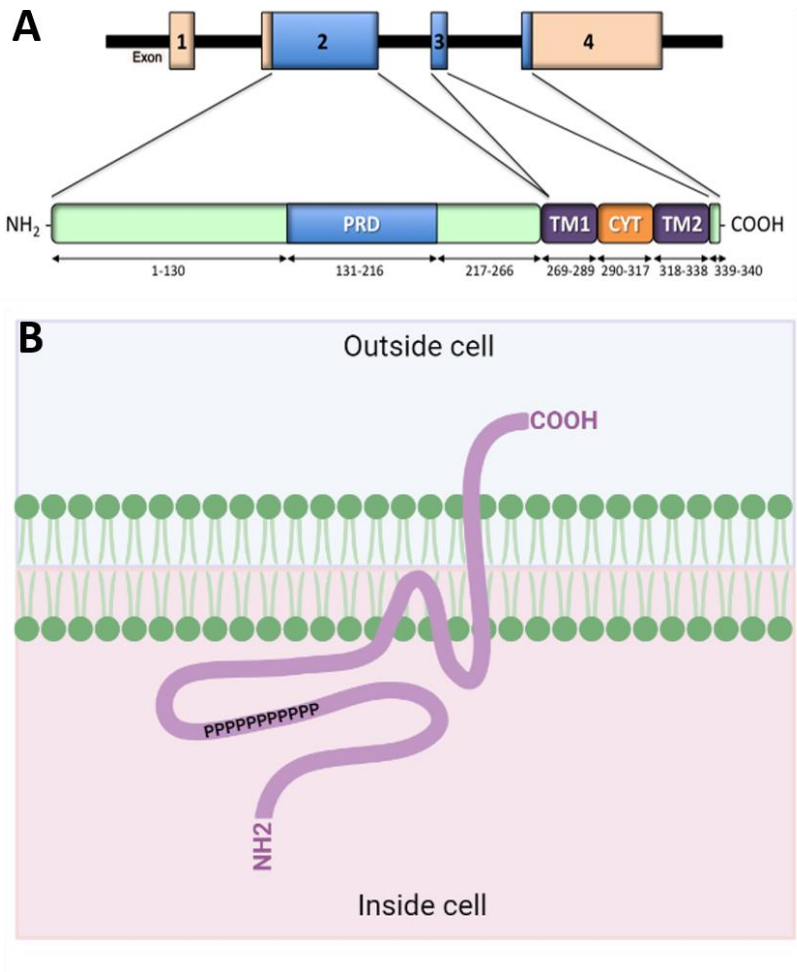


**Figure 4.** (**A**) The PRRT2 gene contains four exons, with exons 2-4 encoding a multidomain protein of 340 amino acids formed by a long N-terminal domain (1–268) containing a proline-rich region (PRD); two putative transmembrane helices, M1 (269–289) and M2 (318–338), separated by an intracellular loop (CYT, 290–317), and a C-terminal dipeptide (339–340). Despite the similarity with the proteins of the dispanin family, only M2 is a true transmembrane helix, while M1 is folded into two halves (M1a and M1b) by a hinge formed by two proline residues. As a consequence, M1 does not cross the membrane (Valtorta et al., 2016). (**B**) Membrane topology of PRRT2 (created with BioRender.com).

### 1.2.1. PRRT2 mutations

To date, more than 70 *PRRT2* mutations have been reported, with a percent of 5.5% occurring *de novo* and 87.1% with a familial origin (Figure 5) [29]. The amount of nonsense/frameshift or missense mutations is scattered along the entire sequence of the gene with a hot spot consisting in the c.649dupC frameshift mutation that accounts for nearly 80% of the cases. The DNA sequence in the "mutational hotspot" region is composed by a homopolymer of four guanine bases followed by nine consecutive cytosine bases. This peculiar sequence seems particularly prone to mutations given the frequent duplication, deletion and point mutations in the very same cytosine stretch. Most of the mutations involve the insertion of a precocious stop codon, leading to an unstable mRNA and/or a protein that is degraded or mistargeted [18]. This haploinsufficient state is consistent with a loss-of-function mechanism (LOF) in PRRT2-associated diseases.

Besides the truncated variants, about 30 missense variants of PRRT2 are documented in PRRT2-related disorders [30] (Figure 5). Several pathogenic missense mutations of PRRT2 do not change in the total and plasma membrane expression levels [30] [31] [32] (Table 1). Therefore, the pathogenicity of PRRT2 missense variants in paroxysmal disorders is difficult to evaluate.

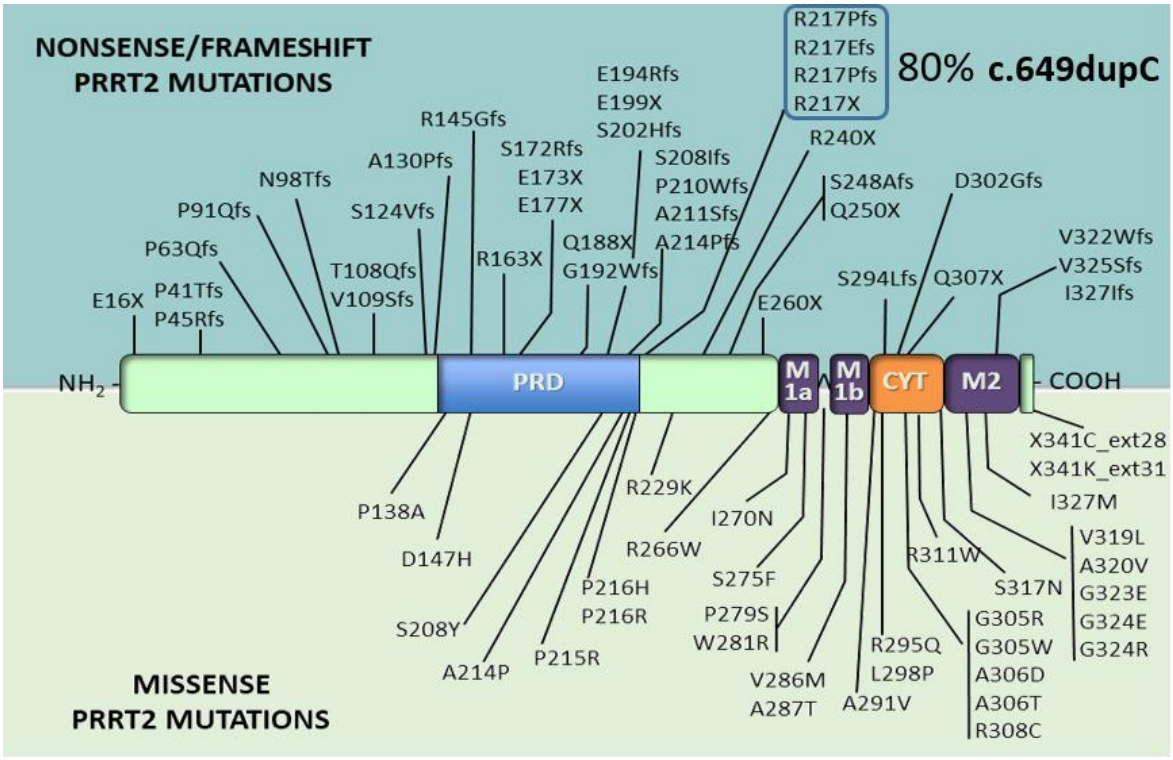


**Figure 5.** Mapping of PRRT2 mutations superimposed to the domain structure of PRRT2. Mutations in PRRT2 have been recently identified as the cause for a heterogeneous group of paroxysmal neurological diseases. The identified nonsense/frameshift and missense mutations are reported on the PRRT2 domain structure in the upper and lower panels, respectively (Valtorta et al., 2016, *modified*).

Particularly interesting are the mutations at the transmembrane region of PRRT2. The PRRT2 protein, from the amino acid in position 266 of the transmembrane part to the C-terminal end, has a very stable configuration, suggesting a crucial role in the PRRT2 function, as well as in the binding with potential interactors. However, a very low number of PRRT2 mutations in general and in the transmembrane in particular, has been functionally studied thus far [33] [34] [35].

Recently, the discovery of a novel PRRT2 pathogenic variant inherited in an autosomal dominant pattern was reported in a family with PKD and BFIS [36]. This pathogenic variant shows a mutation to valine of the highly conserved alanine located at position 320 (A320V) in the M2 transmembrane region. The high evolutionary conservation suggests an important role of alanine-320. Other four missense mutations were found in the transmembrane region, namely R266W, R308C, R311W, I327M. The mutations R266W, R311W and I327M maintain a protein expression similar to the wild type, while the R308C mutation produces a

significant decrease of the protein expression [37] [38]. Moreover, a new mutation, I270V, in the same region was recently discovered, with a still unknown effect on PRRT2 expression [39]. Recently, other novel PRRT2 mutations have been identified, such as the mutation V286M identified in PKD patients [40] and the de novo heterozygous missense mutation V319L in exon 3 of the gene [41]. In general, all PRRT2 mutations are responsible of heterogeneous clinical signatures that go beyond the mere paroxysmal disorders. However, among these, we can discern frequent pathological phenotypes caused by PRRT2 mutations, as well as pathological phenotypes rarely related to PRRT2 mutations.

| PRRT2 variant | | Phenotype | Poly-phen 2 | Protein expression | Plasma membrane targeting | References |
|---|---|---|---|---|---|---|
| **c.796C>T** | R266W | PKD | Probably damaging/damaging | Expression similar to WT (100%) | Expression similar to WT (100%) | Zhao et al., 2020 |
| **c.809T>A** | I270N | PKD | Unknow | Unknow | Unknow | Balagura et al., 2020 |
| **c.856G>A** | V286M | PKD | Probably damaging | Unknow | Unknow | Li et al., 2018 |
| **c.922C>T** | R308C | PKD | Probably damaging/damaging | Expression 50% of WT | Expression 50% of WT | Zhao et al., 2020, Tsai et al., 2019 |
| **c.931C>T** | R311W | PKD, EA | Probably damaging | Expression similar to WT (100%) | Expression similar to WT (100%) | Zhao et al., 2020, Tsai et al., 2019 |
| **c.955G>T** | V319L | PKD | Probably damaging | Unknown | Unknown | Fang et al., 2020 |
| **c.959C>T** | A320V | PKD, BFIS | Probably damaging | Unknown | Unknown | Lu et al., 2018 |
| **c.981C>G** | I327M | PKD, BFIS | Probably damaging/damaging | Expression similar to WT (100%) | Expression similar to WT (100%) | Zhao et al., 2020, Tsai et al., 2019 |

**Table 1**. List of the selected missense mutations in the PRRT2 membrane-associated domain and their phenotypic characterization.

## 1.3. PRRT2 predominant phenotypes

At now, PKD is considered the most frequent type of paroxysmal dyskinesia, with an incidence rate estimated as about 1:150,000 [42]. PKD, together with BFIE and ICCA, represents the core of PRRT2-associated disorders [12] [43] In PKD patients, the prevalence of PRRT2 mutations ranges from 40% to 90% depending on case ascertainment, suggesting a high genetic heterogeneity [44] [29]. However, PRRT2 mutations do not account for all PKD cases, suggesting the existence of additional gene mutations, or possible misdiagnosis due to overlapping clinical manifestations. In this context, several other genetic disorders have been recently suggested to be an alternative cause of the PKD syndrome including, but not limited to, those associated with SCN8A, ADCY5, and SCL16A2 mutations [45]. PRRT2 mutations in PKD are mainly inherited in an autosomal-dominant manner [29], but about 10-30% are sporadic, suggesting a *de novo*

origin [29] [46]. The PRRT2 mutations in PKD displayed a male predominance, with a male-to-female ratio of about 2:1.5 [47] [48].

Several PKD related families were studied over the years, describing the precise clinical diagnostic criteria for PKD (Table 2) [49]. PKD is characterized by unilateral or bilateral involuntary movements triggered by other sudden and voluntary movements, such as standing up from a sitting position, being startled or changing motion velocity (e.g., accelerating from walking to running) [42]. The most common attacks include dystonia, followed by chorea and athetosis [49][29]. Less frequently, attacks can include ballism or hemiballism [50] and do not involve loss of consciousness) [42]. Since common movements represent potential triggers, attacks can be as frequent as 100 per day to as few as one per month, but with a very brief duration.

| Diagnostic criteria for PKD | |
|---|---|
| 1 | Attacks provoked by kinesigenic trigger |
| 2 | Short duration of attacks (<1 min) |
| 3 | No loss of consciousness or pain during attacks |
| 4 | No evidence of other organic diseases and normal neurological examination between the attacks |
| 5 | Good control of the attacks with phenytoin or carbamazepine |
| 6 | Age of onset between 1 and 20 years, if there is no family history of PKD |

**Table 2.** Diagnostic criteria for PKD. Clinical manifestations used to diagnose the PKD pathology (Bruno et al., 2004, *modified*).

The age of onset in PKD varies generally between 6 months and 33 years, but more frequently between 7 and 15 years [44] [29]. Patients with PKD and IC (PKD/IC) usually develop epilepsy within the first 2 years of age and subsequently attacks of PKD. Normally, the frequency of attacks decreases with age with a complete remission typically occurring in the third and fourth decades of life [49]. Conversely, a tendency for improvement in the number and severity of attacks was observed during pregnancy and was observed in 50% of affected women [49].

Despite all cases linked to PRRT2 mutations have a kinesigenic trigger [29], [49][51], additional triggers can be observed, including loud sounds, emotional stress, startle or hyperventilation [44] [52]. Often, a sensory aura precedes the attacks, manifesting like paresthesia, stiffness, or a “fluttery feeling” usually in the body part where PKD develops [44] [49]. Some patients report that they could minimize their attacks if they stop or slow

down their movements when the aura appears [49]. The attacks may range from mild to severe, with the mild ones limited to a sensory aura followed by slight dystonic or choreic movements, while severe episodes might result in falls and injuries [53]. Another important diagnostic criterion concerns the ability of PRRT2-related PKD to respond to antiepileptic drugs (AEDs), especially the voltage-gated sodium ($Na^+$) channel (Nav) blocker carbamazepine (CBZ), with effective dosages lower than those used in epilepsy [44] [29][54]. In general, $Na^+$ channel blockers are among the most used drugs for the treatment of both focal and primary generalized tonic-clonic seizures. Other drugs belonging to this family are lamotrigine and oxcarbazepine [54], that are both effective in PRRT2-related pathologies [49] [29]. Other AEDs that were found to be effective in controlling PRRT2-related symptoms are levetiracetam and topiramate [49]. The exact mechanism by which levetiracetam acts to treat epilepsy is still unknown, but multiple lines of evidence suggest that a membrane glycoprotein named SV2A, expressed in the synaptic vesicles is the molecular target of this molecule [55][56]. The putative targets of topiramate include Nav, $GABA_A$, AMPA and kainate receptors, as well as carbonic anhydrase isoenzymes type II and IV [57]. Very important, unlike other AEDs, the effects of topiramate on ion channels are not likely to occur through direct modulation of channel gating, but rather through an indirect effect on channel phosphorylation [58].

Among the predominant phenotypes of PRRT2-related dysfunctions, there are also infantile convulsions and choreoathetosis (ICCA), also called paroxysmal kinesigenic dyskinesia with infantile convulsions (PKD/IC) [59] [60]. ICCA patients show both BFIE and PKD, the first one during childhood and the second one in the adult life [60] [61] [62], [63]. The range of the mean onset of PKD is 3-12 years and the clinical features consists in daily short paroxysmal episodes of dystonia/dyskinesia [64]. Many affected patients are misdiagnosed or prescribed multiple antiepileptic drugs. Patients usually show a good response to anticonvulsants and favorable prognosis [29]. A low-dose carbamazepine causes a dramatic improvement with the complete disappearance of dyskinetic episodes after 3 days [64].

Finally, another common onset of PRRT2-linked diseases is the BFIE, a self-limiting seizure disorder of infancy characterized by afebrile partial complex or generalized tonic-clonic seizures [62]. Brief spells with motor arrest, eye or head deviation, cyanosis, generalized hypertonia and limb jerks are very often reported in patients [65]. The onset age is between 3 to 12 months, while seizures usually remit by 2 years of age or, more frequently, by 16

months for PRRT2-associated cases [29]. Neurological tests and imaging studies, such as electroencephalogram (EEG) and magnetic resonance imaging (MRI), are usually normal. BFIE has no known long-term neurological *sequelae* and the development is usually normal, and normal are also neurological tests [29]. The transmission pattern of BFIE is consistent with autosomal dominant inheritance with incomplete penetrance [66]. BFIE affect both females and males in populations with various ethnic backgrounds [29]. Although more male patients have been reported in PKD, BFIE distributes more evenly between male and female patients [29]. Mutations in PRRT2 have been identified in the majority of families with BFIE, with the c.649dupC frameshift mutation found in 81.4% of cases [29]. Watanabe and colleagues observed that the seizures were easily controlled with antiepileptic drugs, such as phenobarbital, carbamazepine or valproate, and a combination of two or more anticonvulsants is rarely necessary [65][62]. Because of the benign course of the syndrome and the spontaneous remission of seizures, patients with low seizure frequency do not necessarily have to be treated [67].

## 1.4. PRRT2 rare phenotypes

Together with the predominant phenotypes, there are a few others, which are rarely induced by PRRT2 mutations. PNKD is a rare movement disorder occurring at an estimated prevalence of around one in a million people [68]. PNKD differs from PKD because of the longer duration and smaller frequency of the attacks. In fact, PNKD attacks last for minutes to hours, but they are much more infrequent compared to PKD [68] [69] [70]. In PNKD patients, attacks are triggered by different conditions, such as by consuming alcohol, coffee, or tea, psychological stress, excitement or fatigue. Frequently, PNKD attacks are characterized by dystonic posture, chorea, athetosis, and ballism, affecting a single region of the body or generalized, and begin with premonitory symptoms such as sensation of tightness (80% of those) in one limb, involuntary movements of the mouth, or anxiety [71] [72]. As for PKD, also PNKD attacks are not associated with loss of consciousness or seizures and never occur during sleep [73] [74]. PNKD onset is typically during childhood from 1 to 20 years, with a mean age of 12 years. Only a few patients have the onset after 18 years of age [74]. Normally, attacks tend to diminish with age [72]. PNKD can be idiopathic or genetic (in both cases either sporadic or familial) or secondary to a known etiology. When familial, PNKD is inherited as autosomal dominant trait and is due to

mutations in*MR*-1, also called *PNKD* gene [75] [76]. In addition, several studies reported cases of PNKD-like phenotypes in different families carrying the PRRT2 c.649dupC mutation [34] [77]. Although the preponderance is not as striking as for PKD (M:F, 3-4:1), more males than females are affected (1.4:1) [72].

Concerning treatment of PNKD, avoidance of the triggering factors (e.g., alcohol or caffeine) can be helpful. Anticonvulsants should be tried in any case, although PNKD does not readily respond to anticonvulsants, and the medical treatment is less rewarding [51]. Several drugs have been used, although without consistent success [78] [79] [80]. In this context, only clonazepam appears to be the most successful drug [73]. Interestingly, deep brain stimulation appears a useful treatment for drug resistant severe PNKD [81].

Another rare phenotype associated with PRRT2 mutations is PED, a clinical syndrome described for the first time in 1977, characterized by recurrent episodes of involuntary movement usually precipitated by sustained walking or running [73]. About 30-40% of patients with PED carry a *SLC2A1* mutation [82] [44]. However, a PRRT2 mutation was found in a Chinese family presenting PD occurring both at rest and after prolonged exercise, showing an overlap between PNKD and PED subgroups [83].

Mutations in *PRRT2* gene cause a spectrum of pathologies that may be also associated with HM, a rare and peculiar disorder in which affected individuals experience migraine with transient weakness or hemiparesis [84]. Usually, attacks begin during childhood or adolescence and, in addition to hemiparesis, can gradually involve sensory symptoms, always accompanied by headaches [84]. Hemiplegic migraine may be sporadic or familiar with a dominant autosomal inheritance. In recent years, mutations in ion channel genes were identified to cause HM (*CACNA1A, ATP1A2*, and *SCN1A*), but do not cover a large proportion of patients [85] [86]. To date, several patients with HM were found to carry PRRT2 mutations localized in residue c.649/650 [87].

In the literature, the association between movement disorders and epilepsy is well known, indicating an overlap in the pathogenesis of the diseases [88] [89]. Frequently, febrile seizures are present in PRRT2 patients, with a prevalence in children between six months and five years [90] [66] [91] [92] [93].

Some patients with PRRT2 mutation experiment EA, a rare group of disorders characterized by attacks of truncal ataxia and incoordination lasting minutes to hours [94]. To date, several

gene mutations have been identified to cause EA (*EA1, KCNA1; EA2, CACNA1A; EA5, CACNB4; EA6, SLC1A3; EA8, UBR4*) [95], [96] [97].

PRRT2-linked pathologies can be associated with more severe phenotypes in the presence of homozygous or compound heterozygous mutations. In 2011, five individuals of an Iranian family showing severe non-syndromic intellectual disability were found to carry a homozygous PRRT2 mutation (c.649dupC) [98]. In addition, Labate and colleagues in 2012 described a small group of patients carrying homozygous mutations and showing a more severe encephalopathic phenotype, including cognitive and neurological deficits associated with the most common paroxysmal movement disorder [99]. Further studies reported further fifteen patients with homozygous or compound-heterozygous mutations [100] [23] [101]. The increased presence of intellectual disability in patients with biallelic *PRRT2* mutations indicates a gene-dosage effect in which a strong reduction or the absence of PRRT2 leads to a more severe phenotype with additional disease manifestations [29] [17]. The dominant effect of *PRRT2* mutations associated with several paroxysmal disorders points out the important functional role of the protein in the mammalian central nervous system (CNS). The study of PRRT2 mutations is thereby important to advance the understanding of the homeostatic processes in the brain and elucidate the PRRT2-related pathogenetic mechanisms leading to paroxysmal disorders.

## 1.5. PRRT2 distribution

A recent study shows that PRRT2 is a neuron-specific protein that has an important role in synaptic development and function in the brain [102]. Several lines of evidence, obtained in the mouse show that the PRRT2 mRNA levels are regulated during brain development. The expression of the protein was found to be high in brain and spinal cord, with the highest levels in the cerebellum, basal ganglia, and neocortex [103][104][105] [102] [17]. In particular, low levels of both PRRT2 mRNA and protein were detected during early development in the murine nervous system followed by a marked increase during the postnatal phase with a peak during synapse formation and neuronal network rearrangement [103] [102]. In primary cultures of hippocampal and cortical neurons, PRRT2 expression already discernible at early stages, increases between 10 and 21 days in vitro, the temporal window of intense synaptogenesis. On the contrary, PRRT2 expression is undetectable in primary astroglial cultures, consistent with its neuron-specific expression [102].

Recently, to investigate in detail the role of PRRT2 at synapses, Michetti and colleagues characterized a murine model in which the PRRT2 gene has been constitutively inactivated (PRRT2 KO) [17]. From a behavioral point of view, both pups and adult PRRT2 KO mice were not affected by spontaneous seizures. However, these animals displayed a phenotype recapitulating the most common clinical manifestations of patients suffering PRRT2 mutations. KO animals displayed behaviors characterized by loss of balance and back walking that are similar to the episodic ataxia found in patients, suggesting a strong implication of the cerebellum in pathogenesis of PRRT2-related diseases [17]. Moreover, PRRT2 KO mice were also highly prone to audiogenic paroxysms with wild running, back walking and jumping and displayed a higher propensity for generalized pentylenetetrazol-evoked seizures. In both phenotypes, the seizure propensity was not severe, consistent with the mild epileptic phenotype observed in patients bearing PRRT2 mutations. In this study, was characterized for the first time a genetically altered mouse constitutively lacking PRRT2 that also allow to analyze the protein expression by means of a knocked-in lacZ sequence. Through β-galactosidase (β-gal) staining, the regional expression of PRRT2 was found more intense in the cerebellum, hindbrain and spinal cord, while it was localized to restricted areas in the forebrain. On a macroscopic level, β-gal appeared strongly expressed in the cerebellum and hindbrain with respect to more rostral areas.

Examination of the entire nervous system from PRRT2 KO mice confirmed an average low expression level of β-gal in the forebrain, but with expression hot spots in restricted areas. The analysis of rostral sections revealed high expression levels in layer VIb of the neocortex, septal nuclei and claustrum. At more caudal levels, the β-gal signal was high in the hippocampus, particularly in the hilus, dentate gyrus and CA3 regions, with lower β-gal activity in the CA1 and CA2 areas. Specific signals were also observed in the amygdala, collicula and periaqueductal grey. In more caudal sections, a strong expression of PRRT2 was detected in the granular layer of cerebellum, whereas Purkinje cells and the molecular layer were negative except for sparse positive interneurons in the latter. Finally, PRRT2 expression was observed in the spinal cord, with intense β-gal staining in the substantia gelatinosa, as well in the dorsal horn. No β-gal staining was detected in the white matter, confirming the neuron-specificity of PRRT2 expression. PRRT2 expression was very low at postnatal day (P) 4 and 8, while at P16 its expression markedly increased, with a regional distribution similar to the adult [17]. This finding is in line with previous studies in which

PRRT2 mRNA, low at birth, was found to increase postnatally over the first month of life [102].

## 1.6. PRRT2 as a molecular actuator

To date, the molecular mechanisms by which PRRT2 mutations cause the disease and how are mostly unknown. Recently, several laboratories have thoroughly explored this topic. The current understanding assumes that the PRRT2 protein plays a crucial role in the release of neurotransmitters, in the formation and maintenance of synaptic networks and in the fine modulation of firing activity of neurons [18] [102], [106].

Due to its multifaceted function, PRRT2 might not be devoted to a single membrane actuator. PRRT2 was shown to act at both presynaptic and postsynaptic levels by interacting with several actors, ranging from the components of the neurotransmitters release machinery to ion channels and pumps. For these reasons, understanding the PRRT2 physiology and the functional impact of its mutations may help to elucidate the pathogenetic mechanisms leading functional derangement of brain networks in paroxysmal disorders.

### 1.6.1. PRRT2 and the neurotransmitter release machinery

The yeast two-hybrid screen experiments show that PRRT2 co-distributes with proteins associated with the neuronal synaptic area, such as the synaptosomal-associated protein 25 kDa (SNAP-25) [107]. SNAP-25 is a presynaptic membrane protein belonging to the Soluble N-ethylmaleimide-Sensitive Factor Attachment Proteins Receptor (SNARE) complex involved in synaptic vesicle membrane docking and fusion that plays a pivotal role in $Ca^{2+}$-dependent neurotransmitter release [108][109]. The interaction of PRRT2-SNAP25 was subsequently confirmed both *in vitro* and *in vivo* [70].

Since PRRT2 mutations display a LOF mechanism, an acute silencing approach through RNA interference was used to dissect out the physiological role of the protein at the synaptic level [102]. Together with SNAP-25, PRRT2 was found to co-distribute also with other presynaptic proteins such as synaptophysin, confirming that PRRT2 targeting to the synapse (Figure 6). To test for the localization of the protein in neuronal cells, hippocampal neurons were transduced with lentiviruses encoding for PRRT2-mCherry. In agreement with the biochemical experiments, PRRT2 immunoreactivity largely overlapped with the staining of the two presynaptic proteins in axonal and nerve terminal areas [102].

Functionally, it was observed that the acute lack of PRRT2 produces a dramatic downregulation of neurotransmitter release with a marked impairment in spontaneous and synchronous release, providing the important role of PRRT2 on presynaptic function [102]. To better investigate other possible PRRT2 interactors, an array of major presynaptic proteins whose constitutive KO strongly impairs evoked transmission was screened [102]. The association of PRRT2 with Vesicle-Associated Membrane Protein 2 (VAMP2) and with synaptotagmins 1/2 (Syt1/2) was found, both proteins involved in synchronous neurotransmitter release. In particular, the interaction between PRRT2 and Syt1/2 suggests that PRRT2 participates in the regulation of the $Ca^{2+}$ sensing apparatus responsible for fast synchronous release [102]. These data suggest a model in which PRRT2, binding SNAP-25 and Syt1/2, increases the affinity of the SNARE complex for the $Ca^{2+}$ sensor for fast release. The lack of PRRT2 lowers the $Ca^{2+}$ sensitivity of SNARE complexes, resulting in a strong decrease of neurotransmitter release probability. Consequently, the interactions between PRRT2 and Syt1/2 are necessary to boost the $Ca^{2+}$ sensitivity of evoked fast release, whereas they would be dispensable for the synaptotagmin-mediated spontaneous release (Figure 6).

Another important effect of acute PRRT2 deletion is a reduction of the density of synaptic connections, followed by changes in synaptic ultrastructure. In this context, both a reduction in the synaptic vesicle volume and an increase in the docked synaptic vesicles were observed [102]. In addition, the acute downregulation of PRRT2 in mouse embryos led to a delay in neuronal migration that was accompanied by defects in synaptic development [70].

Low levels of PRRT2 are also detected in fractions enriched in post-synaptic densities [102][110]. Thus, while its distribution indicates that PRRT2 is primarily a presynaptic protein, proteomics [111] [57] and coimmunoprecipitation [112] studies suggest that it plays some role also in the postsynaptic compartment. Specifically, at this level, PRRT2 was found to interact with GluA1 subunit (GRIA) of the AMPA-type glutamate receptor complex (AMPARs), formed by a core together to variable complex of more external proteins [113] [114]. Specifically, PRRT2 and PRRT1, together with Leucine-Rich Repeat Transmembrane Neuronal Protein 4 (LRRT4) and four isoforms of the membrane-associated guanylate kinase (MAGUK) family, (Noelins1-3 and C9orf4/FRRS1l) [24], constitute the receptor neighbor. These proteins assemble with the core subunits either through direct binding to the receptor or through interactions with each other [24]. The receptor core is composed by

tetramers of the pore-forming GluA1-4 proteins [115] [116][117] and up to four members of three distinct families of membrane proteins: the transmembrane AMPAR regulatory proteins (TARPs, g-2, g-3, g-4, g-5, g-7, g-8; [118] [119], the cornichon homologs 2 and 3 (CNIH2, 3)[24] , and the GSG1l protein [57] [24]. Functional data suggests that PRRT2, by this localization, limits the membrane distribution of GluA1 subunit in the postsynaptic membrane [112], confirming a potentially important role also at the postsynaptic level.

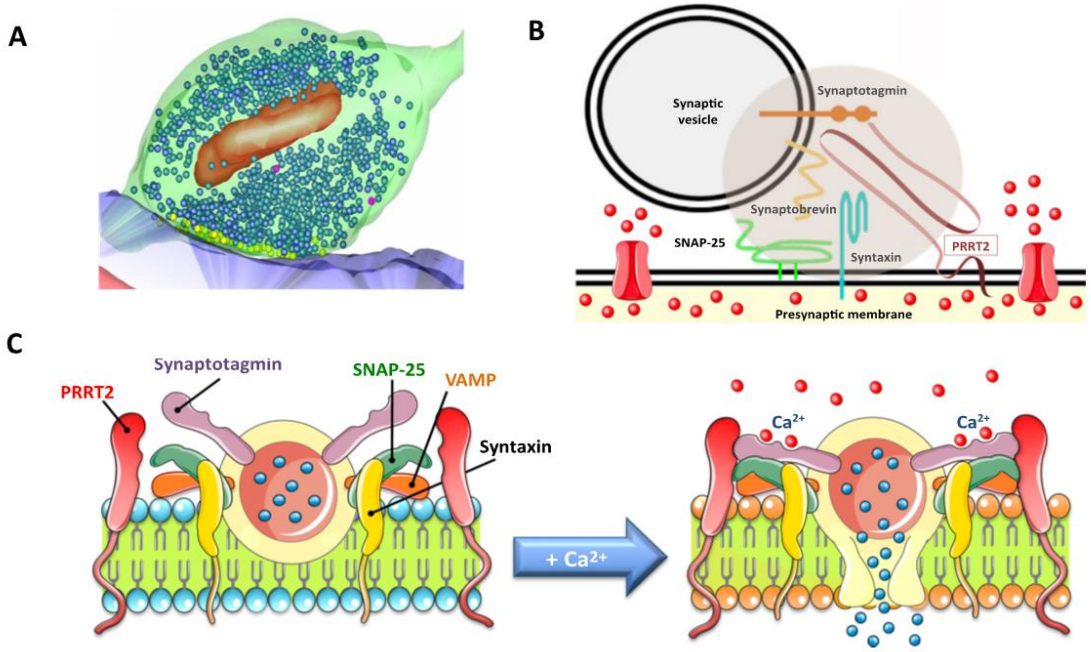


**Figure 6.** (**A**) 3D reconstruction of the ultrastructure of a presynaptic terminal from serial sections. (**B**) Schematic view of the presynaptic portion of the nerve terminal at the active zone. PRRT2, associated with the presynaptic plasma membrane, interacts with components of SNARE complex (SNAP-25, VAMP and synaptobrevin) and with the fast $Ca^{2+}$ sensor synaptotagmin. The panel also shows $Ca^{2+}$ ions (red spheres) and presynaptic $Ca^{2+}$ channels. (**C**) Mechanistic model for the role of PRRT2 in fast synaptic vesicle exocytosis. At rest (left), PRRT2 is in the proximity of both the $Ca^{2+}$ sensor synaptotagmin and the SNARE complex. Upon stimulation, when $Ca^{2+}$ concentration increases, PRRT2 interacts with both SNARE proteins and synaptotagmin. Consequently, PRRT2 endows the SNARE complex with $Ca^{2+}$ sensitivity and increases the probability of synchronous neurotransmitter release (Valtorta et al., 2016).

### 1.6.2 PRRT2 and the Na+/K+ ATPase pump

The α-subunit of $Na^+/K^+$ ATPase (NKA) is a fundamental polarized and electrogenic pump that transports 3 $Na^+$ ions outside the cell and two $K^+$ ions inside for each ATP hydrolyzed. Thanks to this activity, NKA maintains the ion gradient across the plasma membrane and

contributes to determine the neuronal resting membrane potential [120]. The NKA is formed by two subunits. The α-subunit carries out the catalytic and ion transport functions and associates with the β-subunit that modulates its membrane exposure and activity. Three isoforms of NKA α-subunit (α1- α3) are expressed in the brain, the ubiquitous α1 subunit and the α3 and α2 subunits that are specifically expressed in neurons and glial cells, respectively [121]. Since firing activity, inward synaptic currents, and the resting $Na^+$ permeability all enrich neurons with $Na^+$, neurons have a high requirement for $Na^+$ extrusion activity [122] [123]. Previous studies in cell lines showed that the α1-subunit has higher $Na^+$ affinity than the α3-subunit. This suggests that the α3 subunit becomes crucial when the intracellular $Na^+$ concentration rises during sustained neural activity, whereas the α1-subunit in neurons is dedicated to basal ion pumping activity [124] [125].

Numerous diseases are linked to mutations in NKA-isoforms. For example, familial hemiplegic migraine is associated with mutations in the *ATP1A2* gene encoding for α2-NKA, whereas a variety of paroxysmal neurological disorders are linked to mutations in the *ATP1A3* gene encoding for α3-NKA [123]. Among these disorders, including alternating hemiplegia of childhood, rapid-onset dystonia Parkinsonism, and epilepsy a significant overlap exists with PRRT2-associated diseases [122] . Moreover, recently discovered mutations in the *ATP1A1* gene encoding for α1-NKA are linked to refractory seizures and intellectual disability [126].

PRRT2 was demonstrated to specifically interact with both the α1 and the α3 subunits of NKA [127]. PRRT2 deficiency affects α3-NKA membrane distribution and impairs NKA function during neuronal stimulation, a phenotype that was specifically rescued by PRRT2 expression in PRRT2-lacking neurons [127]. These defects in NKA activity may contribute to the hyperexcitability described in PRRT2 KO neuronal networks and hence to the pathogenesis of PRRT2-linked paroxysmal disorders.

To fully understand the physiopathology of the PRRT2 clinical phenotypes and test the hypothesis of an interplay between NKA and PRRT2, the PRRT2 interactome was investigated in the mouse brain by a pulldown-based proteomic approach [127]. Interestingly, PRRT2 and NKA were found to colocalize at neuronal surface, and the lack of PRRT2 led to an increased clustering of α3-NKA at the neuronal membrane [127]. This abnormal clustering was due to the aggregation of the smallest nanoclusters forming large aggregates, without affecting the overall expression and membrane exposure of NKA but

producing a reduced mobility of α3-NKA that impaired $Na^+$ extrusion [127]. These observations are consistent with previous research demonstrating a dynamic equilibrium between clustered and free α3-NKA molecules on the membrane surface via diffusion-dependent mechanisms [123]. Electrophysiological recordings showed that the lack of PRRT2 in primary neurons does not affect the pump activity under resting conditions but decrease it during sustained neuronal activity. These data were confirmed by experiments performed in PRRT2-deficient neurons, where PRRT2 re-expression normalized both the electrophysiological profile and the pump membrane distribution [127]. Consequently, due to the functional interaction with NKA, the PRRT2 LOF has a larger impact on neuronal function under sustained electrical activity, leading to neuronal network hyperactivity, consistent with the proposed PRRT2 function as a stabilizer of neural network activity [17].

### 1.6.3 PRRT2 and $Ca^{2+}$ channels

Voltage-gated $Ca^{2+}$ channels (VGCCs) are complex proteins, consisting of distinct subunits encoded by multiple genes, plays a crucial role in translating changes in the cell surface membrane potential into local intracellular $Ca^{2+}$ transients that start a variety of physiological processes [128]. They are complexes of a central pore-forming α1 subunit with multiple auxiliary subunits [128]. The α1 subunit of 190 to 250 kDa is the largest subunit, and incorporates the conduction pore, the voltage sensor and gating apparatus, and most of the known sites of channel regulation by second messengers, drugs, and toxins. This subunit is arranged in four homologous domains (I-IV) each with six transmembrane segments (S1-S6) similar to the subunits of $Na^+$ channels, with the voltage sensor located in the S4 segment.

The transmembrane portion of the channel contains a re-entrant loop between helices S5 and S6, which forms the small, ion-selective filter at the extracellular end of the pore. The four S6 segments combine to form the pore's larger intracellular end. The largest extracellular loops connect the S5 or S6 segments to the membrane re-entrant loop. Small extracellular loops link the transmembrane segments. Larger intracellular loops link the four homologous domains. Large N-terminal and C-terminal tail domains also contribute to the internal face of the $Ca^{2+}$ channel. Biochemical, electrophysiological, and structural studies have essentially verified this view of $Ca^{2+}$ channel architecture [129].

In addition to α1 subunit, an intracellular β subunit and a transmembrane, disulfide-linked, α2δ subunit complex compose the majority of $Ca^{2+}$ channel types. A γ subunit has also been found in skeletal muscle $Ca^{2+}$ channels, and related subunits are expressed in heart and brain [130]. Although these auxiliary subunits alter the features of the channel complex, the pharmacology and electrophysiology properties of $Ca^{2+}$ channels are due principally to the α1 subunit [131].

As we have seen above, PRRT2 interacts with the SNARE proteins SNAP25, synaptobrevin and with the fast $Ca^{2+}$ sensors Synaptotagmin 1/2, suggesting a role in the $Ca^{2+}$-dependent transition from synaptic vesicle priming to fusion [18]. It was also observed that the knockdown of PRRT2 sharply decreases the $Ca^{2+}$-sensitivity of the release machinery. This effect leads to an impairment of basal synaptic transmission and a dramatic increase of facilitation of excitatory synapses that translates into hyperactivity and instability of primary culture of hippocampal/cortical neuronal networks [102], [132][106]. This phenomenon was observed both in primary granule cultures and in acute cerebellar slices from constitutive PRRT2 KO mice [102].

The above results suggest that PRRT2 deficiency may reduce the excitatory strength through a putative negative modulation of presynaptic VGCCs coupled with synaptic vesicles fusion. This possibility led to investigate the effects of PRRT2 deficiency on the properties of the two major groups of VGCCs present in nerve terminals, namely N-type and P/Q-type channels [130]. At synapses, P/Q-type and N-type $Ca^{2+}$ channels serve as the primary sources of cytosolic $Ca^{2+}$ used for fast neurotransmission [133] [134]. $Ca^{2+}$ entry through them generates a local microdomain of high $Ca^{2+}$ concentration that has molecular dimensions, on the order of 10-fold the diameter of the $Ca^{2+}$ channel itself [135] [136]. Co-immunoprecipitation and pull-down assays showed that PRRT2 interacts directly with P/Q-type VGCCs subtypes in glutamatergic hippocampal neurons. In addition, in nerve terminals, the lack of PRRT2 reduces the P/Q type channel clustering at the active zone dispersing P/Q-type $Ca^{2+}$ channels and decreasing their contribution to the $Ca^{2+}$ transients evoked by actions potentials [137]. This effect of PRRT2 on $Ca^{2+}$ sensitivity of excitatory strength of glutamatergic neurons, was also confirmed by specific pharmacological experiments by use of subtype-specific antagonists [137].

These results highlight the central role of PRRT2 in presynaptic $Ca^{2+}$ dynamics, by indirectly affecting SNARE proteins, and directly modulating the P/Q subtypes of VGCCs. The findings

emphasize PRRT2's crucial function in presynaptic $Ca^{2+}$ dynamics, which ensures a physiological $Ca^{2+}$ sensitivity of synchronous release at glutamatergic synapses.

### 1.6.4 PRRT2 and $Na^+$ channels

In addition to its role in the control of synaptic activity by modulating $Ca^{2+}$ inflow and sensitivity and NKA function, PRRT2 was recently demonstrated to interact with Nav [132][138] [106]. Nav are heteromeric channels that open in response to a change of membrane potential to provide selective permeability for $Na^+$ ions to initiate action potentials (for a recent review, see [139]). In the mammalian brain, Nav are composed of a 260 kDa α subunit associated with one or two auxiliary β subunits (β1-β4) of 33 to 36 kDa [139]. The α subunits, sufficient to produce a functional channel [140] are composed of approximately by 2000 amino acids and organized in four homologous domains (I-IV), each containing six α helices transmembrane segments (S1-S6) (Figure 7). Segments S1-S4 of Nav α subunits from each domain form the voltage sensor [139]. Positively charged arginine and lysine residues are positioned at every third residue within each S4 helix, conferring the flexibility of the voltage sensor domain connected directly with the pore domain by an intracellular linker between transmembrane segments S4 and S5 [139]. During depolarization, the positively charged S4 segments move toward the extracellular surface, directly affecting the pore domain structure through intracellular linkers and causing a conformational change that results in the opening of the channel pore. The segments S5 and S6, together with the extracellular connecting pore-loops, form the channel pore and the selectivity filter, the narrowest part of the pore that distinguish ions with similar charges and radii [139] [141]. The intracellular loop that connects the homologous domains III and IV occludes the cytoplasmic end of the pore when channel inactivates and is called inactivation gate. The intracellular loop folds into the channel structure and blocks the pore from the inside during sustained depolarization of the membrane [139]. Finally, four hydrophobic residues, one from each intracellular end of the S6 segments, form the activation gate, a small intracellular cavity.

In humans, nine genes (*SCN1A, SCN2A, SCN3A, SCN4A, SCN5A, SCN8A, SCN9A, SCN10A*, and *SCN11A*) encode nine distinct α subunits (Nav1.1-Nav1.9). Recently, an atypical $Na^+$ channel known as Nax, was identified [142]. The different α subunits define the Nav channel subtypes that also contain receptive amino acids for drugs and toxins [141]. The α subunit isoforms are expressed in tissue-specific patterns and exhibit differences in

gating behaviour, making them useful for distinct physiological roles [143]. Specifically, Nav1.1, Nav1.2, and Nav1.3 subtypes are abundantly expressed only in the CNS, Nav1.6 in both central and peripheral NS, Nav1.7, Nav1.8, and Nav1.9 are mostly restricted to the peripheral NS, and finally, Nav1.4 and Nav1.5 channels are abundant in skeletal and cardiac muscles, respectively [144] [141]. Nax, also known as Nav2, is expressed in the CNS and is involved in the control of salt intake [145].

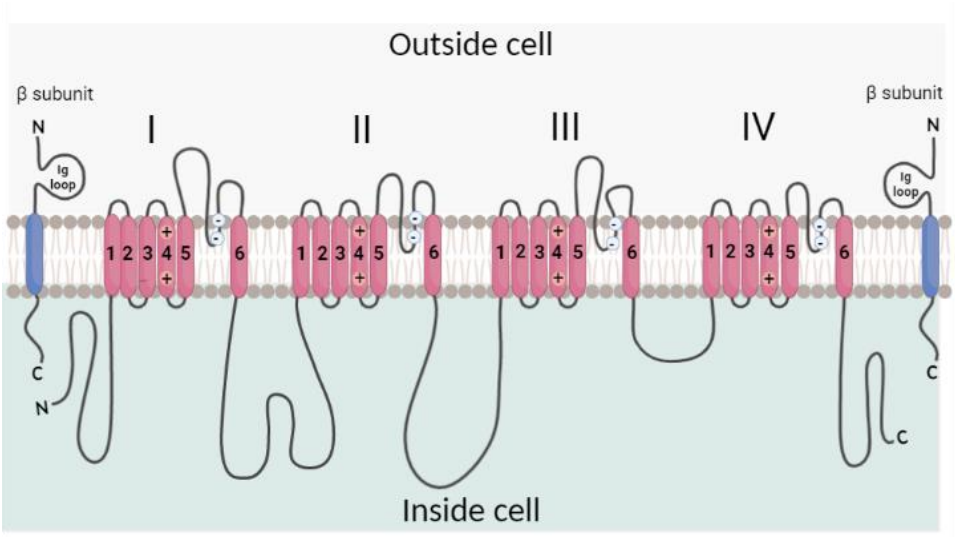


**Figure 7.** The primary structure of the subunits of the voltage-gated $Na^+$ channels (Nav). Nav contain a pore-forming α subunit consisting of four homologous domains (I-IV) of six transmembrane segments (1-6). Cylinders represent alpha helical segments. Bold lines represent the polypeptide chains of each subunit. The "+" signs in S4 represent the positively charged voltage sensor (arginine or lysine residues). The β subunits contain an extracellular immunoglobulin loop, transmembrane domain, and an intracellular C-terminal domain. (Created with BioRender.com).

Ionic current flowing through Nav generates the upstroke of action potentials in excitable cells, including neurons. In neuronal cells, depolarizations evoke rapidly activating and inactivating $Na^+$ currents, hence "transient", that are similar across cell types. Nevertheless, neurons differ both in the amplitude of "persistent" $Na^+$ current remaining after the inactivation of the transient current [146] and in the expression of "resurgent" current evoked by repolarization from positive potentials [147] [148]. Persistent current (also known as late current), is due to either incomplete inactivation or brief dissociations of the inactivation gate from the conductive pore. Resurgent currents occur when an intracellular molecule acts blocking the transient current upon depolarization, hindering the interaction of the inactivation gate with the conductive pore. Upon repolarization, the blocking molecule

dissociates and current briefly resurges through the conductive pore before it is again cut off by the inactivation gate. By increasing channel opening and availability at subthreshold voltages, persistent and resurgent currents generally increase neuronal firing rates, and hence are associated with hyperexcitability [149][150]. In particular, resurgent currents play an important role as drivers of both repetitive and spontaneous action potential activity and spontaneous action potential generation [147] [151]. Persistent currents were described to support burst neuronal firing [152] [153].

By using heterologous system stably expressing distinct Nav channel subtypes, it has been demonstrated that the expression of PRRT2 decreases the membrane exposure and $Na^+$ current of Nav1.2/1.6, but not of Nav1.1, channels [132]. Moreover, PRRT2 modulates biophysical properties of Nav1.2/1.6 by inducing a negative shift in the voltage-dependence of inactivation and a slow-down in the recovery from inactivation. The demonstration that the lack of PRRT2 leads to a hyperactivity of Nav channels in mouse neurons, in addition to the reported alteration of synaptic transmission and NKA function, represents the molecular basis of hyperexcitability of neurons in which the PRRT2 gene has been constitutively inactivated (PRRT2 KO) [17].

This Nav hyperactivity induced by PRRT2 LOF was also observed in neurons differentiated from induced pluripotent stem cells (iPSCs) from previously described heterozygous and homozygous siblings carrying the c.649dupC mutation. Electrophysiological experiments, performed on iPSCs from homozygous patients, showed increased $Na^+$ currents that were fully rescued by expression of wild-type PRRT2. This phenotype was associated with an increased length of the axon initial segment and with markedly augmented spontaneous and evoked firing activities [132]. These electrophysiological features were very similar to those observed in primary neurons from PRRT2 KO mice [17][106]. In this context, several studies suggest that the episodic nature of the attacks is the consequence of hyperexcitable networks bearing an imbalance between excitatory and inhibitory transmission and/or an intrinsic instability in response to external triggers [154] [155] [156] [157].

Interestingly, a significant increase in the axon initial segment (AIS) length of mouse PRRT2-KO neurons was found. Changes in length and location of the AIS with respect to the cell body are known as an important form of structural/functional homeostatic plasticity [158]. In agreement with these results, at the network level, several signs of hyperexcitability were found in PRRT2-KO hippocampal networks. This instability makes the brain areas

responsible for processing sensory information more prone to generate aberrant and undesired movements when suddenly stimulated by sensory inputs [17]. Hence, given the predominant paroxysmal character of PRRT2-linked diseases, the disturbance in cellular excitability by lack of negative modulation of Nav appears a fundamental pathogenetic mechanism to investigate.

Interestingly, diseases caused by mutations of Nav1.2 and Nav1.6 share some features with the PRRT2-related disorders, especially regarding epilepsy, intellectual disability and in some cases movement disorders. Sodium channels are the molecular targets for several common antiepileptic drugs, including phenytoin, carbamazepine, and lamotrigine [159], [160]. Consequently, the finding that sodium channels are important molecular targets for mutations that cause epilepsy is not surprising. Epilepsy mutations, which result in epileptic syndromes with a wide range of severity and comorbidities, target all sodium channel types that are highly expressed in the brain [161] [162] [163]. The most frequently mutated gene in sodium channel epilepsies is SCN1A, encoding the Nav1.1 channel. A wide range of epilepsy syndromes, from mild febrile seizures to persistent, drug-resistant developmental and epileptic encephalopathies, are caused by mutations in this gene [164] [165]. Interestingly, also Nav1.2 mutations were found to be involved in epilepsy. Nav1.2 mutations were first suggested to be related to epilepsy in 2001, with the identification of the variant R187W in a family in which the proband developed complex partial seizures after an initial diagnosis of FS [166]. However, BFNIS were the first epileptic syndrome that was clearly associated with SCN2A mutations [167], [168]. Later, there was a significant growth in the phenotypic spectrum of epilepsies caused by SCN2A mutations, including severe developmental and epileptic encephalopathies (DEE) [169] [170] [171]. In addition to epilepsy, SCN2A mutations have also been identified in patients with neurodevelopmental dysfunctions including autism spectrum disorders (ASD) and/or intellectual disability (ID), as well as other neuropsychiatric phenotypes such as schizophrenia [169] [171]. Nav1.6 is the main sodium channel in AIS and nodes of Ranvier of myelinated axons of excitatory neurons and was found to be implicated in epilepsy and movement disorders [159]. The first mutation on human SCN8A was identified in a heterozygous proband with cognitive impairment and cerebellar ataxia without seizures [172]. Now, a few hundred patients with SCN8A mutations have been reported with a wide phenotypic spectrum. The majority of SCN8A patients exhibit severe developmental and epileptic encephalopathy characterized by early onset

epilepsy with multiple seizure types, infrequent febrile seizures, EEG abnormalities mainly in the temporo-occipital regions, severe intellectual disability, and movement disorders [173]. Other patients showing milder phenotypes, exhibit BFIS, PD [174] and epilepsies with intermediate phenotypes [175].

As mentioned before, although α subunits alone formed a functional channel, under physiological conditions, this subunit, is coupled to one or two β subunits that play an essential role in the fine-tuning of channel kinetics and channel expression on the cell surface (for a review see:[176]).

In mammalian, four genes (*SCN1B*-*SCN4B*) encode for five types of β subunit (β1, β1B, β2, β3, and β4). Subunits β2 or β4 bind to the α-subunit via a disulfide bond, whereas β1 and β3 associate non-covalently [141]. Nav β subunits are expressed in excitable cells in the CNS, peripheral nervous system (PNS), skeletal muscle, and the heart [177] [178] [129] [179], [180] [180]. β subunits are also expressed in non-excitable cells such as astrocytes, radial glia, and Bergmann glia although particular focus has been given to the β subunit expressed in neurons and myocytes [181] [182]. Nav β subunits are members of the immunoglobulin (Ig) superfamily of cell adhesion molecules and possess an extracellular Ig domain that participates in a number of cell adhesion-related activities [183]. In general, β1B and β3 are most abundant during fetal development and their expression decreases after birth [184] [185] [186]. Expression of β1 and β2 rises during postnatal development and predominates in the adulthood [184][185]. β4 is expressed in postnatal tissues, although the developmental time course for β4 expression has not been determined [129]. The β4 subunit was found to exhibit a high expression in the cerebellum playing a role in regulating resurgent $Na^+$ current [176]. A peptide corresponding to β4 was found to be sufficient to invoke resurgent $Na^+$ current in Hek293 cells [187], strongly suggesting a role for β4 in the generation of resurgent $Na^+$ current in vivo.

Most β subunits share a similar type I membrane topology [176]. The association of the α-subunits with β-subunits facilitates the membrane targeting and the activation of the α-subunits with an opposite of those observed for PRRT2 [132]. Hence, due to the opposite behaviors, it is unclear at now, whether PRRT2 and the β-subunits cooperate or compete for the same binding sites, leading to the putative formation of Nav channel complexes with distinct functional characteristics.

# 2. AIMS

The main objective of this research project is to characterize the molecular and functional PRRT2-Nav interactions to investigate the basis of PRRT2-associated paroxysmal disorders. Based on the previous studies, we decided to focus on the interaction between PRRT2 and Nav1.2. Because Nav1.2 channels, as all Nav channels, are embedded in a multicomponent membrane signaling complex that involves, among others, the β-subunits, we aimed at studying whether they interact or compete with PRRT2 for their modulation of channel binding and functions. Moreover, given the characteristic membrane topology of PRRT2, we studied the structure-function relationships of the PRRT2-Nav1.2 interaction by molecular dynamics simulations, biochemical and electrophysiological techniques.

Specifically, in this project the following aims were addressed:

I. Determine how PRRT2 and the β-subunit interact or compete for the α-subunit's shared binding sites to generate Nav complexes with different functional characteristics. To address this question, we used Hek293 cells stably expressing Nav1.2 sequentially transfected with different constructs. Because the β4-subunit was highly expressed in the cerebellum, the main brain region responsible for the PRRT2 LOF phenotype, we mostly studied the interplay with the β4-subunit.

II. Study which are the PRRT2 domains responsible for both interaction with Nav1.2 and modulation of channel turnover and biophysics. To do this, we generated two deletion mutants of PRRT2, the first one composed of the C-terminal transmembrane domain of PRRT2 including the short cytoplasmic loop and lacking the N-terminus domain (PRRT2ΔN-HA), and the second one encoding the cytosolic PRRT2 domain fused to a transmembrane anchor (PRRT2ΔC-HA). Full-length PRRT2-HA and the two constructs were then transfected in stable Hek293 clones expressing Nav1.2 (or Nav1.1, used to study the specificity of the effect).

III. Analysis of some PRRT2 mutations involved in the binding to the Nav directly implicated in PRRT2-related pathologies. The majority of the PRRT2 pathogenic mutations cause the loss of protein expression, making in vitro studies difficult or impossible. However, a restricted number of missense mutations maintains the protein expression and the trafficking to the membrane allowing their characterization. Hence, their expression and function were studied in the same system used for the previous points.

# 3. EXPERIMENTAL PROCEDURES

## 3.1 Plasmids

The following human PRRT2-based constructs are used in the study:

(I) PRRT2-HA, i.e., pKH3-PRRT2-HA vector encoding for full length PRRT2 with 3XHA tag fused at the C-terminal [19].

With the aim to introduce the mutations of interest in the PRRT2 gene, a site-directed mutagenesis was performed using the QuikChange Lightning Site-Directed Mutagenesis Kit (Agilent). The site-directed mutagenesis primers containing the mutation in the middle of the sequence, were designed in order to have some specific features, about melting temperature (Tm ≥ 78 °C), length (between 25 and 45 nt) and GC% (>40%). All primers were purchased from Eurofins Genomics (Ebersberg, Germany).

The following PRRT2 mutation primers were used:

V286M: forward, GTGGCCTGTCAACATCATGGCCTTCGCTTATGC

A320V: forward, CTCTTAAGCATCGTGGTGCTGGTGGGGGGA

(II) BAP-HA, i.e., pKH3-BAP-HA vector encoding for bacterial alkaline phosphatase (BAP) with 3XHA tag fused at the C-terminal [132]

(III) PRRT2ΔN-HA, i.e., pKH3-PRRT2ΔN-HA encoding for the PRRT2 membrane domain with 3XHA tag fused at C-terminal

(IV) PRRT2ΔC-HA, i.e., pKH3-PRRT2ΔN-HA encoding for the PRRT2 cytosolic domain fused, for membrane targeting, to the second membrane domain of IFTM1 (a kind gift of dr. J. Yount; RRID: Addgene_58415). For the PRRT2ΔC-HA plasmid, the second membrane domain of IFTM1 was amplified by PCR from pCMV-HA-mIFITM1 with the following primers:

forward, ACGTAAGCTTACCGCCAAGTGCCTGAACAT

reverse, TCAGGTCGACTCTAATGGCACAGACAACGATGAC

and cloned in Hind3-Sal1 sites of the pKH3 plasmid (a gift of dr. I. Macara, Addgene_12555). The sequence corresponding to the intracellular domain of PRRT2 (nucleotides: 1-780) was PCR amplified from pKH3-PRRT2-HA vector with the primers:

forward, CTGAAAGCTTATGGCAGCCAGCAGCTCTGAGATC

reverse, GATCAAGCTTTTCACCCCCCTCCACCCCAGGA

and cloned in Hind3 single site of the vector pKH3 encoding the second transmembrane domain of the IFITM1 previously generated. The correct orientation and sequence of the cloned fragment were controlled by restriction analysis followed by DNA sequencing.

## 3.2 Cell cultures and transfection

Hek293 cells stably expressing human Nav1.2 or Nav1.1 were kind gifts from Drs. Enzo Wanke and Marzia Lecchi (Milano-Bicocca University, Italy). All Hek293 cell lines were maintained in DMEM/F12 (1:1) supplemented with 10% fetal bovine serum, 100 U/ml penicillin, 100 µg/ml streptomycin and, for selection of stable Nav clones, 500 µg/ml G418. Cell lines were transfected with 2 µg of each plasmid according to the manufacturer's recommendations at 70% confluency using Lipofectamine 2000. All reagents were purchased from ThermoFisher Scientific. To identify transfected cells for electrophysiology, the reporter EGFP or Tomato protein reporter (Clontech) was co-transfected. For electrophysiological experiments, transfected cells were dissociated, re-plated at low density about 24 h post-transfection and recorded after other 24 h.

For testing β1-β4-subunit/Nav1.2 interactions, Nav1.2 expressing Hek293 cells were transfected with either FLAG-tagged β-subunit (SCN1B [NM_001037], SCN2B [NM_004588], SCN3B [NM_018400], SCN4B [NM_174934]; Origene) or FLAG-tagged bacterial alkaline phosphatase (BAP; Sigma-Aldrich). To evaluate PRRT2 and β1-β4-subunit interactions, Hek293 cells were transfected with either HA-tagged PRRT2 or the unrelated BAP as a control. For competition assays, Nav1.2-expressing Hek293 cells were transfected with HA-tagged PRRT2 and incubated with FLAG-tagged β4-subunit expressed in wild type cells. Alternatively, HA-tagged PRRT2 and FLAG-tagged β4-subunit were co-expressed in Nav1.2-expressing Hek293 cells. For biotinylation assays and electrophysiological experiments, Nav1.2-expressing Hek293 cells were transfected with the empty pKH3 vector (MOCK), HA-tagged PRRT2 and/or FLAG-tagged β4-subunit.

To map the PRRT2/Nav interactions, Hek293 Nav1.2 and Hek293 Nav1.1 cells were transiently transfected with MOCK, full length PRRT2-HA or its deletion mutants PRRT2ΔN-HA and PRRT2ΔC-HA.

To study the effect of PRRT2 pathogenetic mutants, Hek293 Nav1.2 were transfected with the MOCK, full length PRRT2-HA, PRRT2 A320V or PRRT2 V286M.

## 3.3 SDS-PAGE and Western blotting

SDS-PAGE was performed according to Laemmli [188]. Samples heated to 50°C for 5 min without boiling were run on SDS-PAGE polyacrylamide gels and blotted onto nitrocellulose membranes (Whatman). Blotted membranes were blocked for 1 h in 5% milk in Trisbuffered saline (10 mM Tris, 150 mM NaCl, pH 8.0) plus 0.1% Triton X-100 and incubated overnight at 4 °C with the appropriate primary antibody. Membranes were washed and incubated at room temperature for 1 h with peroxidase-conjugated anti-mouse (1:3000; BioRad, Hercules, CA) or anti-rabbit (1:3000; BioRad, Hercules, CA) antibodies. Bands were revealed with the ECL chemiluminescence detection system (ThermoFisher Scientific). Immunoblots were quantified by densitometric analysis of the fluorograms (Quantity One software; Bio-Rad, Hercules, CA) obtained in the linear range of the emulsion response.

## 3.4 Pull down and Surface biotinylation assays

Naïve Hek293 cells expressing the PRRT2 variants were harvested in lysis buffer (150 mM NaCl, 50 mM Tris, 1 mM EDTA and 1% Triton X-100 supplemented with protease inhibitor cocktail) 48 h after transfection and centrifuged at 10,000 x g for 10 min at 4 °C. Kept an aliquot for input, the supernatant was incubated with 50 µL of monoclonal anti-HA-agarose affinity beads (Sigma-Aldrich) for 2 h at 4 °C. After 3 washes in lysis buffer, beads were incubated with cell extracts from Hek293 cells expressing either Nav1.2 or Nav1.1 for 2 h at 4 °C. After extensive washes in lysis buffer and detergent-free lysis buffer, samples were resolved by SDS-PAGE and subjected to western blotting with pan-Nav (1:300, Sigma-Aldrich Cat.S8809, RRID:AB_477552) and HA (1:1000, Thermo Fisher Scientific Cat.71-5500, RRID:AB_2533988) specific antibodies. Actin immunoreactivity (anti-actin antibody 1:1000, Sigma-Aldrich Cat.A4700, RRID:AB_476730) was used as control of equal loading. For biotinylation experiments, 48 h after transfection, Nav1.2 expressing Hek293 cells were incubated with 1 mg/ml of EZ-Link™ Sulfo-NHS-SS-Biotin (ThermoFisher Scientific) in cold phosphate buffered saline (PBS) for 35 min at 4 °C, with constant mixing. Free biotin was quenched, twice with 100 mM Tris pH 8, and once with cold PBS to remove the excess of biotin. Cells were then lysed in lysis buffer (150 mM NaCl, 50 mM Tris, 1 mM EDTA and 1% Triton X-100) supplemented with protease inhibitor cocktail (Cell Signaling). Total cell lysates were centrifuged at 10,000 x g at 4 °C for 10 min. Kept an aliquot for the input sample, the supernatant fraction was incubated with 150 µl of NeutrAvidin conjugated agarose beads

(ThermoFisher Scientific) at 4°C for 3 h. After extensive washes of the beads, samples were eluted, resolved by SDS-PAGE and subjected to western blotting with anti-panNav (1:300; Sigma-Aldrich), anti-NKA 1 (1:1,000; Merck), anti-FLAG (1:2,000; Sigma Aldrich) or HA (1:1,000; ThermoFisher Scientific) antibodies.

## 3.5 Live and conventional cell immunolabeling

Hek Nav1.2 cells transfected with PRRT2-HA, PRRT2ΔC-HA or PRRT2ΔN-HA constructs were live labelled by diluting primary antibodies (mouse anti-HA, 1:500, Millipore) in culture medium for 30 min at 37 °C / 5% $CO_2$ to detect surface epitopes, followed by fixation with 4% paraformaldehyde (PFA) and incubation with Alexa Fluor-594 secondary antibodies.

After several washes in phosphate-buffered saline (PBS), coverslips were mounted using Prolong Gold antifade reagent (Invitrogen) containing 4′,6′-diamidino-2-phenylindole (DAPI) for nuclear staining. Hek293-Nav1.2 cells transfected with PRRT2-HA, PRRT2ΔC-HA or PRRT2ΔN-HA constructs were fixed in 4% PFA at room temperature for 20 min, washed in PBS and blocked with 10% bovine serum albumin (BSA) for 20 min.

Samples were sequentially incubated with mouse anti-pan-Nav (Sigma; 1:100 in 5% BSA) and rabbit anti-HA, (Invitrogen; 1:500 in 5% BSA) primary antibodies, followed by Alexa 564-conjugated or 488-conjugated secondary antibodies (Invitrogen; 1:200 in 5% BSA) at room temperature. After several washes in PBS, coverslips were mounted using Prolong Gold antifade reagent (Invitrogen) containing DAPI for nuclear staining.

The Live Labeling protocol used for the characterization of *hPRRT2* mutant isoforms; it is a variant of the standard one. In the Live Labeling protocol, the cells are incubated with the primary antibody diluted in the culture medium; without the permeabilization step, the primary antibodies can bind just to components exposed on the extracellular side of the cell membrane. Successively to the incubation, cells are fixed and treated with the secondary antibody. Transfected live cells are maintained for 10 min at 4 °C, and then incubated with the primary antibody anti-HA (rabbit anti-HA Invitrogen, 1:500 diluted in culture medium) for 20 min at 4 °C; cells are treated with the secondary antibody Alexa Fluor 488 for 20 min at 4 °C and then are fixed by 4% PFA for 20 min at room temperature. Cell nuclei are stained with DAPI. The images were acquired with the confocal microscope. With this protocol, it is

possible to visualize the HA epitope in PRRT2-HA exposed on the external side of the cell membrane.

## 3.6 Electrophysiological recordings

Patch pipettes, prepared from thin-borosilicate glass (Hilgenberg) were pulled and fire-polished to a final resistance of 2-4 MΩ when filled with standard internal solution. Whole-cell currents were recorded using an EPC-10 amplifier (HEKA Electronic). Recordings with leak currents >200 pA or series resistance >10 MΩ were discarded. Linear capacity and leakage currents were eliminated by P/N leak subtraction procedure. For all electrophysiological experiments data acquisition was performed using PatchMaster programs (HEKA Elektronic). Series resistance ($R_s$) was compensated 80% (2 μs response time) and the compensation was readjusted before each stimulation. All recordings were performed at room temperature. Voltage-clamp recordings of voltage-gated $Na^+$ currents were performed using the following solutions: extracellular (in mM): 140 NaCl, 3 KCl, 1 $MgCl_2$, 1 $CaCl_2$, 10 HEPES, 10 Mannitol (pH 7.3 with NaOH); intracellular (in mM): 140 CsCl, 10 NaCl, 2 EGTA, 10 HEPES (pH 7.3 with CsOH). To induce resurgent currents, 200 μM Nav β4 peptide (KKLITFILKKTREK-OH; Proteogenix) corresponding the C-terminal tail of full-length β4-subunit, was included in the pipette solution.

For the experiments with PRRT2ΔN-HA/PRRT2ΔC-HA and the pathogenetic mutantions whole-cell family currents of fast inactivating Nav channels were evoked by 5 mV steps depolarization from -80 to 40 mV and cells were held at -100 mV. For the experiments with the β subunits, whole-cell family currents of fast inactivating Nav channels were evoked by 5 mV steps depolarization (100 ms in duration) from -80 to 65 mV and cells were held at a holding potential ($V_h$) of -120 mV.

Steady state inactivation curves were constructed by recording the peak currents amplitude evoked by 20-ms test pulses to -10 mV after 500-ms pre-pulses to potentials over the range of -130 to 20 mV. Time-dependent rate of recovery from inactivation was calculated by pre-pulsing the cell with a 20-ms step to -20 mV to inactivate $Na^+$ channels and then bringing back the potential to -100 mV for increasing recovery durations (0.5, 1, 2, 4, 8, 32, 64, 128, 148 ms) before the test pulse of -20 mV. Time constants for recovery from inactivation were calculated by fitting data from each recorded cell to a first order exponential function and averaging time constants across cells. To investigate the frequency dependent inhibition, a

series of depolarizing pulses to +10 mV from a holding potential of -100 mV for 12 ms at a frequency of 20 Hz was applied. Peak current was normalized to the first pulse in each experiment. Persistent currents were evoked from $V_h$=-120 mV by 5-mV depolarization steps of 600 ms from -60 to 50 mV. Resurgent currents were evoked with depolarization steps from $V_h$ of -120 mV to 30 mV (20 ms) to open channels, allowing them to undergo open-channel block, and subsequently repolarizing to potentials ranging from -50 to 20 mV (60 ms) to allow the blocker to unbind. Persistent currents were measured in the last 60 ms of a 600 ms depolarizing step pulse. Resurgent currents were measured after 2.5 ms into the repolarization step to bypass fast tail currents. The percentage of persistent/resurgent currents were calculated by dividing the current amplitude by the peak transient current in each recorded cell. To minimize space-clamp problems, we selected only isolated cells with a soma diameter of about < 30 µm for recordings.

The $Na^+$ current density (J) was obtained by dividing the peak inward current by the cell capacitance (nA/pF). The conductance/voltage relationship (G-V) curves were obtained by converting the maximal current values, evoked with the voltage step protocols, to conductance using the relation $G_{Na}=I_{Na}/(V-E_{Na})$, where $G_{Na}$ is the $Na^+$ conductance, $I_{Na}$ is the peak $Na^+$ current, V is the command pulse potential, and $E_{Na}$ is the theoretical reversal potential of $Na^+$ current calculated by Nernst equation. G-V curves were normalized and fitted with the Boltzmann function $G/G_{max} = 1/(1 + \exp[(V - V_{1/2})/k])$, where G is the conductance, $G_{max}$ is the maximal conductance, $V_{1/2}$ is the half-maximal voltage of activation, and k is the slope factor. Inactivation curves were fitted with the Boltzmann equation in the following form: $1/[1 + \exp(V_{1/2} - V)/k]$.

## 3.7 Molecular Dynamics Simulations

Molecular dynamics (MD) simulations were performed using NAMD3.0 [189] with the all-atom CHARMM36m force field [190] [191]. The membrane builder application of the CHARMM-GUI server [192] [114] was used for the preparation of all the input files. The protein transmembrane domain (G261 to K340 of the human PRRT2 sequence) was oriented with the PPM web server [193], inserted into a 1-palmitoyl-2-oleoyl-*sn*-glycero-3-phosphocholine lipid bilayer and solvated with water molecules, using the TIP3P model [194]. $Na^+$ and $Cl^-$ ions were added to neutralize the total system charge at a physiological concentration of 0.15 M. The whole system counted 108,608 atoms in a rectangular box.

Periodic boundary conditions were applied to replicate the system and remove box surface effects, and the particle mesh Ewald (PME) method was used for long-range electrostatics [195], with a grid spacing of 1 Å and sixth-order B-splines. A cutoff of 12 Å and smooth switching at 10 Å was used for Lennard-Jones interactions. Chemical bond distances involving hydrogen atoms were constrained using the SHAKE/RATTLE algorithm [196]. Before production**,** the system was energy minimized and later it was equilibrated by running 15-ns NPT simulation using positional restraints on the protein atoms with $p$ = 1 atm and $T$ = 310 °K. Subsequently, two independent 1 μs-long MD simulations were produced in the NPT ensemble at the same temperature and pressure maintained by a Langevin thermostat and Nosé-Hoover Langevin piston pressure control [197]. A time-step of 2 fs was employed for one replica, while the hydrogen mass repartitioning (HMR) method [198]was used to allow the use of a 4-fs time-step for the second one [199]. The MD trajectories were inspected and analyzed to validate the structural stability of PRRT2 protein using VMD [200] and PyMOL. Alpha carbon Root Mean Square deviation and cross distances analysis were performed for PRRT2 replicas trajectories through tcl scripting [200].

## 3.8 Statistical analysis

Data are expressed as means ± standard error of the mean (SEM) for number of independently preparations as detailed in the figure legends. Normal distribution of data was assessed using the D'Agostino-Pearson's normality test. To compare two normally distributed sample groups, the two-tailed Student's unpaired *t*-test was used. To compare two sample groups that were not normally distributed, the non-parametric Mann-Whitney's U-test was used. To compare more than two normally distributed sample groups, one-way ANOVA, followed by post hoc multiple comparison tests (either the Bonferroni's or the Dunnett's test) was used. In cases in which data were not normally distributed, non-parametric one-way ANOVA (Kruskal-Wallis' test) was used, followed by the Dunn's multiple comparison test. Alpha levels for all tests were 0.05% (95% confidence intervals). Statistical analysis was carried out using Prism (GraphPad Software, Inc.) software.

# 4. RESULTS

## 4.1 The Nav β4-subunit and PRRT2 do not interact or compete for binding to Nav1.2.

It is well known that Nav β-subunits influence the biophysical features and membrane exposure of the Nav channels (for a review see: [176]). Moreover, β-subunits are involved in numerous pathological processes such as cardiac arrhythmias, neuropathic and inflammatory pain, and epilepsy. Most of these conditions are based on neuronal hyperexcitability. Consequently, it was necessary to determine whether the effects of PRRT2 on Nav activity, which led to cellular and network hyperexcitability, was related to the sequestration of β-subunits by PRRT2 or an inhibition of β-subunits binding to the Nav α-subunit. Affinity-binding assays were used to measure the interactions between Nav1.2, β4-subunits and PRRT2. We decided to focus our experiments on the β4-subunit because this subunit is highly expressed in the cerebellum [176], the main brain area responsible for the phenotype of PRRT2 KO mice and where PRRT2 reaches the highest expression under physiological conditions [17] [201]. Furthermore, among the four β-subunits, only β4 is necessary for the resurgent $Na^+$ current often associated with high-frequency firing and network hyperexcitability [176] [202] [203]. Hek293 cell clones stably expressing the α subunit of human Nav1.2, were transiently transfected with HA-tagged PRRT2 and β-subunits. The PRRT2/Nav1.2 α/β complexes were pulled down with anti-HA beads and identified by western blotting with anti-Nav α- and β-subunit antibodies. This investigation allows us to assess whether PRRT2 binds directly to the transmembrane or cytosolic domains of β-subunits reducing their availability for the Nav1.2 α/β complex. Affinity binding assays were performed in wild type Hek293 cells expressing HA-tagged PRRT2 and either the negative control BAP or the various β-subunits. This experiment revealed that PRRT2 pulled down by anti-HA beads did not significantly associate with none of the four β-subunits detected by western blotting with β1/β4-subunit specific antibodies (Figure 8A). Next, using the Nav1.2 α-subunit as a hub, we investigated whether PRRT2 and the β4-subunit can bind to the Nav1.2 α-subunit independently at distinct sites or they compete for a single association site of the protein. When both HA tagged PRRT2 and β4-subunit were transiently expressed in Hek293 cells stably expressing Nav1.2, pull down of PRRT2 with anti-HA beads resulted in the co-precipitation of similar amounts of Nav1.2 α-subunit together with detectable amounts of β4-subunit (Figure 8B).

To assay for a direct competition of PRRT2 and β4-subunit for a shared binding site on the α-subunit, HA-tagged PRRT2 or BAP was expressed in Hek293-Nav1.2 cells. The HA-PRRT2/Nav1.2 immunoprecipitated complex was challenged in the absence or presence of an excess of β4-subunit expressed in wild type Hek293 cells. Also under these conditions, the presence of an excess β4-subunit did not inhibit the binding of PRRT2 to Nav1.2 α subunit, as the amount of α-subunit present in the immunocomplexes was not affected in the presence/absence of β4-subunit, as shown by western blotting with anti-Nav antibodies (Figure 8C). Hence, all these data indicate that PRRT2 and the Nav β4-subunit do not interact with each other and bind the Nav1.2 α-subunit independently.

The β-subunits of Nav channels are known to enhance the trafficking of the α-subunits to the plasma membrane, resulting in a larger population of active channels exposed to the extracellular *milieu* [137]. On the other hand, we have recently shown that PRRT2 inhibits Nav1.2/Nav1.6 channel membrane exposure, resulting in a decrease in Na+ current [132].

Consequently, we investigated whether the simultaneous presence of the β4-subunit and PRRT2 affected the surface exposure of the α-subunit to the plasma membrane. To this aim, we performed surface biotinylation experiments of Hek293 cells stably expressing Nav1.2 α-subunit transiently transfected with HA-tagged PRRT2, β4-subunit or both and quantified the amount of surface-labelled Nav1.2 α-subunits. The results obtained show that, while PRRT2 and β4-subunit have the reported opposite actions on the exposure of the α-subunit on the plasma membrane, the combined expression of the two membrane proteins was not significantly different from the control sample. These data indicate that PRRT2 and β4-subunit have opposite actions on Nav1.2 channel trafficking that occur independently of each other, so that the two proteins operate as additive modulators of Nav1.2 α-subunit targeting to the plasma membrane (Figure 9).

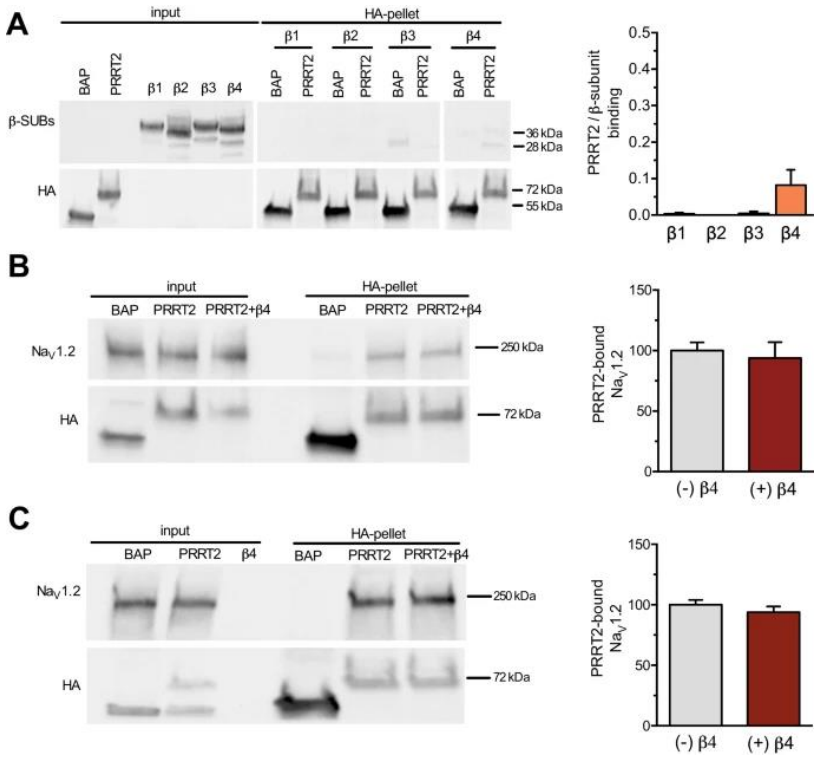


**Figure 8.** PRRT2 and the Nav β4-subunit do not interact or compete for binding to Nav1.2. (**A**) Left: Representative immunoblot of co-immunoprecipitation of β1/β4-subunits by PRRT2. HA-tagged PRRT2 (PRRT2), bacterial alkaline phosphatase (BAP) and FLAG-tagged β1/β4-subunits were expressed in wild type Hek293 cells. Cells lysates (INPUT, 10 µg protein) and samples immunoprecipitated by anti- HA beads (HA-pellet) were analyzed by western blotting with anti-FLAG and anti-HA antibodies. The representative blots were cut from the same gel. Right: Quantification of the FLAG immunoreactive signal in PRRT2 immunoprecipitates normalized to the control BAP values. Means ± sem of n = 3 independent experiments. (**B**) Left: Representative immunoblot of co-immunoprecipitation of PRRT2 and Nav1.2 from extracts of Nav1.2-expressing stable Hek293 clones transiently transfected with either HA-tagged PRRT2 alone or with HA-PRRT2 + β4 subunit (β4). BAP was used as a control. Cells lysates (INPUT,10 µg protein) and samples immunoprecipitated by anti-HA beads (HA-pellet) were analyzed by western blotting with anti-panNav and anti-HA antibodies. Right: Quantification of the Nav immunoreactivity in PRRT2 immunoprecipitates expressed as ratios between normalized Nav1.2 and PRRT2 immunoreactivities. Means ± sem of n = 3 independent experiments. (**C**) Left: Representative immunoblot of co-immunoprecipitation of Nav1.2 by PRRT2 in the presence or absence of an excess of β4-subunit. HA- tagged PRRT2 or BAP was expressed in Nav1.2-expressing Hek293 cells, whereas the β4-subunit (β4) was overexpressed in wild-type Hek293 cells. The extract from the β4-subunit expressing cells was added to the HA-immunoprecipitated PRRT2/Nav 1.2 complex. Cells lysates (INPUT, 10 µg protein) and samples immunoprecipitated by anti-HA beads (HA-pellet) were analyzed by western blotting with anti-panNav and anti-HA antibodies. Right: Quantification of the Nav immunoreactivity in PRRT2 immunoprecipitates normalized to the BAP values. Means ± sem of n = 3 independent experiments.

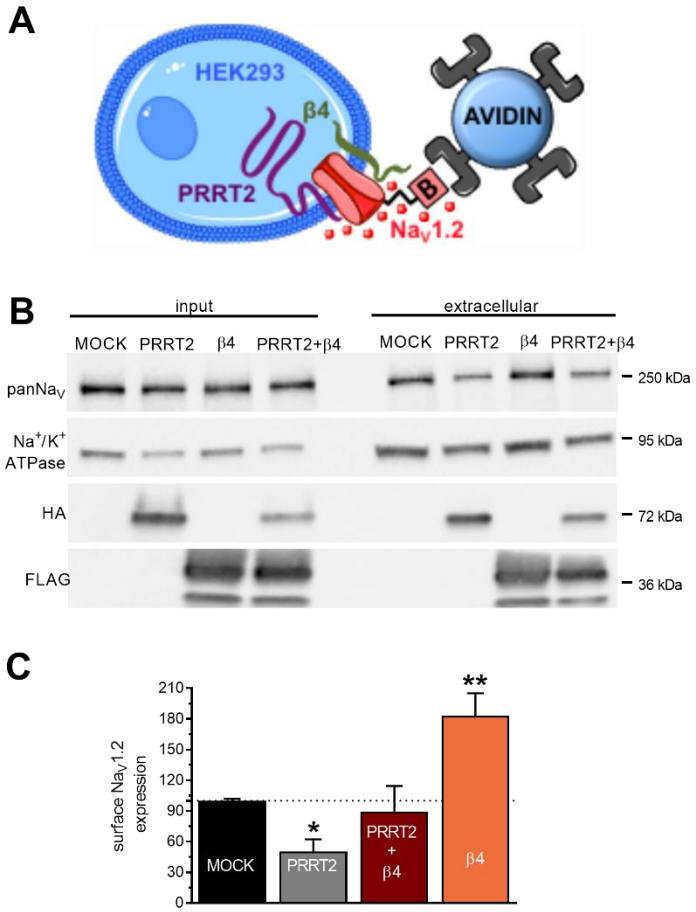


**Figure 9.** PRRT2 and the Nav β4-subunit have opposite effects on membrane targeting and exposure of Nav1.2 channels. (**A**) Schematics of the biotinylation experiment. (**B**) Representative immunoblots of cell surface biotinylation performed in Hek293 cells expressing Nav1.2 and transfected with empty vector (MOCK), PRRT2-HA, β4-FLAG, or both. Total lysates (input; left) and biotinylated (cell surface; right) fractions were analyzed by western blotting. Membranes were probed with antibodies to panNav, HA, FLAG, and Na/K-NKA, with the latter used as marker of cell surface fractions. (**C**) The cell surface Nav immunoreactivity is expressed in percent of the control MOCK value after normalization to NKA immunoreactivity. Means ± sem of n = 4 independent experiments. Two-way ANOVA revealed no significant interaction between PRRT2 and β4-subunit. *p < 0.05, **p < 0.01; one-way ANOVA/Fisher's least significant difference tests versus MOCK.

## 4.2 PRRT2 counteracts the increase in Nav1.2 current density induced by β4-subunit

To study the PRRT2 effects on the properties of $Na^+$ currents mediated by the physiological complex formed by Nav1.2 α-subunit-β4-subunit, macroscopic whole-cell currents were recorded from Hek293 cells expressing Nav1.2 sequentially transfected with empty vector (pKH3; MOCK), PRRT2, β4-subunit or with PRRT2 + β4-subunit (Figure 10A). Families of transient $Na^+$ currents were elicited by applying 100-ms depolarizing steps ranging from -80 mV to 65 mV from a holding potential of -120 mV (inset). The Current density (J)/voltage (V) curves were calculated for all experimental conditions by normalizing the recorded peak current at each applied voltage by the cell capacitance (Figure 10B). Cells expressing PRRT2 showed the previously described reduction of the transient $Na^+$ current across a wide voltage range and in the absence of voltage shifts in the peak of maximal current, when compared to the control condition (MOCK) ([132]; Figure 10B,C). As previously described [129], expression of the β4-subunit had a positive modulatory effect on $Na^+$ current density with a two-fold increase of the Nav1.2 current density, as compared to MOCK-transfected cells with a shift of the peak current towards more negative voltages (Figure 10B,C). The properties of Nav1.2 currents were modified after either β4-subunit or PRRT2 transfection, suggesting that both these membrane proteins were successfully integrated into the channel signaling complex and exerted their modulatory action. However, the positive modulation of the β-subunit on the amplitude of the $Na^+$ current density was neutralized when PRRT2 and the β4-subunit were co-expressed, while the β4-subunit induced left-shift of the J/V curve was preserved (Figure 10B,C). The data indicates that membrane targeting of the Nav1.2 α-subunit is affected by PRRT2 and the β4-subunit in opposite directions via different processes, with additive effects.

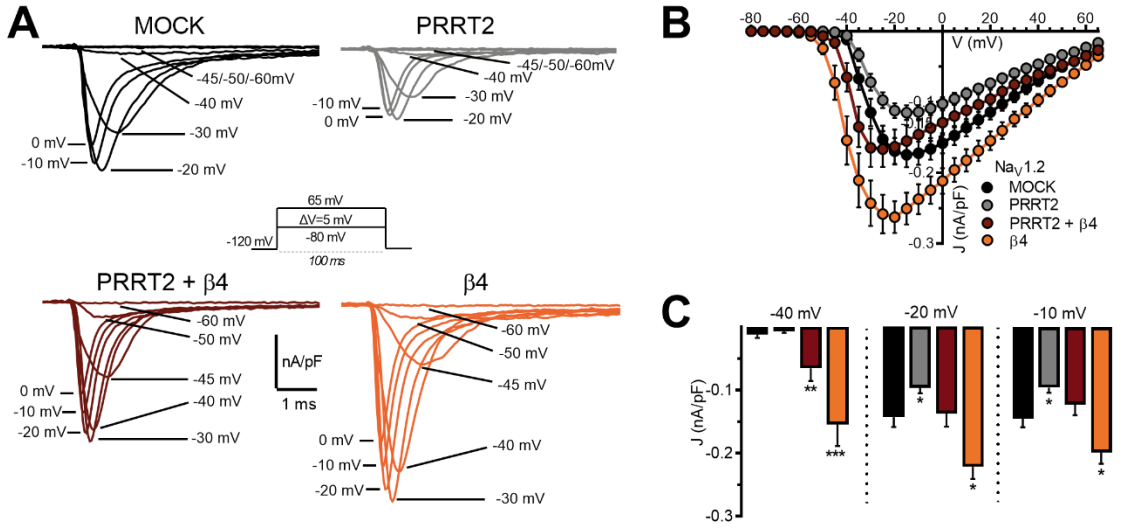


**Figure 10.** PRRT2 and the β4-subunit have opposite effects on the expression of the Nav1.2 transient current. (A) Representative whole-cell transient $Na^+$ currents recorded in Hek293 cells stably expressing Nav1.2 and transiently transfected with empty vector (MOCK, black), PRRT2 (gray), β4-subunit (orange) or PRRT2+β4 subunit (dark red). Currents were elicited by a protocol (inset) consisting of 5-mV depolarization steps from -80 to 65 mV from a holding potential of -120 mV. For clarity, the first 6 ms of the 100-ms steps for eight representative traces per condition are plotted. (**B**) Current density (J) versus voltage (V) relationship for all the studied experimental conditions. The statistical analysis of J values at three representative voltages (-40/-20/-10 mV) is reported (**C**). Data are expressed as means ± sem (MOCK, n = 36; PRRT2, n = 22; β4, n = 18; PRRT2+β4, n = 17). Two-way ANOVA revealed no significant interaction between PRRT2 and β4-subunit on the amplitude of the macroscopic $Na^+$ current. *p<0.05, **p<0.01, ***p<0.001 *versus* MOCK, Kruskal-Wallis/Dunn's tests.

## 4.3 PRRT2 and β4-subunit differentially modulate the of Nav1.2 activation and inactivation kinetics

We next examined the voltage-dependence of channel activation and steady-state inactivation with the aim to investigate the PRRT2 effects on the biophysics of Nav1.2 α-subunits in the presence of the β4-subunit, (Figure 11A,B). In a previous study [132], we observed that PRRT2 did not affect the Nav1.2 activation curves. However, PRRT2 promoted channel inactivation at more negative potentials. On the other hand, the β4-subunit is known to induce a leftward shift of the activation curve of Nav1.2, without affecting the voltage-dependence of inactivation [204]. We found that the specific modulation of the Nav1.2 biophysical properties by PRRT2 and the β4-subunit were fully preserved when the two auxiliary proteins were co-expressed. Specifically, under this condition, the activation curves displayed the leftward shift as signature of the β4-subunit, while the steady-state inactivation curves were shifted at more negative potentials by the concomitant action of PRRT2 (Figure 11A,B). Notably, β4 exerted its action on the activation irrespective of the absence or presence of PRRT2 and PRRT2 exerted its action on the inactivation irrespective of the absence or presence of β4. The quantification of the main biophysical parameters obtained from the Boltzmann fitting of individual activation and inactivation curves confirmed that the voltage of half-maximal activation ($V_{0.5}$), slope and maximum conductance of activation ($G_{max}$) were significantly changed in the presence of the β4-subunit and not affected by PRRT2 (Figure 11C). The voltage of half-maximal inactivation ($V_{0.5\,inact}$) was decreased by PRRT2 and not affected by of the β4-subunit, which only induced a slight decrease of the slope of inactivation (Figure 11D).

Additionally, we measured channel recovery from fast inactivation using a protocol in which we evaluated the peak current by a first depolarizing step to -20 mV and allowed channels to recover from the inactivation state for 10-increasing time intervals at -100 mV before measuring channel availability with a test pulse to -20 mV (Figure 12A, inset). When compared to Hek293-Nav1.2 MOCK transfected cells, the extent of channel recovery was significantly decreased by PRRT2, while it was unaffected by the β4-subunit. Interestingly, the PRRT2-induced decrease of the recovery plateau was only slightly attenuated when both auxiliary proteins were co-expressed, but still significant with respect to MOCK transfected cells, leaving the time constant of recovery unmodified under the tested

experimental conditions (Figure 12B,C). Furthermore, the expression of β4-subunit reduced the use-dependent inhibition of Nav1.2 by PRRT2 as shown by the ratio between the current evoked by the last and first step of the protocol used to study the recovery from fast channel inactivation (Figure 12D). All results suggest that PRRT2 and β4 subunit operate together in the Nav channel signalling complex by producing discrete and distinct modulations of the channel biophysics.

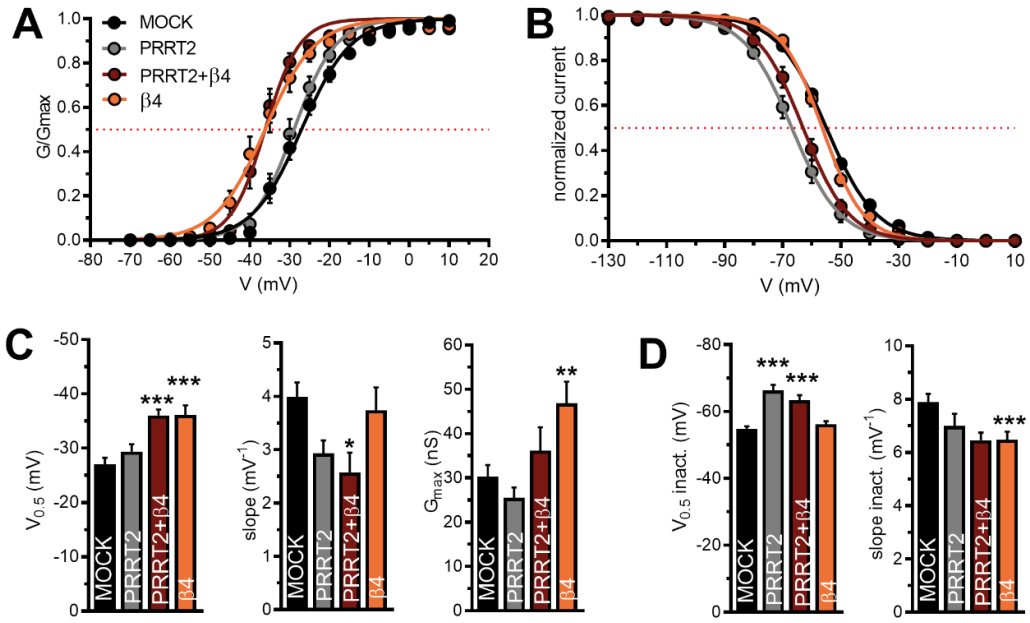


**Figure 11**. PRRT2 and β4-subunit differentially affect the kinetics of activation and inactivation of Nav1.2 channels. Voltage dependence of activation (**A**) and steady-state inactivation (**B**) curves fit with a Boltzmann function for all conditions tested. Activation was studied using recordings obtained with the protocol depicted in Fig. 10A. Steady-state inactivation was obtained with a protocol in which the cell under study was held at a series of voltages ranging from -130 mV to 30 mV for 500 ms followed by a 20-ms step pulse to -10 mV to measure channel availability using a holding potential of -120 mV. Mean parameters of activation (**C**) and steady-state inactivation (**D**) curves fit to data obtained from all condition tested. All data are expressed as means ± sem. Activation: MOCK, n = 36; PRRT2, n = 22; β4, n = 18; PRRT2 + β4, n = 17. Steady-state inactivation: MOCK, n = 44; PRRT2, n = 16; β4, n = 28; PRRT2 + β4, n = 24. No significant differences were found in the activation kinetics between β4-subunit alone and PRRT2 + β4-subunit groups, as well as in the inactivation kinetics between PRRT2 alone and PRRT2 + β4-subunit groups. Two-way ANOVA revealed no significant interaction between PRRT2 and β4-subunit on the analyzed biophysical parameters. *p < 0.05, **p < 0.01, ***p < 0.001 versus MOCK; one-way ANOVA/Bonferroni's tests or Kruskal–Wallis/Dunn's tests.

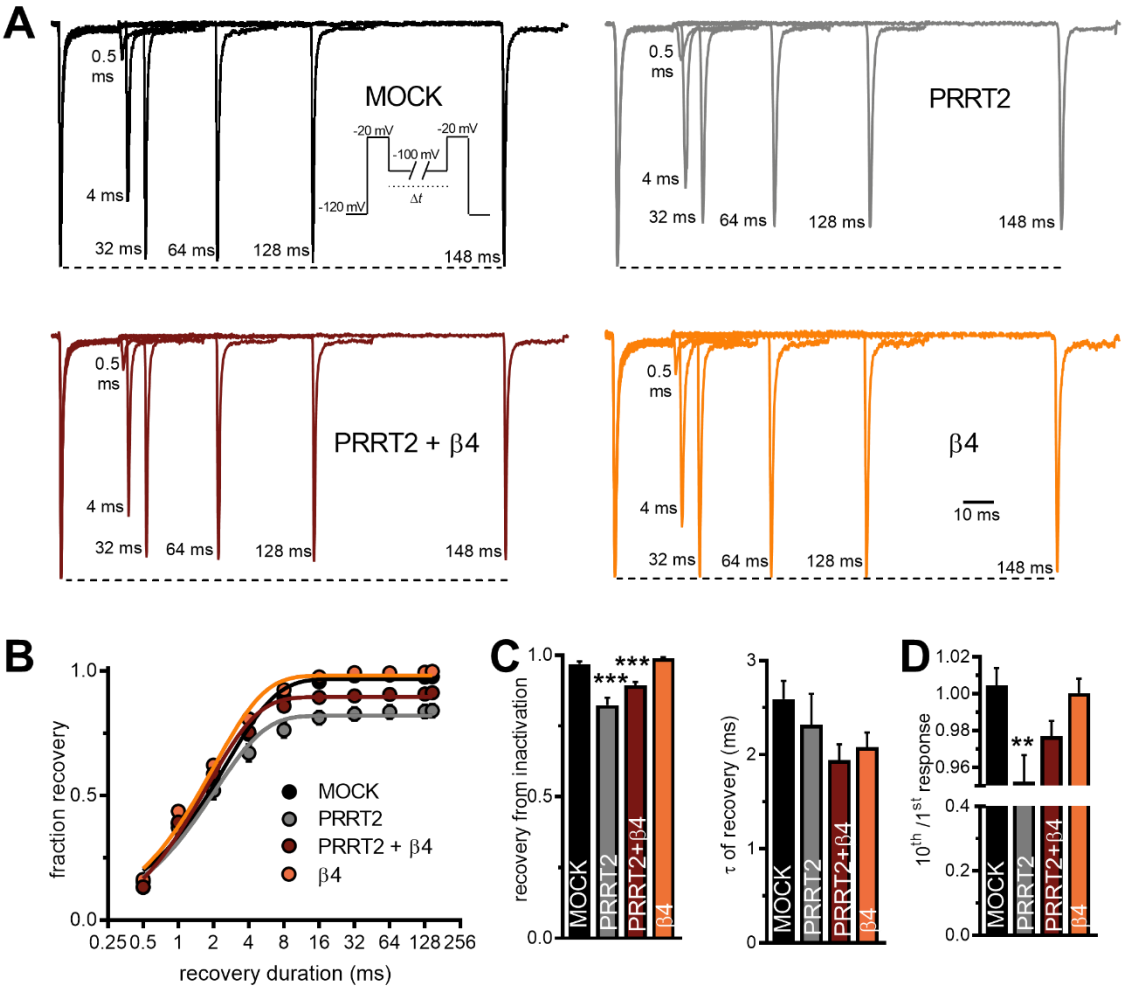


**Figure 12.** PRRT2, but not the β4-subunit, modulates the Nav1.2 recovery kinetic from fast inactivation. **(A**) Representative channel recovery from inactivation current traces recorded for all the experimental conditions. Recordings were obtained pre-pulsing cells to -20 mV for 20 ms to inactivate $Na^+$ currents and then coming back to a recovery potential of -100 mV for increasing durations before the repetition of test pulse to -20 mV. For clarity, 6 of the 9 time-intervals are shown. The dotted line represents the first pulse peak amplitude. (**B**) Time courses of the recovery from inactivation of peak currents at -100 mV for all conditions studied are plotted on a semi-logarithmic scale. (**C**) Mean (± sem) values of plateau and τ of recovery estimated from one-phase decay fit to the data. (**D**) Relationship between the $10^{th}$ and the $1^{st}$ test pulses evoked by the protocol displayed in A. All data are expressed as means ± sem (MOCK, n = 46; PRRT2, n = 25; PRRT2 + β4, n = 28; β4, n = 29). Two-way ANOVA revealed no significant differences between PRRT2 alone and PRRT2 + β4-subunit groups. **p < 0.01, ***p < 0.001 versus MOCK; Kruskal-Wallis/Dunn's tests.

## 4.4 PRRT2 and β4-subunit independently modulate the Nav1.2 persistent and resurgent currents

Next, we analyzed the effects of the combined expression of PRRT2 and β4-subunit on resurgent and persistent currents. In fact, increases in both these currents are associated with neuronal hyperexcitability and increase in firing rates [149] [150]. The persistent $Na^+$ current is a non-inactivating (or very slowly-inactivating) current, consequently, we measured it over the last 60 ms of the 600 ms incremental conditioning steps for each condition tested (Figure 13A, inset). This current can amplify subthreshold currents facilitating neuronal repetitive neuronal firing [146] [205]. Due to the variability of current density across cells, the persistent current amplitude was normalized to the peak amplitude of the transient current for each cell, and the percentage of persistent current was plotted versus the applied voltage. We found that the percent amplitude of the Nav1.2 persistent current was decreased by PRRT2 and increased by the β4-subunit, when compared to mock-transfected cells, when PRRT2 and β4-subunit were individually expressed. With both modulatory proteins co-expressed, the amount of persistent current was similar to that recorded in MOCK transfected cells (Figure 13B,C). These results closely resemble the behavior of the macroscopic transient $Na^+$ current (see Figure 10) and demonstrate that PRRT2 and β4-subunit modulate independently the Nav1.2 persistent current when expressed in the same channel complex and with a purely additive effect.

The resurgent $Na^+$ current is due to the influx of $Na^+$ ions through Nav channels during repolarization [206]. To elicit that, we applied an initial depolarizing step from -120 to 60 mV, followed by subsequent incremental repolarizing steps from -50 mV to 20 mV (Figure 14A, inset). Since the expression of the full length β4-subunit is not sufficient to produce resurgent currents in Nav1.2-expressing Hek293 cells, we included a β4 peptide (β4-ptd) derived from the C-terminal of the full-length β4-subunit in the pipette solution (see Experimental procedures). The inclusion of the peptide in the pipette solution is known to induce resurgent currents, although this is controversial because, despite the β4 peptide works, there are no evidence that *in vivo* resurgent current is actually produced by β4. [176][203] [207]. All voltage protocols used to study these currents were started at least 10 min after entering the whole-cell configuration to allow the β4-ptd dilution in the intracellular space.

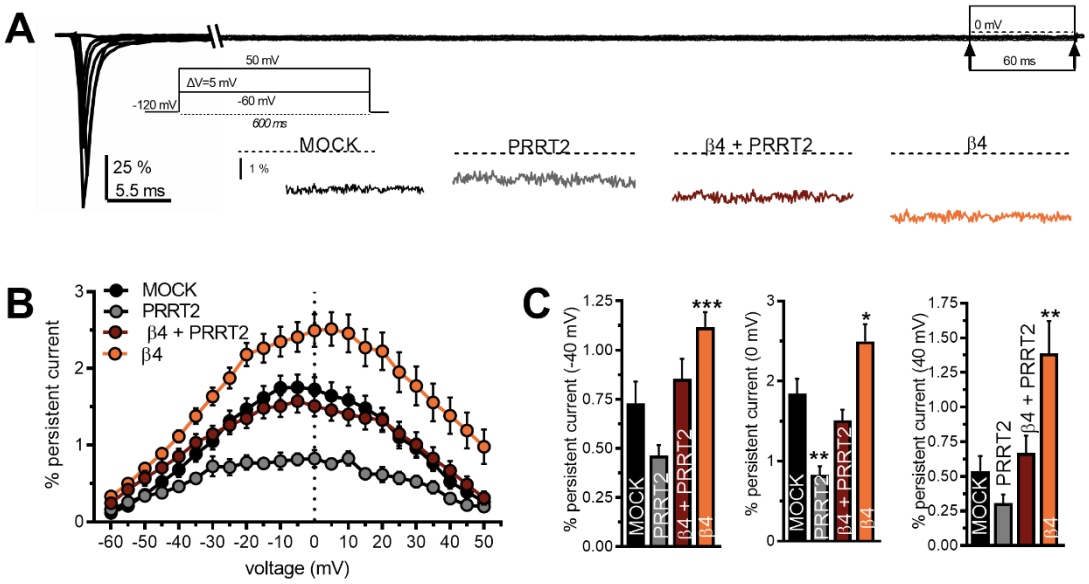


**Figure 13.** PRRT2 and β4-subunit independently modulate the Nav1.2 persistent current. (**A**) Representative MOCK persistent Nav1.2 currents evoked by depolarizing steps from -60 to 50 mV with 5-mV increments, lasting 600 ms (inset) in MOCK-transfected Nav1.2-expressing Hek293. For clarity, only currents evoked at -60, -40, -20, 0, 20, and 40 mV are reported. The highlighted box at the end of stimulation indicates the region of the trace in which the persistent current was measured. The insets show zoomed views of the maximal persistent current for all the conditions tested. (**B**) Persistent current, measured as the mean current in the last 60 ms of each 600 ms step and normalized to the transient current peak, is plotted versus voltage in each cell. (**C**) Bar plots of the mean (± sem) values of the normalized persistent current amplitude recorded at three distinct voltages (-40, 0, and 40 mV) for all tested conditions. Data are expressed as means ± sem (MOCK, n = 24; PRRT2, n = 10; PRRT2 + β4, n = 20; β4, n = 21). Two-way ANOVA revealed no significant interaction between PRRT2 and β4-subunit on the amplitude of the persistent $Na^+$ currents. *p < 0.05, **p < 0.01, ***p < 0.001, versus MOCK; one-way ANOVA/Bonferroni or Kruskal-Wallis/Dunn tests.

Then, we recorded $Na^+$ resurgent currents in Nav1.2-expressing Hek293 cells which had been transfected either with the empty vector or with PRRT2 cDNA in the absence or presence of the β4-peptide in the intracellular pipette recording solution (MOCK and MOCK + β4-ptd, respectively) (Figure 14A). Also in this case, to reduce the variability in current density across recorded cells, the resurgent current at each repolarizing voltage step was normalized to the peak amplitude of the transient current recorded in the same cell under the same experimental condition. As expected, the presence of β4-peptide greatly increased the resurgent current in a wide range of voltages, while PRRT2 was totally ineffective in modulating the resurgent current in MOCK-transfected cells in both presence and absence of the β4-peptide (Figure 14B,C). Hence, all these data it appears that the expression and

modulation of the Nav1.2 resurgent current depends exclusively on the presence of the β4-peptide and is independent of PRRT2.

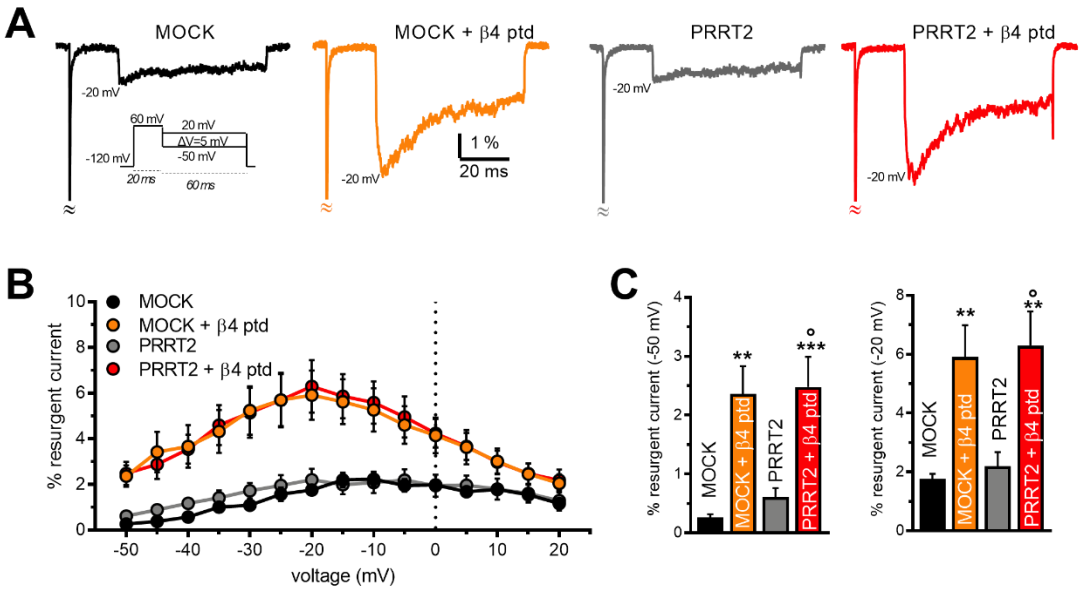


**Figure 14. PRRT2 and β4-subunit independently modulate the Nav1.2 resurgent current.** (**A**) Representative peak resurgent current traces generated by Nav1.2-expressing Hek293 cells either mock-transfected or transfected with PRRT2 recorded in the presence (yellow/red) or absence (black/gray) of the β4 C-terminal peptide (β4 ptd) in the intracellular recording solution. Currents were evoked with a family of steps depolarizations from -120 mV to 30 mV for 20 ms to open the channels, allow them to undergo open-channel block, and subsequently repolarize to a different potential ranging from -50 mV to 20 mV for 60 ms to allow the blocker to unbind. For clarity, only the peak resurgent current trace for all condition is plotted. (**B**) Resurgent currents evoked during repolarization were normalized to peak transient current at each voltage for all experimental conditions. The peak resurgent current was measured for each voltage after 2.5 ms into the repolarization step to bypass fast tail currents. (**C**) Bar plots of the mean (± sem) values of the normalized resurgent current amplitude recorded at three distinct voltages at -20 and -50 mV for all conditions tested. All data are expressed as means ± sem (MOCK, n = 6; MOCK + β4 ptd, n = 12; PRRT2, n = 6; PRRT2 + β4 ptd, n = 14). Two-way ANOVA revealed no significant interaction between PRRT2 and β4-subunit on the amplitude of the resurgent $Na^+$ currents. *p < 0.05, **p < 0.01, ***p < 0.001, versus MOCK; one-way ANOVA/Bonferroni or Kruskal-Wallis/Dunn tests.

## 4.5 PRRT2 deletion mutants are correctly expressed and targeted to the membrane

Given the specific interaction between PRRT2 and Nav1.2/1.6, but not with Nav1.1 channels, it was interesting to investigate which part of the full-length protein was responsible of this effect. Consequently, we generated two PRRT2 deletion mutants alternatively lacking the two regions of interest, the N- or C-terminal, and fused to a HA reporter sequence, namely: PRRT2ΔC-HA, a chimeric protein composed of the N-terminal cytoplasmic PRRT2 domain anchored to the membrane by the transmembrane domain of the structurally homologous protein Interferon Induced Transmembrane Protein 1 (IFITM1; [208]) and PRRT2ΔN-HA composed of the C-terminal transmembrane domain of PRRT2 including the short cytoplasmic loop (Figure 15A). Full-length PRRT2-HA or either deletion mutant was then transfected in stable Hek293 clones expressing Nav1.2. The PRRT2-linked HA immunoreactivity was found in association with Nav1.2 channels stained with pan-Nav antibodies and all mutants were correctly expressed at the membrane level (Figure 15B). Live staining of non-permeabilized Hek-Nav1.2 cells with anti-HA antibodies confirmed the membrane targeting of the PRRT2 variants, as deduced from the staining of the surface-exposed C-terminal HA (Figure 15C). In addition, HA-tagged PRRT2 variants were expressed to the same extent in Hek-Nav1.2 cells (Figure 16 A,B).

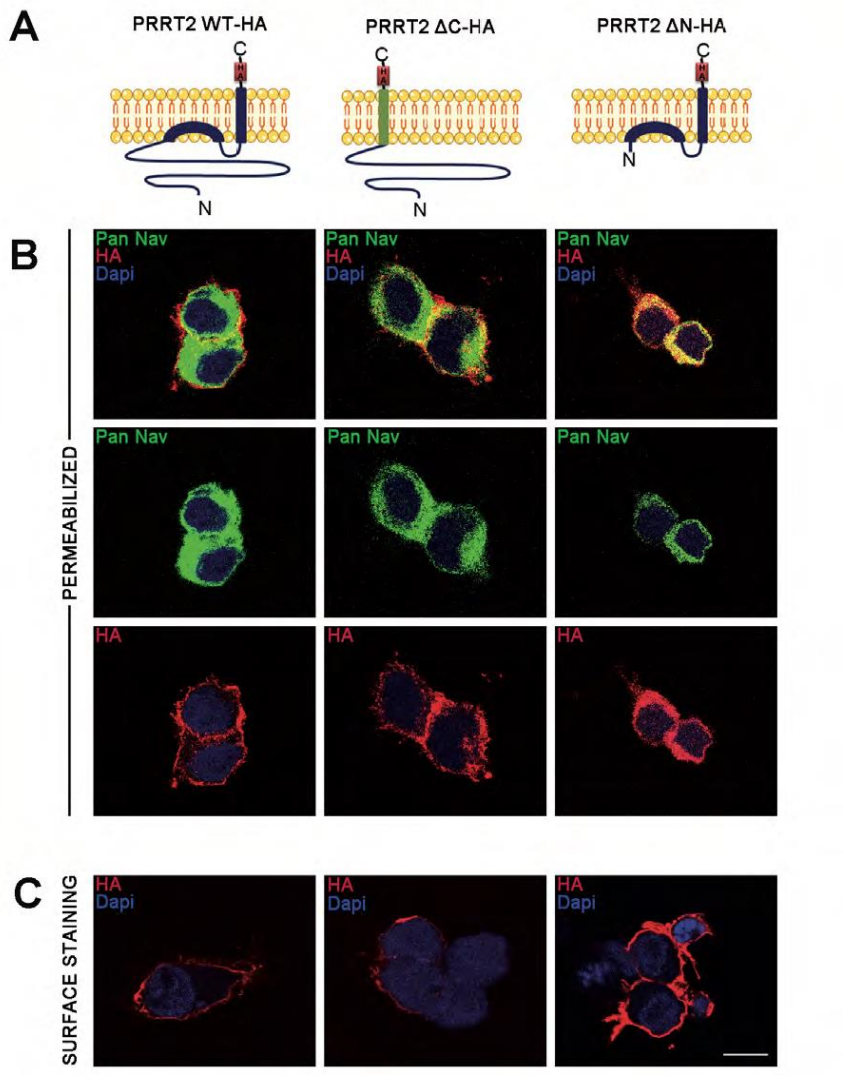


**Figure 15.** Generation and characterization of the PRRT2 deletion mutants. (**A**) Schematics of the PRRT2 domain constructs. PRRT2 WT-HA is the entire protein (violet). PRRT2 ΔC-HA is a chimeric protein composed of the cytoplasmic PRRT2 (violet) domain anchored to the membrane by the transmembrane domain of IFITM1 (green). PRRT2 ΔN-HA is composed of the transmembrane domain of PRRT2. (**B**) Hek- Nav1.2 cells transfected with (from left to right) PRRT2-HA, PRRT2ΔC-HA and PRRT2ΔN-HA were permeabilized and subsequently labeled for anti-HA and pan-Nav antibodies, respectively, with nuclei marked with DAPI. The individual HA and pan-Nav staining are shown together with the respective merge images (top row). (**C**) Hek-Nav cells transfected with PRRT2-HA, PRRT2ΔC-HA and PRRT2ΔN-HA were surface-labeled with anti-HA to stain the membrane-exposed domains of the proteins. Scale bar, 10 µm.

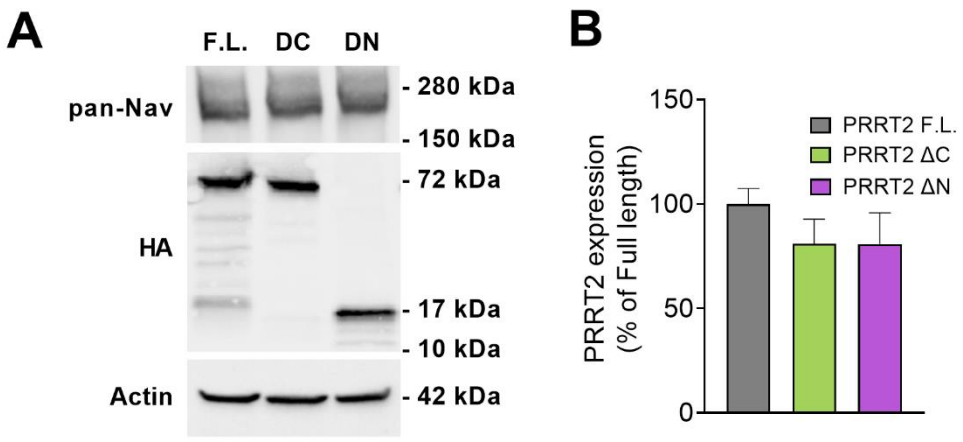


**Figure 16.** Expression of full length PRRT2 and its deletion mutants in Hek293-Nav1.2 cells. (**A**) HA-tagged full-length PRRT2 (PRRT2-FL) or its deletion mutants PRRT2ΔN and PRRT2ΔC were transfected in Hek293 cells stably expressing Nav1.2 channels. Cell lysates (10 µg protein) were analyzed by western blotting with pan-NaV and HA antibodies. Actin immunoreactivity was used as a control of equal loading. The representative blots were cut from the same gel. Molecular mass standards are reported on the right. (**B**) Quantification of HA immunoreactivity. Box plots of n = 4 independent experiments.

## 4.6 Both the N- and C-terminal regions of PRRT2 bind Nav1.2 channels

Previous data reported that PRRT2 is an atypical dispanin, presenting a long and unstructured intracellular N-terminus region, a first membrane domain that folds at a proline residue (TM1), a short cytosolic loop, a full membrane spanning domain (TM2) and minimal extracellular C-terminus (Figure 17A; [19] [209]. We refined the 3D structure of C-terminus PRRT2 by extending two distinct simulations to 1 µs, using 2 fs time steps and 4 fs time steps with HMR, respectively. This validation supports the previously proposed structural model of PRRT2 based on much shorter simulation times (50 ns; [19]). Indeed, the $\alpha$-carbon RMSD evolution for both replicas of PRRT2 showed high stability over time (Figure 17B), and the evolution of the cross distances between S272, A294 and A313 belonging to the three distinct membrane stretches for the two PRRT2 trajectories (Figure 17C,D) remained notably stable over time. We next compared our MD Robetta model with the PRRT2 structure predicted by the AlphaFold2 algorithm, using PyMOL and found a full superposition of the two structures (Figure 17E), confirming the reliability and stability of the structure of the PRRT2 membrane domain.

Next, to ascertain which region of PRRT2 directly interacts with the Nav1.2 α-subunit and the basis for its specificity, we performed affinity binding assays by challenging HA-PRRT2 variants purified from naïve Hek293 cells with extracts of Hek293 clones stably expressing either Nav1.2 or Nav1.1 α-subunits in the absence of β-subunits. After incubation, HA-tagged PRRT2 variants were pulled down with anti-HA beads and the associated Nav channels identified by western blotting with anti-pan-Nav antibodies (Figure 18A). As previously described [132], we found that full-length PRRT2 efficiently pulled down Nav1.2, but not Nav1.1, α-subunits. The Nav1.2 binding activity was retained when either PRRT2ΔN (C-terminal PRRT2) or PRRT2ΔC (N-terminal PRRT2) were assayed, but to a different extent. In fact, while C-terminal PRRT2 bound Nav1.2 to the same extent of full length PRRT2, N-terminal PRRT2 exhibited only about 50% of full-length PRRT2 binding. However, the binding specificity for Nav1.2 α-subunits was strictly preserved by both deletion mutants, while the binding to Nav1.1 α-subunit was negligible (Figure 18B).

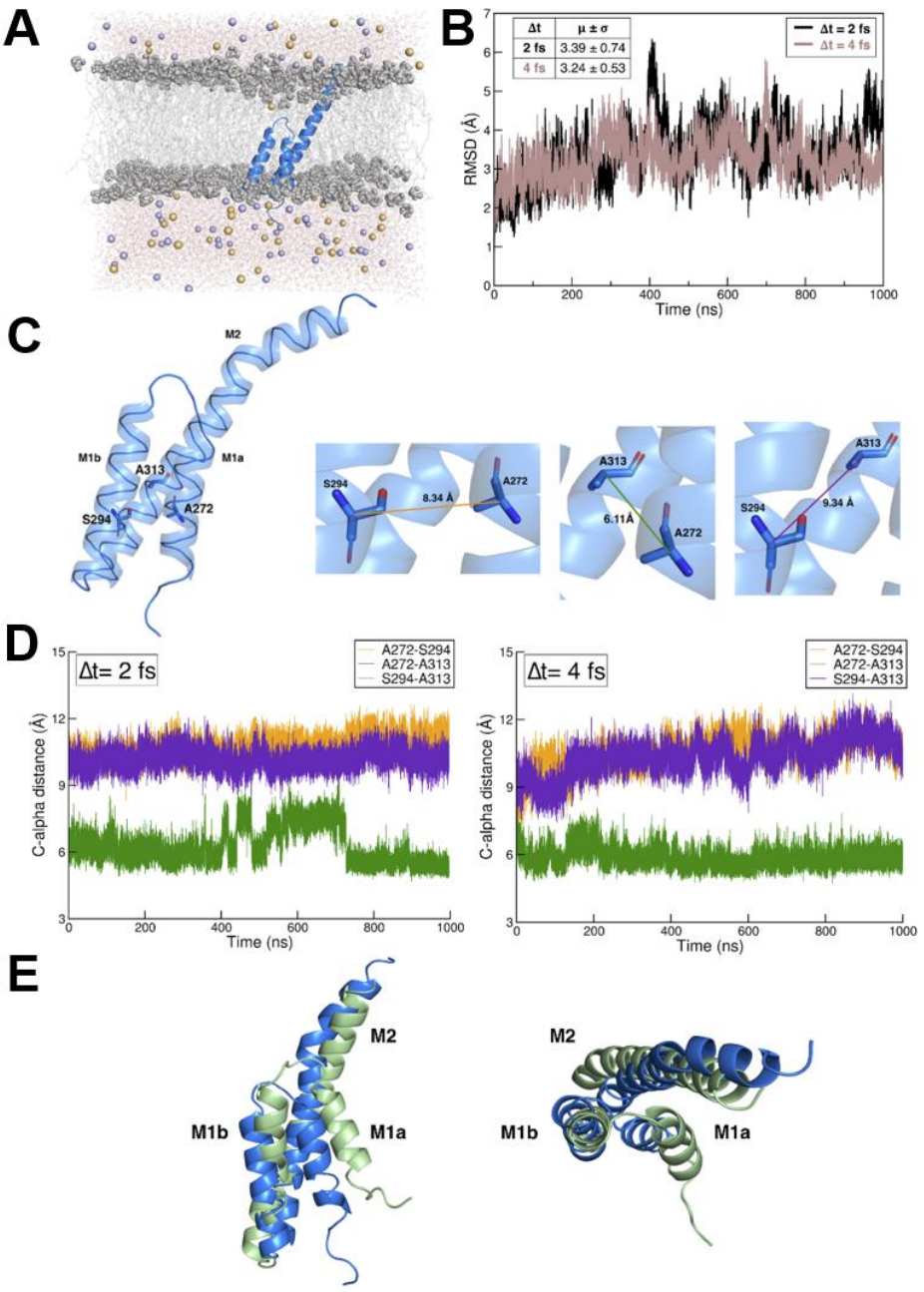


**Figure 17.** Molecular modelling of PRRT2 transmembrane segment. (**A**) Snapshot of PRRT2 molecular dynamics simulation. The protein was embedded into a 1-palmitoyl-2-oleoyl-sn-glycero-3-phosphocholine (POPC) lipid bilayer; spheres represent phospholipids heads. (**B**) Alpha-carbon RMSD evolution for both replicas of PRRT2. (**C**) Cartoon representation of PRRT2 transmembrane portion; residues involved in cross distances analysis are represented in sticks. (**D**) Cross distances evolution for PRRT2 trajectories. (**E**) Lateral and extracellular views of Robetta PRRT2 model (teal) and AlphaFold2 PRRT2 model (marine) superimposition via PyMOL.

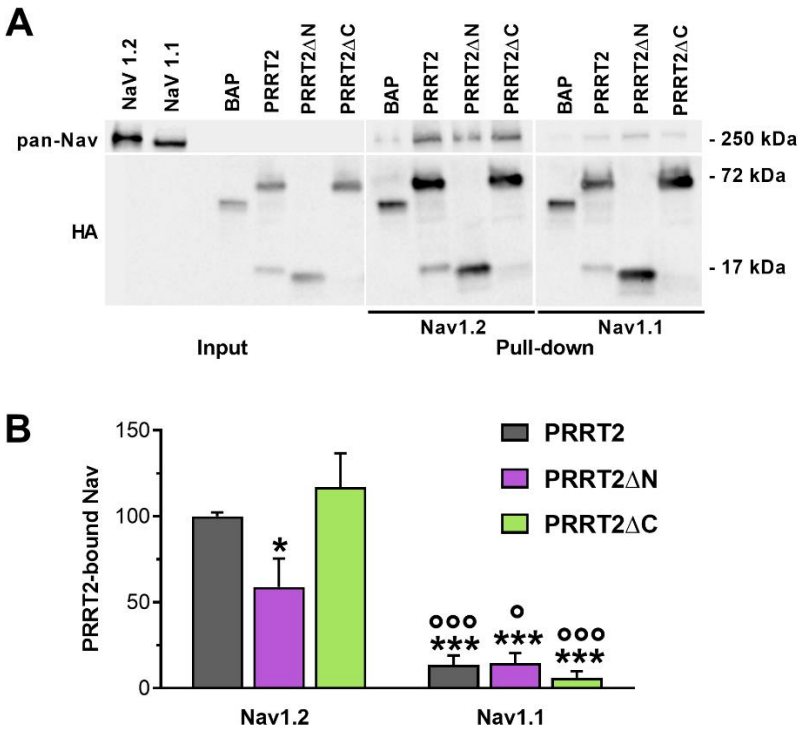


**Figure 18**. Binding of PRRT2 deletion mutants to Nav1.2 and Nav1.1 channels. (**A**) Representative immunoblot of co-immunoprecipitation of PRRT2 variants. HA-tagged full-length PRRT2 (PRRT2) or its deletion mutants PRRT2ΔN and PRRT2ΔC were expressed in Hek293 cells stably expressing either Nav1.2 or Nav1.1 α-subunits. Cells lysates (INPUT, 10 µg protein) and samples immunoprecipitated by anti-HA beads were analyzed by western blotting with anti-pan Nav and anti-HA antibodies. Molecular mass standards are reported on the right The representative blots were cut from the same gel. (**B**) Quantification of the FLAG immunoreactive signal in PRRT2-HA immunoprecipitates. Means ± sem of n = 6 independent experiments. *p<0.05, ***p<0.001 vs full-length PRRT2; °p<0.05, °°°p<0.001 Nav1.1 vs Nav1.2 for each PRRT2 variant. Two-way ANOVA/Fisher's tests.

## 4.7 The PRRT2 C-, but not N-terminal region, modulates specifically Nav1.2 biophysics

We then looked at the PRRT2 deletion mutants' ability to reproduce the effects of full-length PRRT2 in modulating the transient Na+ current in Nav1.2-expressing Hek293 cells using whole-cell patch-clamp in voltage-clamp configuration (Figure 19A). As previously demonstrated [132], full length PRRT2 significantly decreased the $Na^+$ current density compared to MOCK-transfected cells. Interestingly, the effects of PRRT2ΔN (C-terminal PRRT2) were indistinguishable from those of full length PRRT2, while PRRT2ΔC (N-terminal PRRT2) was substantially ineffective (Figure 19B). The modulation of the Na+ current density by full length PRRT2 and C-terminal PRRT2 were highly significant in the -20 to 0 mV range (Figure 19C) while no significant voltage shift of the current density/voltage (J/V) curves was observed (Figure 19B).

As previously reported, the expression of PRRT2 also negatively modulated intrinsic excitability by affecting the inactivation and recovery from inactivation of Nav1.2/1.6 channels [132]. To study in detail this structural modulation operated by PRRT2, we investigated the functional activity of its N- and C-terminal regions by challenging its deletion mutants with Hek293 cells stably expressing Nav1.2. The $V_{0.5}$ and the slope of the activation curve of the Nav1.2 $\alpha$-subunit was not significantly affected by either the expression of full length PRRT2 or both deletion mutants compared to MOCK transfected cells in terms of slope and voltage of half-activation (Figure 20A). Conversely, full length PRRT2 induced a significant left-shift of the curve of steady-state inactivation of Nav1.2 causing a significant decrease of the voltage of half-inactivation towards more negative values compared to MOCK-transfected cells (Figure 20B). The expression of the PRRT2ΔN mutant (C-terminal PRRT2) was able to reproduce the same effect, while the expression of the PRRT2ΔC mutant (N-terminal PRRT2) was ineffective (Figure 20B). Similar effects were observed on the Nav1.2 recovery from inactivation (Figure 21A). In addition, the C-terminal region of PRRT2 recapitulated the decrease in the plateau of recovery induced by full length PRRT2, while the cytosolic $NH_2$-terminal region of PRRT2 was inactive (Figure 21B).

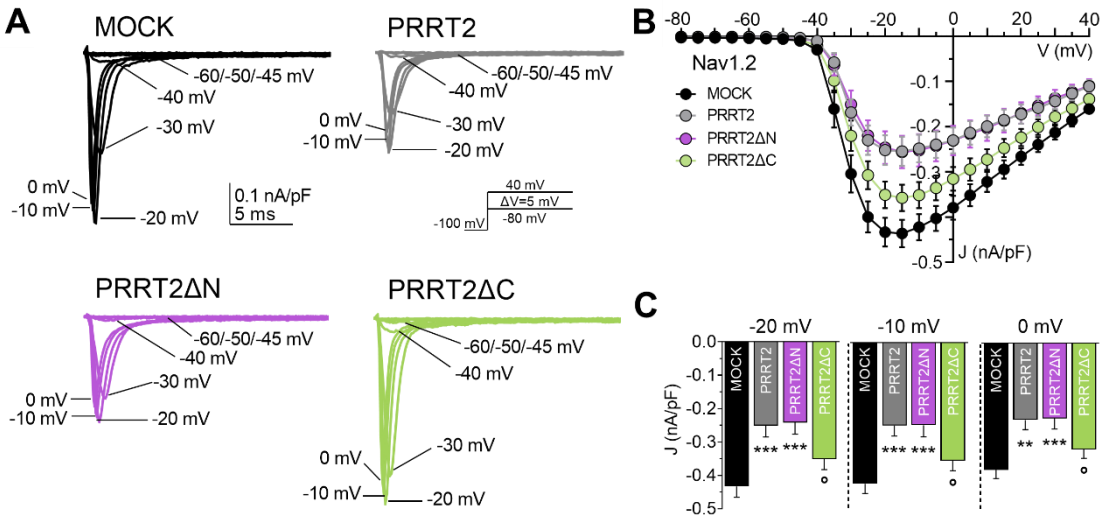


**Figure 19.** Effects of PRRT2 deletion mutants on the transient Nav1.2 current. (**A**) Representative whole-cell transient $Na^+$ currents recorded in Hek293 cells stably expressing Nav1.2 $\alpha$-subunits and transiently transfected with empty vector (MOCK, black), full-length PRRT2 (grey), PRRT2ΔN (violet) and PRRT2ΔC (green). Currents were elicited by a protocol (*inset*) consisting of 5-mV depolarization steps from -80 to 40 mV from a holding potential of -100 mV. For clarity, the first 20 ms of the 100-ms steps for eight representative traces per condition are plotted. (**B**) Current density (J) *versus* voltage (V) relationship for the four experimental conditions. (**C**) The statistical analysis of J values at three representative voltages (-20/-10/0 mV) is reported. Data are expressed as means ± sem (MOCK, n = 24; full-length PRRT2, n =15; PRRT2ΔN, n = 19; PRRT2ΔC, n = 21). ***p<0.001 *vs* MOCK; °p<0.05 vs full-length PRRT2. One-way ANOVA/uncorrected Fisher's LSD test.

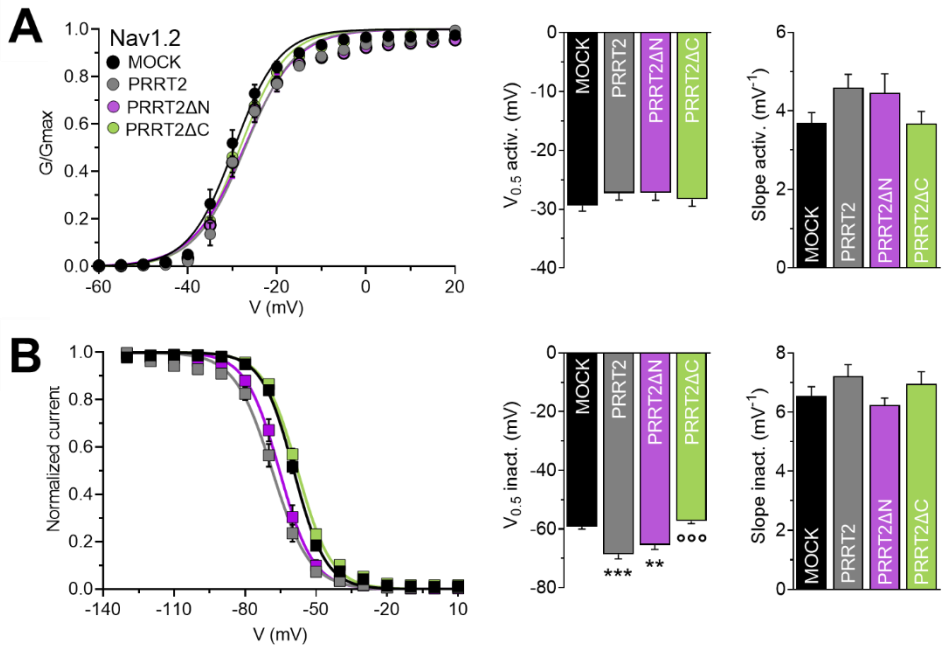


**Figure 20.** Effects of PRRT2 deletion mutants on the biophysical properties of Nav1.2 channels. Hek293 cells stably expressing Nav1.2 $\alpha$-subunits were transiently transfected with empty vector (MOCK, black), full-length PRRT2 (grey), PRRT2ΔN (violet) and PRRT2ΔC (green). (**A**) Left: Voltage-dependence of activation. The lines are the best-fitted Boltzmann curves. Right: Means (± sem) values of the half-maximal voltage of activation ($V_{0.5}$) and slope (MOCK, n = 24; full-length PRRT2, n = 15; PRRT2ΔN, n = 19; PRRT2ΔC, n = 21). (**B**) Left: Steady-state inactivation curves. The lines are the best-fitted Boltzmann curves. Right: Means (± sem) values of the half-maximal voltages for inactivation ($V_{0.5\ inact.}$) and slopes (MOCK, n = 20; full-length PRRT2, n = 18; PRRT2ΔN, n = 15; PRRT2ΔC, n = 21). **p<0.01, ***p<0.001 vs MOCK; °°°p<0.001 vs full-length PRRT2. One-way ANOVA/ Dunnett's test.

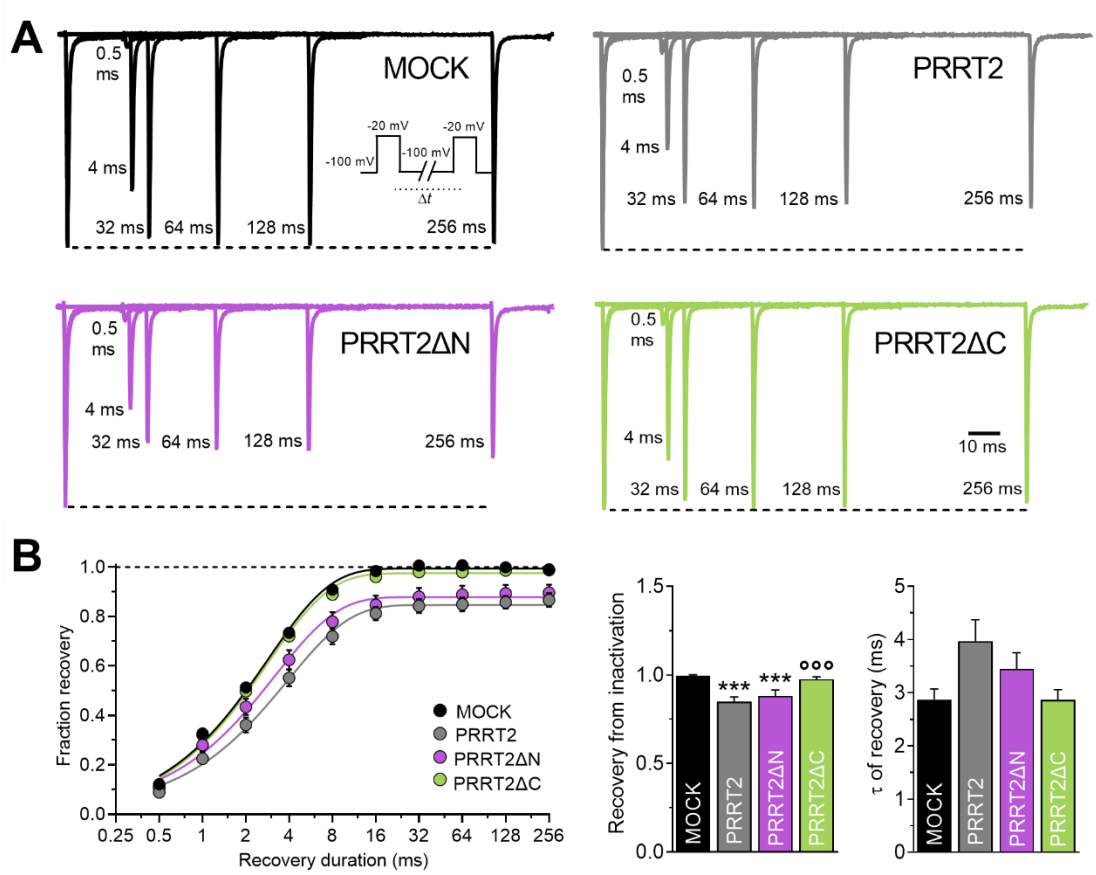


**Figure 21**. Effects of PRRT2 deletion mutants on the recovery from inactivation of Nav1.2 channels. Hek293 cells stably expressing Nav1.2 α-subunits were transiently transfected with empty vector (MOCK, black), full-length PRRT2 (grey), PRRT2ΔN (violet) and PRRT2ΔC (green). (**A**) Representative traces showing current recovery from inactivation for all the experimental conditions. Recordings were obtained pre-pulsing cells to -20 mV for 20 ms to inactivate $Na^+$ currents and then coming back to a recovery potential of -100 mV for increasing durations before the repetition of test pulse to -20 mV. For clarity, 6 of the 9 time-intervals are shown. (**B**) *Left:* The time courses of the recovery from inactivation of peak currents at -20 mV are plotted on a semi-logarithmic scale for the four experimental conditions. *Right:* of τ and plateau of recovery estimated from one-phase decay fit to the data (MOCK, n = 24; full-length PRRT2, n =16; PRRT2ΔN, n = 18; PRRT2ΔC, n = 21). ***p<0.001 *vs* MOCK; °°°p<0.001 *vs* full-length PRRT2. Kuskal-Wallis/Dunn's tests.

Additional electrophysiological experiments were conducted to investigate whether the functional specificity of full length PRRT2 for Nav subtypes was preserved in its deletion mutants, as suggested by co-immunoprecipitation experiments. Patch-clamp recording show that both full length PRRT2 and its PRRT2ΔN and PRRT2ΔC mutants did not significantly affect the density of the transient $Na^+$ currents or its voltage dependence with

respect to MOCK-transfected Nav1.1-expressing Hek293 cells (Figure 22A). Also the constructs under study were totally ineffective in altering the activation (Figure 22B,C), steady-state inactivation (Figure 22D,E) and recovery from inactivation (Figure 22F) curves of Nav1.1 channels. All these data confirmed the specific modulatory effects of PRRT2, as well as of its domains, on Nav1.2 channels.

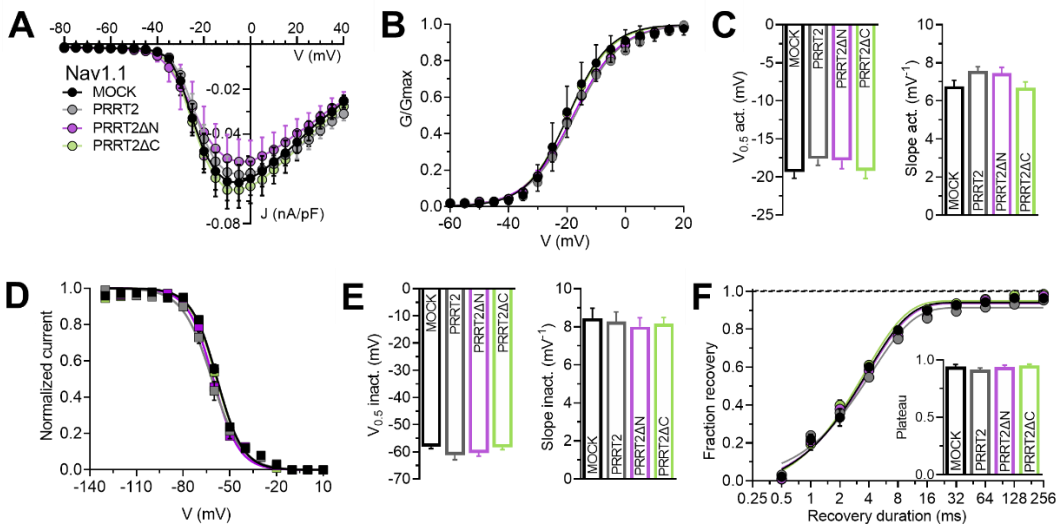


**Figure 22.** PRRT2 deletion mutants are ineffective on the transient current and biophysical properties of Nav1.1 channels. Hek293 cells stably expressing Nav1.1 α-subunits were transiently transfected with empty vector (MOCK, black), full-length PRRT2 (grey), PRRT2ΔN (violet) and PRRT2ΔC (green). (**A**) Current density (J) versus voltage (V) relationship for the four experimental conditions, (**B**) Voltage-dependence of activation. The lines are the best-fitted Boltzmann curves (**C**) Means (± sem) values of the half-maximal voltage of activation ($V_{0.5}$) and slope (MOCK, n = 21; full-length PRRT2, n = 20; PRRT2ΔN, n = 18; PRRT2ΔC, n = 23). (**D**) Steady-state inactivation curves. The lines are the best-fitted Boltzmann curves. (**E**) Means (± sem) values of the half-maximal voltages for inactivation ($V_{0.5}$ inact.) and slopes (MOCK, n = 18; full-length PRRT2, n = 18; PRRT2ΔN, n = 16; PRRT2ΔC, n = 18). (**F**) Time courses of the recovery from inactivation of peak currents at -100 mV for the four experimental conditions studied plotted on a semi-logarithmic scale. Inset: Mean (± sem) values of the plateau of recovery estimated from one-phase decay fit to the data. Data are expressed as means ± sem (MOCK, n = 19; full-length PRRT2, n = 18; PRRT2ΔN, n = 17; PRRT2ΔC, n = 18). One-way ANOVA/Dunnett's tests.

## 4.8 PRRT2 pathogenetic mutants have a normal expression but distinct properties

As previously described, the majority of the PRRT2 pathogenic mutations cause loss of protein expression, making it difficult the in vitro studies. We focused on a restricted number of C-terminal missense pathogenic mutations (Figure 23) and studied their impact on the modulation of PRRT2/Nav1.2 interaction to elucidate possible pathogenic mechanisms. To this aim, we chose 4 mutants that were already reported to be expressed in heterologous systems (R266W, R308C, R311W, I327M), plus 4 further point mutations (I270N, V286M, V319L, A320V) that were not previously investigated.

For this reason, to identify the possible site of the interaction between PRRT2 and Nav1.2, we focused on a restricted number of missense pathogenic mutations that maintain the expression and the protein targeting to the cell membrane, although in some cases with variable levels compared to the control (PRRT2 WT). The expression of mutated PRRT2 isoforms was assessed using the same heterologous system used in the previous experiments. To this purpose, Hek293 cells were transfected with mutated constructs and compared to PRRT2 WT full length protein as a positive control. Western blotting was used to assess the expression of the various PRRT2 mutant isoforms tested. PRRT2-HA isoforms were identified by a primary antibody against the HA tag (encoded at the C-terminal of PRRT2) and actin or GAPDH was used as loading normalizer. No significant differences were found between the expression levels of the eight mutants tested when compared to PRRT2 WT (Figure 24A). Missense mutations are often causative of PRRT2 mislocalization and altered trafficking to the plasma membrane. We then investigated the membrane expression of the mutants. Taking advantage of the HA epitopes fused at the C-terminal of PRRT2, the membrane expression was studied using immunofluorescence on live cells (Live Labeling; see experimental procedures). Using confocal microscopy transfected cells were imaged (Figure 24B, left), and the surface fluorescent signals were normalized to the respective transfection efficiency. Interestingly, all variants preserved a correct targeting to the membrane similar to WT-PRRT2 (Figure 24B, right). We conclude that missense mutations analyzed do not affect protein expression and membrane localization and thereby can be subjected to the functional study of the interactions with Nav channels.

Pull-down experiments were performed to investigate whether the pathogenic mutants directly bind the Nav1.2 channel. An additional construct, encoding for the unrelated protein bacterial alkaline phosphatase (BAP) also tagged with HA epitope was used as a negative control. HA-tagged PRRT2 variants were pulled down and the bound Nav1.2 channels detected by western blotting with anti-panNav antibodies (Figure 25A). Interestingly, two PRRT2 mutants, A320V and V286M, showed a significant alteration in the binding of Nav1.2 (Figure 25B). In particular, the mutant V286M pulled down a higher amount of Nav1.2, suggesting an increased binding affinity compared to the PRRT2 WT, while the isoform A320V immunoprecipitated a smaller amount of the channel. Altered binding between Nav1.2 and PRRT2 mutants may cause channel dysregulation and contribute to the onset of PRRT2-related pathologies.

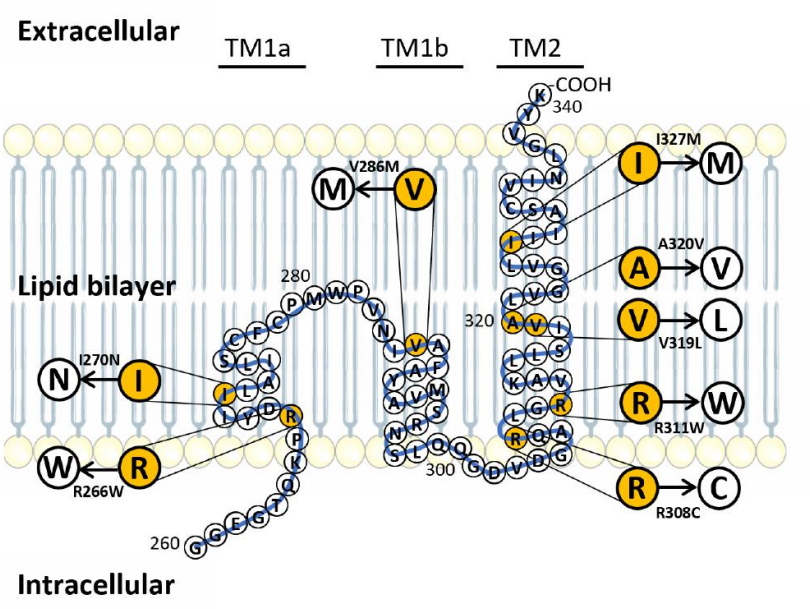


**Figure 23**. Schematic 2D view of the PRRT2 membrane domain. The eight PRRT2 missense pathogenic mutations investigated in this study are highlighted.

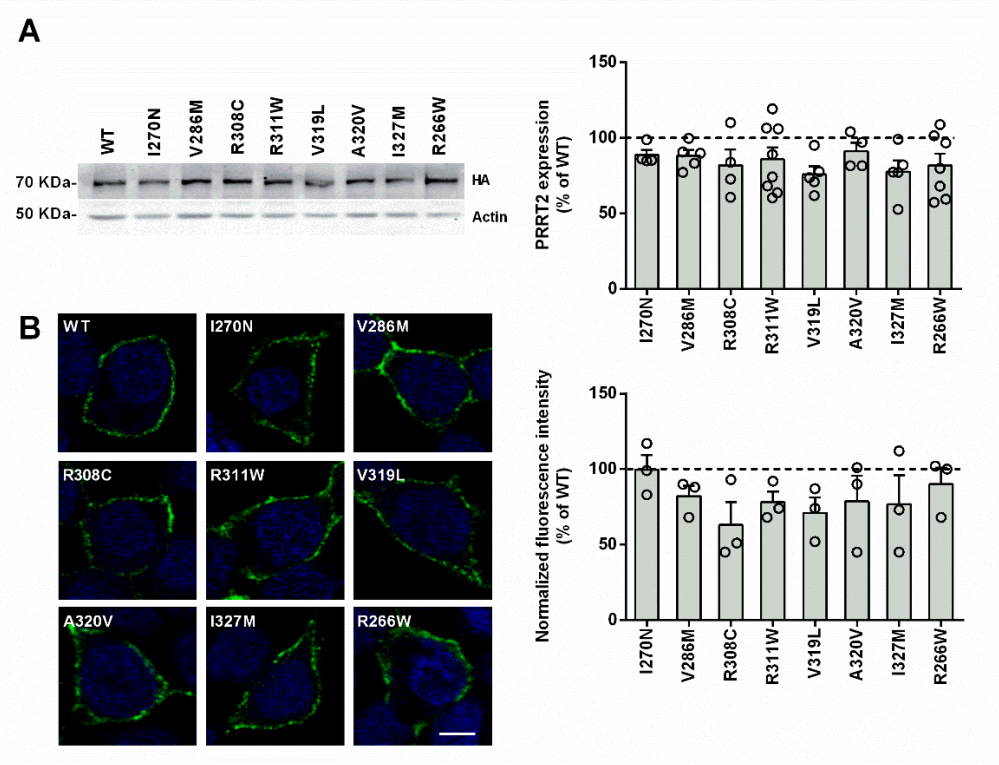


**Figure 24**. Expression levels and membrane targeting of missense PRRT2 mutants (**A**) *Left:* Representative immunoblots. *Right:* Densitometric analysis of the immunoreactive bands. Actin was used as loading control. The expression levels of PRRT2 mutants are shown in percent of the immunoreactivity of WT-PRRT2 as means ± sem of n = 4-8 independent experiments (horizontal line; mean ± sem: 100 ± 0.49). One-way ANOVA/Sidak tests. (**B**) *Left:* Representative confocal images show the PRRT2-HA localization at the membrane level (63x-confocal microscope acquisitions, scale bar 5 µm). Hek293 cells were transfected with either WT or mutant PRRT2-HA variants and live surface-immunolabelled with anti-HA antibodies (green). DAPI staining (blue) was used to visualize nuclei. Scale bar, 5 µm. Right: Quantification of HA fluorescence intensity. Fluorescence intensity was calculated as the ratio between the total anti-HA fluorescence signal and the transfection efficiency in the same field and expressed in percent of WT-PRRT2 (horizontal line). Data represent means ± sem with superimposed individual values from n = 3 independent experiments. One-way ANOVA/Holm-Šídák tests.

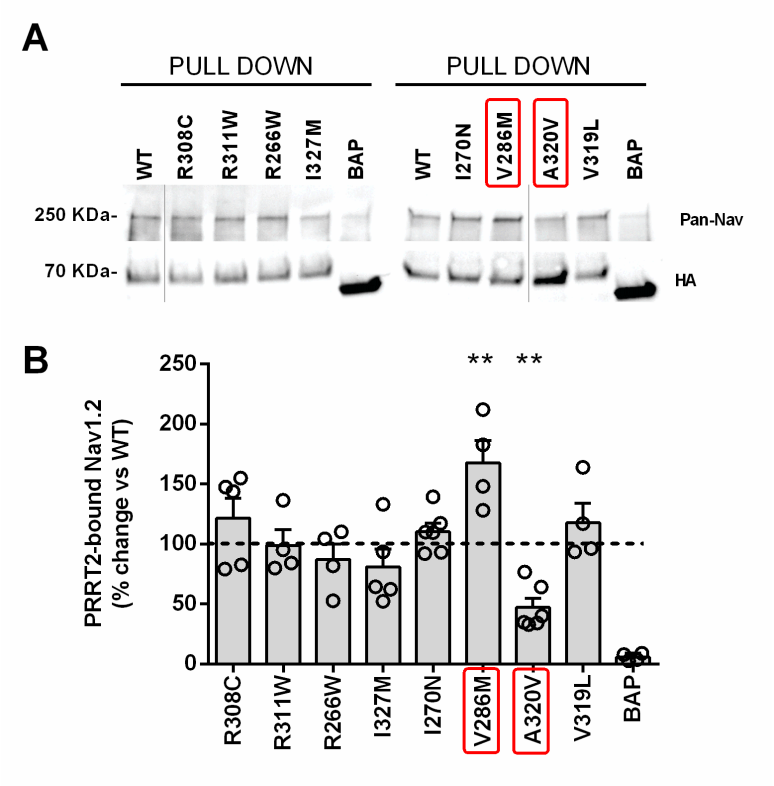


**Figure 25**. The V286M and A320V mutations have opposite effects on the interaction between PRRT2 and Nav1.2 (**A**) Representative immunoblots of co-immunoprecipitation of Nav1.2 by PRRT2; BAP is the negative control. (**B**) Quantification of the PanNav signal in PRRT2 immunoprecipitates. Data are expressed in percent of WT as means ± sem of n = 3 independent experiments. Statistics: one-way ANOVA/Sidak tests (* P<0.05, ** P<0.01, *** P<0.001). Immunoblots were analyzed by densitometry of the fluorograms obtained in the linear range of the emulsion response.

As previous reported, PRRT2 binding reduces the Nav1.2/Nav1.6 plasma membrane expression [132]. Consequently, we investigated whether PRRT2 mutations alter Nav1.2 membrane targeting. To this aim, we performed biotinylation experiments in Hek-Nav1.2 cells transfected with either WT-PRRT2 or its variants and measured the amount of Nav1.2 expressed in the membrane biotinylated protein fraction. In addition to the A320V and V286M, two additional mutants characterized by unchanged Nav1.2 binding (I270N and V319L) were tested as controls in addition to WT-PRRT2. Biotinylation experiments showed that the A320V increases the membrane expression levels of Nav1.2 compared to PRRT2 WT, suggesting that this mutant is not able to negatively regulate Nav1.2 membrane exposure (Figure 26). A trend for an increase of the membrane expression levels of Nav1.2

was also observed with the V286M mutant, but not reaching statistical significance. No differences in Nav channels exposure were found for the I270N and V319L variants.

The A320V and V286M mutations were investigated in detail by whole cell patch-clamp experiments (Figure 27A). Recordings of transient Na+ currents evoked in Hek293-Nav1.2 transiently transfected with both mutants and compared to cells transfected with either empty vectors (MOCK) or PRRT2 WT showed that consistently with the biotinylation studies, the A320V mutant was significantly less effective than WT-PRRT2 in downregulating transient macroscopic Na+ currents, and not significantly different from MOCK-transfected cells. Conversely, the V286M mutant was still able to significantly decrease Na+ conductance with respect to MOCK-transfected cells, and its effect was not significantly different from WT-PRRT2 (Figure 27B,C). The activation dynamics of Nav1.2 was unaffected by PRRT2 WT, as well as by both mutants (Figure 28A,B). The study of the Nav1.2 inactivation kinetics confirmed the significant left-shift of the steady-state inactivation curve by PRRT2 WT with respect to MOCK-transfected cells. Interestingly, the V286M mutant showed an increased magnitude of the effect with respect to PRRT2 WT (gain of function, GOF), while the effect of the A320V mutant was not significant (LOF) (Figure 28C,D, Table 3).

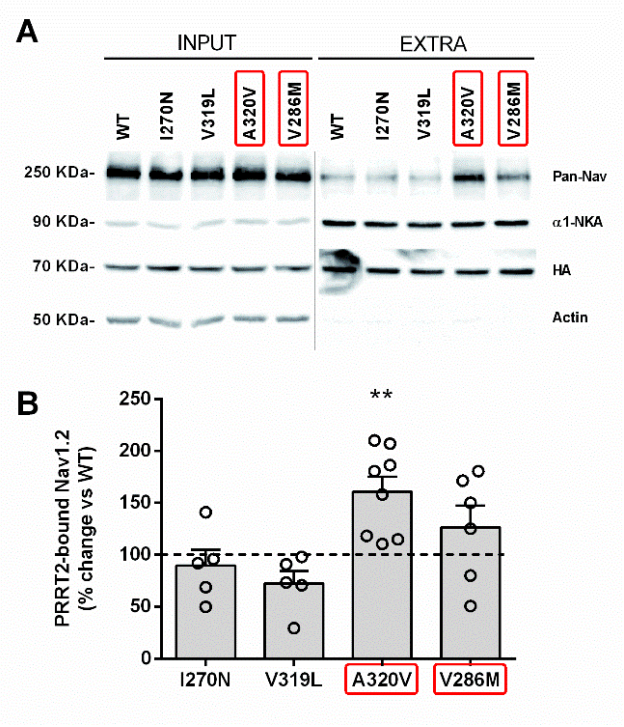


**Figure 26.** Effect of PRRT2 mutants on Nav1.2 channel membrane localization. (**A**) Naïve Hek293 cells were transfected with HA-tagged WT-PRRT2, mutant PRRT2 variants or the control unrelated protein BAP, extracted and immunoprecipitated using anti-HA beads. HA-bound proteins were subsequently incubated with lysates of Nav1.2-expressing Hek293 stable cell clones. HA-pulled-down samples were analyzed by western blotting using anti-panNav antibodies. Representative immunoblots are shown. (**B**) Quantification of the panNav immunoreactivity in PRRT2 immunoprecipitates. Immunoblots were analyzed by densitometry of the fluorograms. The intensity of Nav1.2 immunoreactivity was normalized to the PRRT2 recovery within the same sample. The binding of PRRT2 mutants to Nav1.2 is expressed in percent of WT-PRRT2 (horizontal line; mean ± sem: 100 ± 8.27). Data represent means ± sem with superimposed individual values from n = 4-6 independent experiments. **p<0.01, one-way ANOVA/Holm-Šídák tests.

As already mentioned, in the presence of PRRT2 WT, the recovery from inactivation of the $Na^+$ current is slower and decreased in magnitude, confirming the PRRT2 negative modulation on Nav1.2 described by Fruscione et al. (2018)[132]. Interestingly, this modulation is lost with the A320V mutant, confirming its LOF. This result also suggests a key role for this PRRT2 residue in the modulation of the biophysical properties of the Nav1.2 channel (Figure 29A,B, Table3). The V286M mutant confirmed the GOF observed on the inactivation kinetics by showing an enhanced inhibition of Nav1.2 recovery from inactivation with respect to PRRT2 WT (Figure 29C,D).

Since PRRT2 anticipates the entry of Nav1.2 channels into the inactivated state and reduces their recovery from inactivation, it is likely that, during high-frequency stimulation, an increase of Nav1.2 in the inactivated state would occur. To determine the effects of PRRT2 and its patogenic mutants in accumulating inactivated channels, a series of depolarizing pulses from a holding potential of -120 mV to +10 mV at a frequency of 20 Hz were applied (Figure 29C) [210]. In Hek-Nav1.2 cells expressing WT-PRRT2, stimulation at 20 Hz induced a progressive and significant reduction of Na+ current amplitude with respect to MOCK-transfected cells, consistent with an increased proportion of inactivated Nav1.2 channels (Figure 29D). In this context, the V286M mutant accelerated the depression in current amplitude with respect to PRRT2 WT (GOF), while the A320V mutant induced a significantly slower and reduced depression of the current, confirming its LOF phenotype (Figure 29D,E). For a recapitulatory overview of biochemical and electrophysiolgical results see table 3.

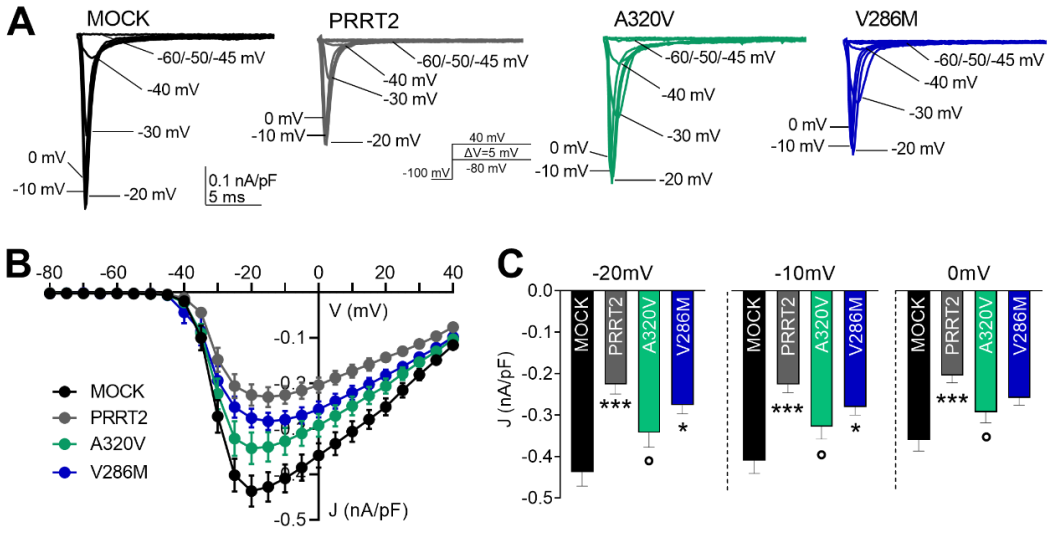


**Figure 27.** (**A**) Representative whole-cell transient $Na^+$ currents recorded from Hek293-Nav1.2 transiently transfected with MOCK (black), PRRT2 WT (grey), PRRT2 A320V (green) or PRRT2 V286M (blue) constructs. Currents were elicited by 5mV steps depolarization from -80 mV to 40 mV and cells were held at -100mV (inset). For clarity, the first 20 ms of the 100-ms steps for eight representative traces per condition are plotted. (**B**) Current density to voltage relationship for conditions as in A. (**C**) The statistical analysis of J values at three representative voltages (-20/-10/0 mV) is reported. (MOCK, n = 11; PRRT2, n = 11; A320V n = 13; V286M n = 15). Data are shown as means ± SEM. (MOCK, n = 21; PRRT2, n = 20; A320V n = 19; V286M n = 18). *p<0.05, **p<0.01, ***p<0.001 vs MOCK; °p<0.05, °°p<0.01, °°°p<0.001 vs WT-PRRT2; One-way ANOVA/Bonferroni's tests or Kruskal-Wallis/Dunn's tests.

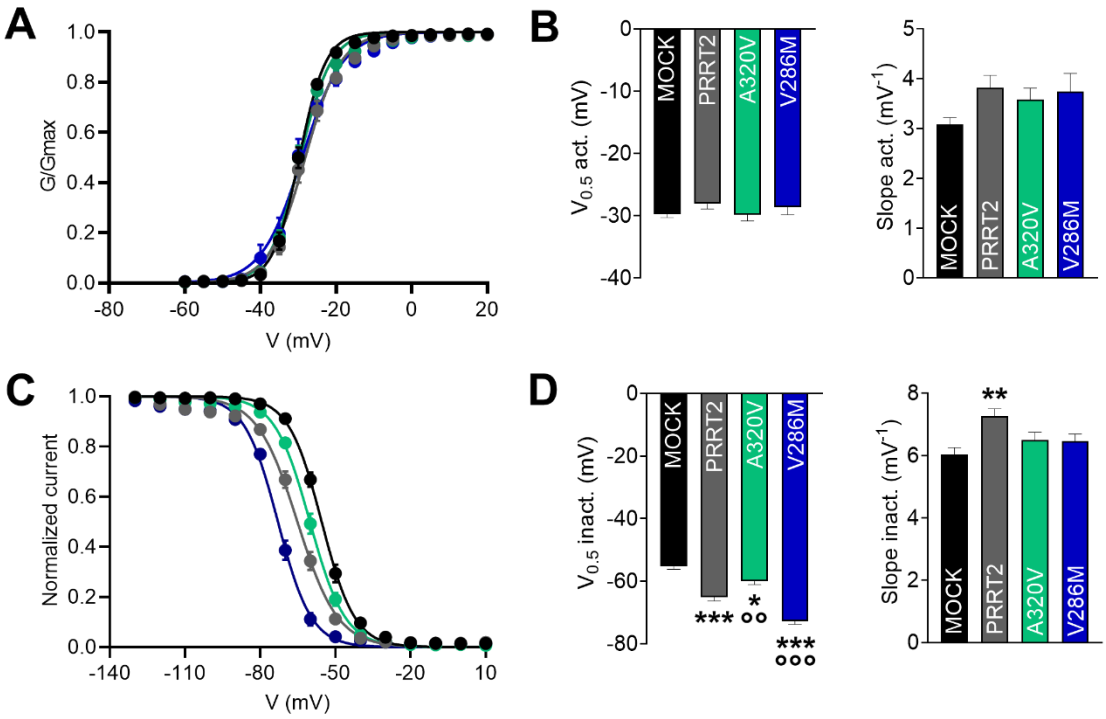


**Figure 28.** (**A**) Voltage-dependence of activation. The lines are the best-fitted Boltzmann curves. (**B**) Means (± sem) values of the half-maximal voltage of activation ($V_{0.5\ act}$) and slope (MOCK, n = 21; PRRT2, n = 20; A320V n = 19; V286M n = 18). (**C**) Steady-state inactivation curves. The lines are the best-fitted Boltzmann curves. (**D**) Means (± sem) values of the half-maximal voltages for inactivation ($V_{0.5\ inact}$) and slopes (MOCK, n = 21; PRRT2, n = 27; A320V n = 18; V286M n = 14). (*p<0.05, ***p<0.001 vs MOCK; °°p<0.01, °°°p<0.001 vs WT-PRRT2. One-way ANOVA/Bonferroni's tests or Kruskal-Wallis/Dunn's tests.

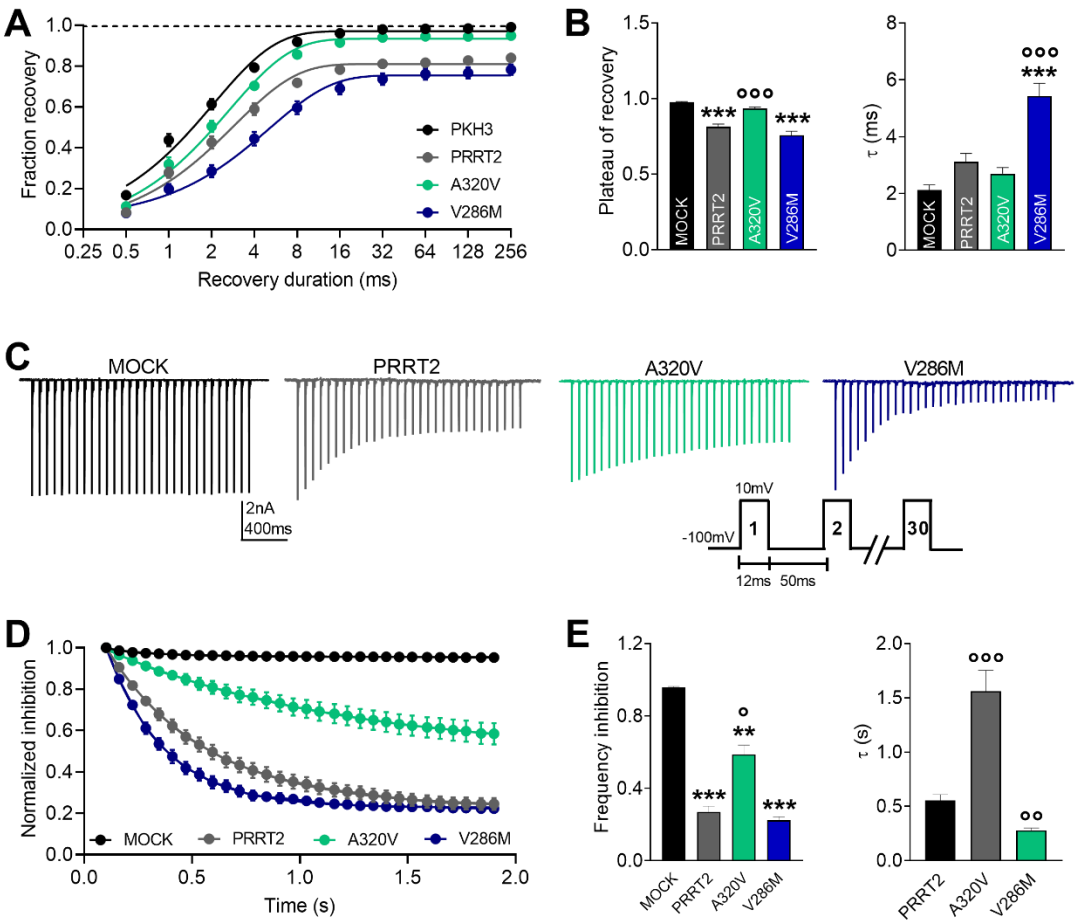


**Figure 29.** (**A**) Time-courses of the recovery from inactivation of peak currents at -100 mV recorded in Hek293 cells stably expressing Nav1.2 and transiently transfected with empty vector (MOCK, black), PRRT2 (grey), A320V (green) or V286M (blue) and plotted on a semi-logarithmic scale. (**B**) τ and plateau of recovery estimated from one-phase decay fit to the data. (MOCK, n = 27; PRRT2, n = 30; A320V n = 27; V286M n = 24). (**C**) Frequency-dependent inhibition for the genotypes described in A in which the τ values were estimated from one-phase decay fit to the data. Since MOCK did not exhibit current depression, the τ value of this group is not reported. Frequency inhibition represents the mean (± sem) of the averaged amplitude of the last three steps of the stimulation (**D,E**). MOCK (n=23); PRRT2 (n=24); A320V (n=19); V286M (n=15). *P < 0.05, **P<0.01, ***P<0.001 vs MOCK; °P<0.05, °°°P<0.001 vs PRRT2 WT. One-way ANOVA/Bonferroni's tests or Kruskal-Wallis/Dunn's tests.

| PHYSIOLOGICAL EFFECT | EXPERIMENT | MUTANT PHENOTYPE | |
|---|---|---|---|
| | | A320V | V286M |
| **Nav1.2 BINDING** | Nav1.2 pull-down | LOF | GOF |
| **Nav1.2 MEMBRANE EXPOSURE** | Biotinylation | LOF | NS |
| **$Na^+$ CURRENT** | Patch-clamp | LOF | NS |
| **ACTIVATION KINETICS** | | NS | NS |
| **INACTIVATION KINETICS** | | LOF | GOF |
| **RECOVERY FROM INACTIVATION** | | LOF | GOF |
| **PLATEAU INHIBITION** | | LOF | NS |
| **INHIBITION KINETICS** | | LOF | GOF |

**Table 3.** Summary of physiological effects exerted by PRRT2 mutants on Nav1.2. GOF: gain of function, LOF: loss of function, NS: non-significant effect.

# 5. DISCUSSION

## 5.1 PRRT2 and β4-subunit exert independent and distinct modulations of Nav1.2 properties

PRRT2 is a neuron-specific protein that was found to act as a modulator of presynaptic functions and intrinsic excitability [132]. In the absence of PRRT2, neuronal circuits are hyperexcitable [17]. Consistently, patients bearing LOF mutations in the PRRT2 gene or PRRT2 KO mice are affected by paroxysmal manifestations. Based on previous studies, these phenotypes result from a mixed synaptopathy/channelopathy [18] [138]. Indeed, PRRT2 acts, in murine and human neurons, as a negative modulator of Nav1.2/1.6, without affecting the 1.1 subtype that is essential for the excitability of inhibitory neurons [132]. These results are in line with the therapeutic efficacy of Nav channel inhibitors in PRRT2-linked diseases [211] [207] [29]. PRRT2 decreases membrane targeting of active Nav channels and modulates their biophysical properties with a left-shift of the inactivation curve and a decreased channel recovery from inactivation [132]. Given the reported results, PRRT2 can be considered novel inhibitory auxiliary subunit of the Nav1.2/1.6 pore-forming α-subunits.

At present, the best-known auxiliary subunits modulating both membrane exposure and kinetics of Nav α-subunit are the β subunits (β1-β4). These membrane proteins structurally resemble PRRT2, being single membrane-spanning domain proteins. Among all β-subunits, the β4 subtype was chosen for being highly expressed in the cerebellum [176], the main brain region responsible for the PRRT2 LOF phenotype [17] [212]. Furthermore, the β4 subunit is the only subtype that enables the resurgent $Na^+$ current involved directly in cell excitability [152]. When expressed in heterologous systems, the β4 subunit increases the $Na^+$ current density by enhancing the membrane exposure of Nav α-subunits, shifts the voltage-dependence of channel activation toward more negative voltages and accelerates the rate of activation [129] [176] .

PRRT2 and β subunits have opposite effects on the membrane exposure and biophysical properties of the pore-forming α-subunit [183] [132]. We investigated whether PRRT2 and β subunits interfere with each other in binding to the α-subunit or act independently as auxiliary subunits on the common Nav target. It is known that β4, as well as β2 subunits covalently interact with the Nav α-subunit by forming an extracellular disulfide bond [213]. However, an

additional interaction site with the transmembrane domain of Nav1.4 α-subunit was found in the intracellular domains of β4 and β2 [214] [215].

In the present study, we showed that: (i) both PRRT2 and β subunits bind to Nav1.2 channels; (ii) PRRT2 does not directly interact with any of the β subunits; (iii) PRRT2 and β subunits do not compete for binding to Nav1.2 channels; (iv) PRRT2 and β subunits have opposite and additive effects on the targeting and membrane exposure of Nav1.2 channels. We further investigated this interplay by electrophysiological experiments.

Specifically, PRRT2 and β4 exert opposite effects on current density and partly distinct and complementary effects on the biophysical properties of Nav1.2 channels. In fact, while the β4 subunit increases the transient $Na^+$ current, PRRT2 decreases it. When PRRT2 and β4 are both expressed pure additive effect was observed through which the $Na^+$ current remains unchanged but shifted to the left due to the specific β4 effect. PRRT2 does not affect the kinetics of activation, while β4 induces a marked shift of the activation curve to negative voltages and an increase in $G_{max}$ that is left unaffected in the presence of PRRT2. On the contrary, β4 is ineffective on the kinetics of inactivation and recovery from inactivation while PRRT2 shifts to negative voltages the kinetics of inactivation and decreases the recovery from inactivation, an effect that remains unaltered in the presence of β4. When both β4 and PRRT2 are co-expressed, the PRRT2-induced decrease of the recovery plateau is only slightly attenuated, but still significant with respect to MOCK transfected cells, leaving the time constant of recovery unmodified under the tested experimental conditions. During long single depolarizations or long trains of depolarizations, sodium channels enter a slow inactivated state, from which recovery requires prolonged repolarization [216] [159] [217]. The difference in the plateau level can be an effect of the recovery from slow inactivation, an important feature of the Nav. In fact, impairments of voltage-dependent activation, fast inactivation as well as slow inactivation have all been associated with channelopathies of skeletal muscle and brain sodium channels [159].

The expression of β4 was able to increase the persistent $Na^+$ current amplitude, while PRRT2 decreased it, replicated those observed in the transient current. When both modulatory proteins were co-expressed, the amount of persistent current was similar that recorded in control transfected cells. These results again demonstrate that PRRT2 and β4-subunit modulate independently the Nav1.2 persistent current when worked in the same channel complex and that their effects are purely additive. On the other hand, the resurgent

$Na^+$ current generated in the presence of the intracellular β4 peptide, was specifically increased by β4, irrespective of the presence or absence of PRRT2 that was previously shown not to modulate this current in cerebellar granule cells [218].

Our findings suggest that the activity of $Na^+$ channels, as well as their targeting and exposure on the membrane, can be regulated by a push-pull mechanism involving PRRT2 and Nav β-subunits. In addition, the two auxiliary proteins have specific and opposite, non-mutually exclusive effects on the channel biophysical properties. Since the cell density of Nav is the determinant for the intrinsic excitability in neurons, a dual control of $Na^+$ channel density is the most efficient way to control the "optimexcitability tone" over time. Moreover, the activity of Nav α-subunits can be modulated by the relative expression of PRRT2 and β-subunits in various neuronal populations, determining heterogeneity in intrinsic excitability.

The Golgi apparatus, secretory vesicles, and endoplasmic reticulum contain the majority of the expressed Nav α-subunits [219]. In these compartments, extensive glycosylation of the α-subunits occurs, which is necessary for the translocation of channel to the cell membrane, as well as for its stability and dynamics [220]. Nav β-subunits interact with the channel at the intracellular level facilitating its targeting to the plasma membrane [221] [222]. Experimental evidence suggests that this requires N-linked glycosylation of β-subunits, as well as a positive effect of the β-subunits on glycosylation of the α-subunits that promotes stabilization of the channel at the plasma membrane [223] [224]. Additionally, β-subunits are members of the CAM family of adhesion molecules; thus, β-subunit interactions with the cytoskeleton appear to be essential for α-subunit expression on the cell surface [225].

The precise mechanism by which PRRT2 inhibits the Nav density on the plasma membrane is still unknown. However, several potential mechanisms are proposed: (i) slowing down exocytosis of intracellular Nav-containing vesicles; (ii) enhancing the turnover of membrane domains containing Nav channels; (iii) modulating Nav channel interactions with the cytoskeleton. Although no direct evidence is as yet available, the described interactions of PRRT2 with SNARE proteins responsible for membrane fusion at nerve terminals [70] [102] [226], as well as potential interactions of the proline-rich cytosolic N-terminal domain of PRRT2 with SH3-domain bearing proteins involved in endocytosis, such as endophilin and intersectin [19] could be involved. Moreover, PRRT2 has been recently shown to modulate the actin-based cytoskeleton and, when expressed in cell lines, inhibits cell motility and focal adhesion turnover [227] [228].

## 5.2 Putative modulation of Nav by the N-terminal and the C-terminal transmembrane domain

In addition to the excitatory/inhibitory imbalance in short-term plasticity [106] [132], the interactions of PRRT2 with $Na^+$ channels provide a basis for the pathogenesis of the PRRT2-linked paroxysmal manifestations [29] [18] [39] [138] [229]. The efficacy of $Na^+$ channel blockers in the therapy of PRRT2-linked diseases [230] [231] provides a strong support to the pathogenic role of the disruption of PRRT2/Nav interactions. Consequently, the study of which protein domains are responsible for interacting with Nav1.2/1.6, modulating their membrane turnover and biophysical properties, are important topics for elucidating disease pathophysiology, genotype-phenotype correlations, and for developing novel targeted therapies.

PRRT2 displays two distinct regions, an N-terminal unstructured proline-rich region, an intramembrane C-terminal region forming a helix-loop-helix, a very short cytosolic loop, and a transmembrane segment ending with a C-terminal dipeptide [19]. In the absence of an experimentally confirmed structure for full length PRRT2, we previously provided an atom-detailed model of the 79 amino acid-long intramembrane region of PRRT2 generated using Robetta and refined with brief MD simulations [19]. Here we have extended the simulations to the µs-time scale and revealed that the protein maintained a stable conformation with all the distinctive features of the model. We also compared our Robetta model with the structure obtained by the AlphaFold2 method, deposited in the AlphaFold database. The two configurations exhibit the same secondary structure patterns and nearly comparable numbers of helix turns, making them highly similar. These results strengthen the validity of the model, which is presently the only structure available for the transmembrane PRRT2 region and is essential to investigate protein-protein interactions in atomic detail.

We generated the N- and C-terminal sections of PRRT2 and tested them with Nav1.2 and Nav1.1 $\alpha$-subunits to determine the extent and specificity of the interactions and determine if one or both regions of PRRT2 are involved in interacting with Nav channels and regulating their biophysical features. PRRT2 fragments retained the subunit specificity of full length PRRT2 and did not interact with Nav1.1 channels. Both PRRT2 deletion mutants bound to Nav1.2 $\alpha$-subunits. However, the N-terminal region displayed a binding comparable to the

full-length protein suggesting an interaction with the C-terminal cytoplasmic tail and/or intracellular loops of the Nav channel. Nevertheless, in spite of the recapitulation of the binding activity and Nav channel specificity, the PRRT2 N-terminal domain was unable to modulate membrane targeting and biophysical properties of the channel.

The presence of a significant Nav binding by the C-terminal region of PRRT2 suggests that, in addition to interactions in the cytosol, PRRT2/Nav1.2 interactions also occur between the intramembrane domains of the two proteins. The observation that the C-terminal region of PRRT2 recapitulates the effects of the full-length form both on channel targeting to the membrane, as well as on the inactivation kinetics and recovery from inactivation testifies the functional importance of this interaction site. Despite the very high homology between the transmembrane domains of Nav1.2 and Nav1.1 $\alpha$-subunits, the C-terminal region of PRRT2 docks to the former and does not interact with the latter. This will open the way to further investigations by performing site-directed mutagenesis of the non-conserved residues present in the voltage sensor and pore forming regions of the I-IV domains of Nav 1.2, using the recently published optimized versions of Nav plasmids [232]. In fact, a considerable obstacle to the study of brain Nav is the unexplained instability of the corresponding recombinant complementary DNA (cDNA) when propagated in commonly used bacterial strains, which is manifested by high spontaneous mutation rates. The stabilization of the Nav1.2 plasmid was obtained by inserting a chimeric intronic sequence capable of disrupting a prokaryotic promoter-like sequence present in the SCN2A plasmid, causative of recombination issues. The recently generated stabilized constructs by DeKeyser and colleagues has made possible for the first time to introduce mutations for the purpose of in vitro study without compromising channel stability [232].

The cytosolic N-terminal region of PRRT2 is rich in proline residues and displays an intrinsically disordered structure when analyzed by AlphaFold2 [19] [21] [233]. However, the significant binding of the cytosolic N-terminal region to Nav1.2 versus Nav1.1 guarantees that the interaction is specific. It is possible that, upon binding to Nav1.2, the N-terminal region of PRRT2 gains a defined structure [234]. A model in which the N-terminal intracellular domain acts as a Nav1.2 docking module that favors the interaction of the intramembrane C-terminal domain on the plasma membrane exposure and biophysical properties is consistent with the marked Nav1.2 binding activity, coupled with the inability to modulate channel turnover and biophysical properties. As mentioned above, binding to Src-

homology-3 domain-containing proteins [19] and/or interactions with the actin cytoskeleton [235] [227] may directly or indirectly responsible for this interaction.

In conclusion, the results support the high-order structure of the intramembrane C-terminal region of PRRT2 and indicate that interactions with the transmembrane domains of Nav1.2 are responsible for the PRRT2-induced constraint to the membrane exposure of Nav1.2 channels and their activation. Further experiments should be dedicated to the dissection of the amino acids involved in the binding between Nav and PRRT2. The elucidation of the molecular bases of the inhibitory effects of PRRT2 on neuronal excitability is the first step toward a targeted therapeutic approach to PRRT2-linked paroxysmal diseases aimed at normalizing the intrinsic excitability of principal neurons without a generalized blockade of Nav channels that, although effective, is associated to undesired side effects.

## 5.3 The PRRT2 A320V and V286M mutants alter the Nav biophysical properties

To understand the pathogenesis of the pleiotropic paroxysmal disorders related to PRRT2, it is crucial to define the PRRT2-Nav interaction sites. We analyzed some point PRRT2 mutations potentially involved in the transmembrane interactions between PRRT2 and Nav that are causative of PRRT2-related pathologies. The study selected the few missense pathogenic mutations of PRRT2 that preserved protein expression and membrane targeting and resulted in the identification of two residues that may play a role in the interaction with the Nav1.2 channel.

In pull-down experiments, the V286M and A320V mutants showed different binding patterns to Nav1.2, with V286M exhibiting increased and A320V exhibiting decreased binding to Nav1.2, respectively. Specifically, the A320V mutant was characterized by a clear LOF phenotype in both the membrane targeting and biophysical properties of Nav1.2 channels. Conversely, the V286M mutant showed a GOF phenotype compared to WT-PRRT2 in the modulation of the Nav1.2 biophysical properties (e.g. steady-state inactivation and recovery from inactivation), without significantly affect the membrane targeting of the channel. The different phenotypes of the two mutants indicate that partially distinct domains of the TM region of PRRT2 may be involved in the inhibition of Nav1.2 channel membrane exposure and the alterations of their inactivation kinetics/recovery from inactivation. The A320V

pathogenic variant in the TM2 region was discovered in a family with PKD and BFIE [236]. Our findings suggest that A320 is an important site for the interaction with the Nav1.2 channel since its mutation decreases or virtually abolishes all the physiological effects of PRRT2, which is supported by the very high evolutionary conservation. The loss of PRRT2's inhibitory control over Nav1.2 membrane exposure in the presence of A320V, provides a potential pathogenetic mechanism for this mutation. Regarding the V286M mutant in the TM1b region, a pathogenetic hypothesis based on the observed GOF activity on Nav1.2 channels appears less consistent with the existing understanding of PRRT2 as a network stability gene [237] [229] [238] [17]. However, it has very recently been reported that overexpression of PRRT2 in the mouse model of 16p11.2 duplication, which in humans is associated with ASD, epilepsy and intellectual disability, causes hypersynchronous activity, increased glutamate release and seizure propensity [239]. Consequently, it is possible to hypothesize that both insufficient or excessive levels of PRRT2, resulting in LOF or GOF PRRT2 mutants, are deleterious to the stability of neuronal networks and cause paroxysmal manifestations. Here, the PRRT2 mutants were only investigated for their Nav1.2 interaction activity, but it is also possible that they also change PRRT2 activities at the presynaptic level. [102] [237] [229] or on other effectors such as Na+/K+-ATPase [39]. In the end, we evaluated the effects of a cohort of 8 PRRT2 missense mutations on the interactions of PRRT2 with voltage-dependent Na+ channels. We identified two pathogenic mutants with opposite phenotypes on Nav1.2 channels that confirm the key role played by voltage-gated Na+ channels in the hyperexcitability underlying the paroxysmal manifestations in PRRT2 patients explaining the therapeutic efficacy of Na+ channel blockers in these diseases. The results may contribute to a better understanding of the pathogenetic mechanisms underlying paroxysmal attacks in PRRT2 patients as well as the molecular underpinnings of PRRT2's inhibitory effects on neuronal excitability.

# BIBLIOGRAPHY

[1] K. Perrine, “Paroxysmal Disorder,” *Encyclopedia of Clinical Neuropsychology*, pp. 1870–1870, 2011, doi: 10.1007/978-0-387-79948-3_1050.

[2] W. H. Raskind *et al.*, “Further localization of a gene for paroxysmal dystonic choreoathetosis to a 5-cM region on chromosome 2q34,” *Hum Genet*, vol. 102, no. 1, pp. 93–97, 1998, doi: 10.1007/S004390050659.

[3] W. Et, “Mutational Analysis of GLUT1 (SLC2A1) in Glut-1 Deficiency Syndrome,” *Hum Mutat*, vol. 16, pp. 224–231, 2000, doi: 10.1002/1098-1004.

[4] W. J. Chen *et al.*, “Exome sequencing identifies truncating mutations in PRRT2 that cause paroxysmal kinesigenic dyskinesia,” *Nature Genetics 2011 43:12*, vol. 43, no. 12, pp. 1252–1255, Nov. 2011, doi: 10.1038/ng.1008.

[5] H. X. Wang, H. F. Li, G. L. Liu, X. D. Wen, and Z. Y. Wu, “Mutation analysis of MR-1, SLC2A1, and CLCN1 in 28 PRRT2-negative paroxysmal kinesigenic dyskinesia patients,” *Chin Med J (Engl)*, vol. 129, no. 9, pp. 1017–1021, May 2016, doi: 10.4103/0366-6999.180529.

[6] J. Wang, W. Zhao, H. Liu, H. He, and R. Shao, “Myofibrillogenesis regulator 1 (MR-1): a potential therapeutic target for cancer and PNKD,” *https://doi.org/10.1080/1061186X.2017.1401077*, vol. 26, no. 8, pp. 643–648, Sep. 2017, doi: 10.1080/1061186X.2017.1401077.

[7] H. Y. Lee *et al.*, “The gene for paroxysmal non-kinesigenic dyskinesia encodes an enzyme in a stress response pathway,” *Hum Mol Genet*, vol. 13, no. 24, pp. 3161–3170, Dec. 2004, doi: 10.1093/HMG/DDH330.

[8] R. Erro, K. P. Bhatia, A. J. Espay, and P. Striano, “The epileptic and nonepileptic spectrum of paroxysmal dyskinesias: Channelopathies, synaptopathies, and transportopathies,” *Mov Disord*, vol. 32, no. 3, pp. 310–318, Mar. 2017, doi: 10.1002/MDS.26901.

[9] J. Klepper *et al.*, “Defective glucose transport across brain tissue barriers: A newly recognized neurological syndrome,” *Neurochem Res*, vol. 24, no. 4, pp. 587–594, 1999, doi: 10.1023/A:1022544131826.

[10] A. Suls *et al.*, “Paroxysmal exercise-induced dyskinesia and epilepsy is due to mutations in SLC2A1, encoding the glucose transporter GLUT1,” *Brain*, vol. 131, no. Pt 7, pp. 1831–1844, Jul. 2008, doi: 10.1093/BRAIN/AWN113.

[11] R. Erro, K. P. Bhatia, A. J. Espay, and P. Striano, “The epileptic and non-epileptic spectrum of paroxysmal dyskinesias: channelopathies, synaptopathies, and transportopathies,” *Mov Disord*, vol. 32, no. 3, p. 310, Mar. 2017, doi: 10.1002/MDS.26901.

[12] W. J. Chen *et al.*, “Exome sequencing identifies truncating mutations in PRRT2 that cause paroxysmal kinesigenic dyskinesia,” *Nature Genetics 2011 43:12*, vol. 43, no. 12, pp. 1252–1255, Nov. 2011, doi: 10.1038/ng.1008.

[13] A. Méneret, C. Gaudebout, F. Riant, M. Vidailhet, C. Depienne, and E. Roze, “PRRT2 mutations and paroxysmal disorders,” *Eur J Neurol*, vol. 20, no. 6, pp. 872–878, Jun. 2013, doi: 10.1111/ENE.12104.

[14] R. Erro, U. M. Sheerin, and K. P. Bhatia, “Paroxysmal dyskinesias revisited: a review of 500 genetically proven cases and a new classification,” *Mov Disord*, vol. 29, no. 9, pp. 1108–1116, 2014, doi: 10.1002/MDS.25933.

[15] G. Spoto *et al.*, “Synaptopathies in Developmental and Epileptic Encephalopathies: A Focus on Pre-synaptic Dysfunction,” *Front Neurol*, vol. 13, p. 826211, Mar. 2022, doi: 10.3389/FNEUR.2022.826211.

[16] D. Trabzuni *et al.*, “Quality control parameters on a large dataset of regionally dissected human control brains for whole genome expression studies,” *J Neurochem*, vol. 119, no. 2, p. 275, Oct. 2011, doi: 10.1111/J.1471-4159.2011.07432.X.

[17] C. Michetti *et al.*, “The PRRT2 knockout mouse recapitulates the neurological diseases associated with PRRT2 mutations,” *Neurobiol Dis*, vol. 99, pp. 66–83, Mar. 2017, doi: 10.1016/J.NBD.2016.12.018.

[18] F. Valtorta, F. Benfenati, F. Zara, and J. Meldolesi, “PRRT2: from Paroxysmal Disorders to Regulation of Synaptic Function,” *Trends Neurosci*, vol. 39, no. 10, pp. 668–679, Oct. 2016, doi: 10.1016/J.TINS.2016.08.005.

[19] P. Rossi *et al.*, “A Novel Topology of Proline-rich Transmembrane Protein 2 (PRRT2): HINTS FOR AN INTRACELLULAR FUNCTION AT THE SYNAPSE*,” *J Biol Chem*, vol. 291, no. 12, p. 6111, Mar. 2016, doi: 10.1074/JBC.M115.683888.

[20] M. Sä llman Almé, N. Bringeland, R. Fredriksson, H. B. Schiö th, and V. N. Uversky, “The Dispanins: A Novel Gene Family of Ancient Origin That Contains 14 Human Members,” *PLoS One*, vol. 7, no. 2, p. 31961, 2012, doi: 10.1371/journal.pone.0031961.

[21] W. J. Chen *et al.*, “Exome sequencing identifies truncating mutations in PRRT2 that cause paroxysmal kinesigenic dyskinesia,” *Nature Genetics 2011 43:12*, vol. 43, no. 12, pp. 1252–1255, Nov. 2011, doi: 10.1038/ng.1008.

[22] E. Kalashnikova *et al.*, “SynDIG1: an activity-regulated AMPA receptor-interacting transmembrane protein that regulates excitatory synapse development,” *Neuron*, vol. 65, no. 1, p. 80, Jan. 2010, doi: 10.1016/J.NEURON.2009.12.021.

[23] J. Chen, L. Zhou, and S. Y. Pan, “A brief review of recent advances in stem cell biology,” *Neural Regen Res*, vol. 9, no. 7, p. 684, Apr. 2014, doi: 10.4103/1673-5374.131565.

[24] J. Schwenk *et al.*, “High-Resolution Proteomics Unravel Architecture and Molecular Diversity of Native AMPA Receptor Complexes,” *Neuron*, vol. 74, no. 4, pp. 621–633, May 2012, doi: 10.1016/j.neuron.2012.03.034.

[25] N. F. Shanks *et al.*, “Differences of AMPA and kainate receptor interactomes identify a novel AMPA receptor auxiliary subunit, GSG1L,” *Cell Rep*, vol. 1, no. 6, p. 590, Jun. 2012, doi: 10.1016/J.CELREP.2012.05.004.

[26] J. Von Engelhardt *et al.*, “CKAMP44: A brain-specific protein attenuating short-term synaptic plasticity in the dentate gyrus,” *Science (1979)*, vol. 327, no. 5972, pp. 1518–1522, Mar. 2010, doi: 10.1126/SCIENCE.1184178/SUPPL_FILE/VON_ENGELHARDT.SOM.PDF.

[27] B. A. Jordan *et al.*, “Identification and verification of novel rodent postsynaptic density proteins,” *Molecular and Cellular Proteomics*, vol. 3, no. 9, pp. 857–871, Sep. 2004, doi: 10.1074/mcp.M400045-MCP200.

[28] L. M. Kirk *et al.*, “Distribution of the SynDIG4/ Proline rich transmembrane protein 1 in rat brain,” *J Comp Neurol*, vol. 524, no. 11, p. 2266, Aug. 2016, doi: 10.1002/CNE.23945.

[29] D. Ebrahimi-Fakhari, A. Saffari, A. Westenberger, and C. Klein, “The evolving spectrum of PRRT2-associated paroxysmal diseases,” *Brain*, vol. 138, no. 12, pp. 3476–3495, 2015, doi: 10.1093/brain/awv317.

[30] S. Y. Zhao *et al.*, “Functional study and pathogenicity classification of PRRT2 missense variants in PRRT2-related disorders,” *CNS Neurosci Ther*, vol. 26, no. 1, pp. 39–46, Jan. 2020, doi: 10.1111/CNS.13147.

[31] G. Balagura *et al.*, “Clinical spectrum and genotype-phenotype correlations in PRRT2 Italian patients,” *European Journal of Paediatric Neurology*, vol. 28, pp. 193–197, Sep. 2020, doi: 10.1016/J.EJPN.2020.06.005.

[32] J. G. Lu *et al.*, “A novel PRRT2 pathogenic variant in a family with paroxysmal kinesigenic dyskinesia and benign familial infantile seizures,” *Cold Spring Harb Mol Case Stud*, vol. 4, no. 1, Feb. 2018, doi: 10.1101/MCS.A002287/-/DC1.

[33] J. Coleman *et al.*, “PRRT2 Regulates Synaptic Fusion by Directly Modulating SNARE Complex Assembly,” *Cell Rep*, vol. 22, no. 3, p. 820, Jan. 2018, doi: 10.1016/J.CELREP.2017.12.056.

[34] Q. Liu *et al.*, “Mutations in PRRT2 result in paroxysmal dyskinesias with marked variability in clinical expression,” *J Med Genet*, vol. 49, no. 2, pp. 79–82, Feb. 2012, doi: 10.1136/JMEDGENET-2011-100653.

[35] M. Li *et al.*, “PRRT2 Mutant Leads to Dysfunction of Glutamate Signaling,” *Int J Mol Sci*, vol. 16, no. 5, p. 9134, Apr. 2015, doi: 10.3390/IJMS16059134.

[36] J. G. Lu *et al.*, “A novel PRRT2 pathogenic variant in a family with paroxysmal kinesigenic dyskinesia and benign familial infantile seizures,” 2018, doi: 10.1101/mcs.a002287.

[37] S. Y. Zhao *et al.*, “Functional study and pathogenicity classification of PRRT2 missense variants in PRRT2-related disorders,” *CNS Neurosci Ther*, vol. 26, no. 1, p. 39, Jan. 2020, doi: 10.1111/CNS.13147.

[38] M. H. Tsai *et al.*, “PRRT2 missense mutations cluster near C-terminus and frequently lead to protein mislocalization,” *Epilepsia*, vol. 60, no. 5, pp. 807–817, May 2019, doi: 10.1111/EPI.14725.

[39] G. Balagura *et al.*, “Clinical spectrum and genotype-phenotype correlations in PRRT2 Italian patients,” *European Journal of Paediatric Neurology*, vol. 28, pp. 193–197, Sep. 2020, doi: 10.1016/j.ejpn.2020.06.005.

[40] H. F. Li *et al.*, “Associations between neuroanatomical abnormality and motor symptoms in paroxysmal kinesigenic dyskinesia,” *Parkinsonism Relat Disord*, vol. 62, pp. 134–140, May 2019, doi: 10.1016/J.PARKRELDIS.2018.12.029.

[41] J. Fang, S. Wang, G. Zhao, and L. Cao, “Novel mutation of the PRRT2 gene in two cases of paroxysmal kinesigenic dyskinesia: Two case reports,” *Biomed Rep*, vol. 12, no. 6, p. 309, Jun. 2020, doi: 10.3892/BR.2020.1293.

[42] S. D. Spacey *et al.*, “Genetic heterogeneity in paroxysmal nonkinesigenic dyskinesia,” *Neurology*, vol. 66, no. 10, pp. 1588–1590, May 2006, doi: 10.1212/01.WNL.0000217332.51740.7C.

[43] S. E. Heron *et al.*, “PRRT2 Mutations Cause Benign Familial Infantile Epilepsy and Infantile Convulsions with Choreoathetosis Syndrome,” *Am J Hum Genet*, vol. 90, no. 1, p. 152, Jan. 2012, doi: 10.1016/J.AJHG.2011.12.003.

[44] R. Erro, U. M. Sheerin, and K. P. Bhatia, “Paroxysmal dyskinesias revisited: a review of 500 genetically proven cases and a new classification,” *Mov Disord*, vol. 29, no. 9, pp. 1108–1116, 2014, doi: 10.1002/MDS.25933.

[45] R. Erro and K. P. Bhatia, “Unravelling of the paroxysmal dyskinesias,” *J Neurol Neurosurg Psychiatry*, vol. 90, no. 2, pp. 227–234, Feb. 2019, doi: 10.1136/JNNP-2018-318932.

[46] J. W. Lance, “Familial paroxysmal dystonic choreoathetosis and its differentiation from related syndromes,” *Ann Neurol*, vol. 2, no. 4, pp. 285–293, Oct. 1977, doi: 10.1002/ANA.410020405.

[47] K. P. Bhatia, “Paroxysmal Dyskinesias”, doi: 10.1002/mds.23765.

[48] A. R. Gardiner *et al.*, “The clinical and genetic heterogeneity of paroxysmal dyskinesias,” *Brain*, vol. 138, no. Pt 12, pp. 3567–3580, Dec. 2015, doi: 10.1093/BRAIN/AWV310.

[49] M. K. Bruno *et al.*, “Clinical evaluation of idiopathic paroxysmal kinesigenic dyskinesia,” *Neurology*, vol. 63, no. 12, pp. 2280–2287, Dec. 2004, doi: 10.1212/01.WNL.0000147298.05983.50.

[50] L. Silveira-Moriyama *et al.*, “Clinical features of childhood-onset paroxysmal kinesigenic dyskinesia with PRRT2 gene mutations,” *Dev Med Child Neurol*, vol. 55, no. 4, pp. 327–334, Apr. 2013, doi: 10.1111/DMCN.12056.

[51] I. Unterberger and E. Trinka, “Diagnosis and treatment of paroxysmal dyskinesias revisited,” *Ther Adv Neurol Disord*, vol. 1, no. 2, pp. 67–74, 2008, doi: 10.1177/1756285608095119.

[52] M. K. Houser, V. L. Soland, K. P. Bhatia, N. P. Quinn, and C. D. Marsden, “Paroxysmal kinesigenic choreoathetosis: a report of 26 patients,” *Journal of Neurology 1999 246:2*, vol. 246, no. 2, pp. 120–126, 1999, doi: 10.1007/S004150050318.

[53] M. Paucar, H. Malmgren, and P. Svenningsson, “Paroxysmal Kinesigenic Dyskinesia,” *Tremor and Other Hyperkinetic Movements*, vol. 7, p. 529, 2017, doi: 10.7916/D8R79N2F.

[54] M. A. Rogawski, W. Löscher, and J. M. Rho, “Mechanisms of Action of Antiseizure Drugs and the Ketogenic Diet,” *Cold Spring Harb Perspect Med*, vol. 6, no. 5, p. 28, May 2016, doi: 10.1101/CSHPERSPECT.A022780.

[55] R. M. Kaminski, M. Gillard, and H. Klitgaard, “Targeting SV2A for Discovery of Antiepileptic Drugs,” *Epilepsia*, vol. 51, no. SUPPL. 5, p. 83, Dec. 2012, doi: 10.1111/j.1528-1167.2010.02869.x.

[56] G. Li *et al.*, “Levetiracetam but not valproate inhibits function of CD8+ T lymphocytes,” *Seizure*, vol. 22, no. 6, pp. 462–466, Jul. 2013, doi: 10.1016/j.seizure.2013.03.006.

[57] N. F. Shanks *et al.*, “Differences in AMPA and kainate receptor interactomes facilitate identification of AMPA receptor auxiliary subunit GSG1L,” *Cell Rep*, vol. 1, no. 6, pp. 590–598, Jun. 2012, doi: 10.1016/J.CELREP.2012.05.004.

[58] R. P. Shank and B. E. Maryanoff, “Molecular Pharmacodynamics, Clinical Therapeutics, and Pharmacokinetics of Topiramate,” *CNS Neurosci Ther*, vol. 14, no. 2, p. 120, Jun. 2008, doi: 10.1111/J.1527-3458.2008.00041.X.

[59] I. E. Scheffer *et al.*, “ILAE classification of the epilepsies: Position paper of the ILAE Commission for Classification and Terminology,” *Epilepsia*, vol. 58, no. 4, pp. 512–521, Apr. 2017, doi: 10.1111/EPI.13709.

[60] P. Szepetowski, J. Rochette, P. Berquin, C. Piussan, G. M. Lathrop, and A. P. Monaco, “Familial infantile convulsions and paroxysmal choreoathetosis: a new neurological syndrome linked to the pericentromeric region of human chromosome 16.,” *Am J Hum Genet*, vol. 61, no. 4, p. 889, 1997, doi: 10.1086/514877.

[61] H. A. Tomita *et al.*, “Paroxysmal Kinesigenic Choreoathetosis Locus Maps to Chromosome 16p11.2-q12.1,” *Am J Hum Genet*, vol. 65, no. 6, p. 1688, 1999, doi: 10.1086/302682.

[62] R. Caraballo *et al.*, “Linkage of Benign Familial Infantile Convulsions to Chromosome 16p12-q12 Suggests Allelism to the Infantile Convulsions and Choreoathetosis Syndrome,” *Am J Hum Genet*, vol. 68, no. 3, p. 788, 2001, doi: 10.1086/318805.

[63] K. J. Swoboda *et al.*, “Paroxysmal kinesigenic dyskinesia and infantile convulsions,” *Neurology*, vol. 55, no. 2, pp. 224–230, Jul. 2000, doi: 10.1212/WNL.55.2.224.

[64] Y. Deng, J. Xu, C. Yao, L. Wang, X. Dong, and C. Zhao, “Characteristics of infantile convulsions and choreoathetosis syndrome caused by PRRT2 mutation,” *Pediatr Investig*, vol. 6, no. 1, pp. 11–15, Mar. 2022, doi: 10.1002/PED4.12308.

[65] K. Watanabe *et al.*, “Benign complex partial epilepsies in infancy,” *Pediatr Neurol*, vol. 3, no. 4, pp. 208–211, Jul. 1987, doi: 10.1016/0887-8994(87)90018-X.

[66] J. Schubert *et al.*, “PRRT2 Mutations are the major cause of benign familial infantile seizures,” *Hum Mutat*, vol. 33, no. 10, pp. 1439–1443, Oct. 2012, doi: 10.1002/HUMU.22126.

[67] P. M. C. Callenbach *et al.*, “Benign familial infantile convulsions: A clinical study of seven Dutch families,” *European Journal of Paediatric Neurology*, vol. 6, no. 5, pp. 269–283, Sep. 2002, doi: 10.1053/ejpn.2002.0609.

[68] A. F. Van Rootselaar, S. S. Van Westrum, D. N. Velis, and M. A. J. Tijssen, “The paroxysmal dyskinesias,” *Pract Neurol*, vol. 9, no. 2, pp. 102–109, Apr. 2009, doi: 10.1136/JNNP.2009.172213.

[69] L. A. Mount and S. Reback, “FAMILIAL PAROXYSMAL CHOREOATHETOSIS: Preliminary Report on a Hitherto Undescribed Clinical Syndrome,” *Arch Neurol Psychiatry*, vol. 44, no. 4, pp. 841–847, Oct. 1940, doi: 10.1001/ARCHNEURPSYC.1940.02280100143011.

[70] Y. C. Lee *et al.*, “PRRT2 Mutations in Paroxysmal Kinesigenic Dyskinesia with Infantile Convulsions in a Taiwanese Cohort,” *PLoS One*, vol. 7, no. 8, Aug. 2012, doi: 10.1371/JOURNAL.PONE.0038543.

[71] M. K. Bruno *et al.*, “Genotype–phenotype correlation of paroxysmal nonkinesigenic dyskinesia,” *Neurology*, vol. 68, no. 21, pp. 1782–1789, May 2007, doi: 10.1212/01.WNL.0000262029.91552.E0.

[72] S. Fahn, “The early history of paroxysmal dyskinesias,” *Adv Neurol*, vol. 89, pp. 377–385, 2002, doi: 10.1007/978-3-030-53721-0_2.

[73] J. W. Lance, “Familial paroxysmal dystonic choreoathetosis and its differentiation from related syndromes,” *Ann Neurol*, vol. 2, no. 4, pp. 285–293, 1977, doi: 10.1002/ANA.410020405.

[74] S. B. Bressman, S. Fahn, and R. E. Burke, “Paroxysmal non-kinesigenic dystonia.,” *Adv Neurol*, vol. 50, pp. 403–413, Jan. 1988, Accessed: Nov. 04, 2022. [Online]. Available: https://europepmc.org/article/med/3400499

[75] G. Zorzi, C. Conti, A. Erba, T. Granata, L. Angelini, and N. Nardocci, “Paroxysmal dyskinesias in childhood,” *Pediatr Neurol*, vol. 28, no. 3, pp. 168–172, Mar. 2003, doi: 10.1016/S0887-8994(02)00512-X.

[76] H. Y. Lee *et al.*, “The gene for paroxysmal non-kinesigenic dyskinesia encodes an enzyme in a stress response pathway,” *Hum Mol Genet*, vol. 13, no. 24, pp. 3161–3170, Dec. 2004, doi: 10.1093/HMG/DDH330.

[77] J. L. Wang *et al.*, “Mutation analysis of PRRT2 in two Chinese BFIS families and nomenclature of PRRT2 related paroxysmal diseases,” *Neurosci Lett*, vol. 552, pp. 40–45, 2013, doi: 10.1016/J.NEULET.2013.07.020.

[78] R. Kurlan and I. Shoulson, “Familial paroxysmal dystonic choreoathetosis and response to alternate-day oxazepam therapy,” *Ann Neurol*, vol. 13, no. 4, pp. 456–457, 1983, doi: 10.1002/ANA.410130415.

[79] M. Alemdar, P. Iseri, M. Selekler, and S. Ş. Komsuoğlu, “Levetiracetam-responding paroxysmal nonkinesigenic dyskinesia,” *Clin Neuropharmacol*, vol. 30, no. 4, pp. 241–244, Jul. 2007, doi: 10.1097/WNF.0B013E31803B9415.

[80] R. Pons *et al.*, “Paroxysmal non-kinesigenic dyskinesia due to a PNKD recurrent mutation: report of two Southern European families,” *Eur J Paediatr Neurol*, vol. 16, no. 1, pp. 86–89, Jan. 2012, doi: 10.1016/J.EJPN.2011.09.008.

[81] T. J. Loher, J. K. Krauss, J. M. Burgunder, E. Taub, and J. Siegfried, “Chronic thalamic stimulation for treatment of dystonic paroxysmal nonkinesigenic dyskinesia,” *Neurology*, vol. 56, no. 2, pp. 268–270, Jan. 2001, doi: 10.1212/WNL.56.2.268.

[82] S. A. Schneider *et al.*, “GLUT1 gene mutations cause sporadic paroxysmal exercise-induced dyskinesias,” *Mov Disord*, vol. 24, no. 11, pp. 1684–1688, Aug. 2009, doi: 10.1002/MDS.22507.

[83] J. L. Wang *et al.*, “Identification of PRRT2 as the causative gene of paroxysmal kinesigenic dyskinesias,” *Brain*, vol. 134, no. Pt 12, pp. 3490–3498, 2011, doi: 10.1093/BRAIN/AWR289.

[84] M. B. Russell and A. Ducros, “Sporadic and familial hemiplegic migraine: pathophysiological mechanisms, clinical characteristics, diagnosis, and management,” *Lancet Neurol*, vol. 10, no. 5, pp. 457–470, May 2011, doi: 10.1016/S1474-4422(11)70048-5.

[85] L. L. Thomsen *et al.*, “The genetic spectrum of a population-based sample of familial hemiplegic migraine,” *Brain*, vol. 130, no. 2, pp. 346–356, Feb. 2007, doi: 10.1093/BRAIN/AWL334.

[86] M. D. Ferrari, R. R. Klever, G. M. Terwindt, C. Ayata, and A. M. J. M. van den Maagdenberg, “Migraine pathophysiology: lessons from mouse models and human genetics,” *Lancet Neurol*, vol. 14, no. 1, pp. 65–80, Jan. 2015, doi: 10.1016/S1474-4422(14)70220-0.

[87] F. Riant *et al.*, “PRRT2 mutations cause hemiplegic migraine,” *Neurology*, vol. 79, no. 21, pp. 2122–2124, Nov. 2012, doi: 10.1212/WNL.0B013E3182752CB8.

[88] D. M. Kullmann and S. G. Waxman, “Neurological channelopathies: new insights into disease mechanisms and ion channel function,” *J Physiol*, vol. 588, no. 11, pp. 1823–1827, Jun. 2010, doi: 10.1113/JPHYSIOL.2010.190652.

[89] J. F. Russell, Y. H. Fu, and L. J. Ptáček, “Episodic Neurologic Disorders: Syndromes, Genes, and Mechanisms,” *https://doi.org/10.1146/annurev-neuro-062012-170300*, vol. 36, pp. 25–50, Jul. 2013, doi: 10.1146/ANNUREV-NEURO-062012-170300.

[90] C. Marini *et al.*, “PRRT2 mutations in familial infantile seizures, paroxysmal dyskinesia, and hemiplegic migraine,” *Neurology*, vol. 79, no. 21, p. 2109, Nov. 2012, doi: 10.1212/WNL.0B013E3182752CA2.

[91] A. Labate *et al.*, “Homozygous c.649dupC mutation in PRRT2 worsens the BFIS/PKD phenotype with mental retardation, episodic ataxia, and absences,” *Epilepsia*, vol. 53, no. 12, pp. e196–e199, Dec. 2012, doi: 10.1111/EPI.12009.

[92] A. Okumura *et al.*, “PRRT2 mutation in Japanese children with benign infantile epilepsy,” *Brain Dev*, vol. 35, no. 7, pp. 641–646, Aug. 2013, doi: 10.1016/J.BRAINDEV.2012.09.015.

[93] T. Djémié *et al.*, “PRRT2 mutations: exploring the phenotypical boundaries,” *J Neurol Neurosurg Psychiatry*, vol. 85, no. 4, pp. 462–465, Apr. 2014, doi: 10.1136/JNNP-2013-305122.

[94] K.-D. Choi and J.-H. Choi, “Episodic Ataxias: Clinical and Genetic Features,” *J Mov Disord*, vol. 9, no. 3, pp. 129–135, 2016, doi: 10.14802/jmd.16028/J.

[95] M. C. D’Adamo, P. Imbrici, F. Sponcichetti, and M. Pessia, “Mutations in the KCNA1 gene associated with episodic ataxia type-1 syndrome impair heteromeric voltage-gated K+ channel function,” *The FASEB Journal*, vol. 13, no. 11, pp. 1335–1345, Aug. 1999, doi: 10.1096/FASEBJ.13.11.1335.

[96] A. R. Gardiner *et al.*, “PRRT2 gene mutations: From paroxysmal dyskinesia to episodic ataxia and hemiplegic migraine,” *Neurology*, vol. 79, no. 21, p. 2115, Nov. 2012, doi: 10.1212/WNL.0B013E3182752C5A.

[97] J.-M. Kim, J. S. Kim, C.-S. Ki, and B.-S. Jeon, “Episodic Ataxia Type 2 due to a Deletion Mutation in the CACNA1A Gene in a Korean Family,” *J Clin Neurol*, vol. 2, no. 4, p. 268, 2006, doi: 10.3988/JCN.2006.2.4.268.

[98] H. Najmabadi *et al.*, “Deep sequencing reveals 50 novel genes for recessive cognitive disorders,” *Nature 2011 478:7367*, vol. 478, no. 7367, pp. 57–63, Sep. 2011, doi: 10.1038/nature10423.

[99] A. Labate *et al.*, “Homozygous c.649dupC mutation in PRRT2 worsens the BFIS/PKD phenotype with mental retardation, episodic ataxia, and absences,” *Epilepsia*, vol. 53, no. 12, pp. e196–e199, Dec. 2012, doi: 10.1111/EPI.12009.

[100] X. R. Liu *et al.*, “Novel PRRT2 mutations in paroxysmal dyskinesia patients with variant inheritance and phenotypes,” *Genes Brain Behav*, vol. 12, no. 2, pp. 234–240, Mar. 2013, doi: 10.1111/GBB.12008.

[101] M. Delcourt *et al.*, “Severe phenotypic spectrum of biallelic mutations in PRRT2 gene,” *J Neurol Neurosurg Psychiatry*, vol. 86, no. 7, pp. 782–785, Jul. 2015, doi: 10.1136/JNNP-2014-309025.

[102] P. Valente *et al.*, “PRRT2 Is a Key Component of the Ca2+-Dependent Neurotransmitter Release Machinery,” *Cell Rep*, vol. 15, no. 1, p. 117, Apr. 2016, doi: 10.1016/J.CELREP.2016.03.005.

[103] W. J. Chen *et al.*, “Exome sequencing identifies truncating mutations in PRRT2 that cause paroxysmal kinesigenic dyskinesia,” *Nature Genetics 2011 43:12*, vol. 43, no. 12, pp. 1252–1255, Nov. 2011, doi: 10.1038/ng.1008.

[104] S. E. Heron *et al.*, “PRRT2 Mutations Cause Benign Familial Infantile Epilepsy and Infantile Convulsions with Choreoathetosis Syndrome,” *Am J Hum Genet*, vol. 90, no. 1, p. 152, Jan. 2012, doi: 10.1016/J.AJHG.2011.12.003.

[105] H. Y. Lee *et al.*, “Mutations in the novel protein PRRT2 cause paroxysmal kinesigenic dyskinesia with infantile convulsions,” *Cell Rep*, vol. 1, no. 1, p. 2, Jan. 2012, doi: 10.1016/J.CELREP.2011.11.001.

[106] P. Valente *et al.*, “Constitutive Inactivation of the PRRT2 Gene Alters Short-Term Synaptic Plasticity and Promotes Network Hyperexcitability in Hippocampal Neurons,” *Cerebral Cortex*, vol. 29, no. 5, pp. 2010–2033, May 2019, doi: 10.1093/CERCOR/BHY079.

[107] U. Stelzl *et al.*, “A Human Protein-Protein Interaction Network: A Resource for Annotating the Proteome,” *Cell*, vol. 122, no. 6, pp. 957–968, Sep. 2005, doi: 10.1016/J.CELL.2005.08.029.

[108] K. Hu, J. Carroll, S. Fedorovich, C. Rickman, A. Sukhodub, and B. Davietov, “Vesicular restriction of synaptobrevin suggests a role for calcium in membrane fusion,” *Nature*, vol. 415, no. 6872, pp. 646–650, Feb. 2002, doi: 10.1038/415646A.

[109] J. B. Sørensen *et al.*, “The SNARE protein SNAP-25 is linked to fast calcium triggering of exocytosis,” *Proc Natl Acad Sci U S A*, vol. 99, no. 3, pp. 1627–1632, Feb. 2002, doi: 10.1073/PNAS.251673298.

[110] Y. T. Liu *et al.*, “PRRT2 mutations lead to neuronal dysfunction and neurodevelopmental defects,” *Oncotarget*, vol. 7, no. 26, p. 39184, Jun. 2016, doi: 10.18632/ONCOTARGET.9258.

[111] J. Schwenk *et al.*, “Regional diversity and developmental dynamics of the AMPA-receptor proteome in the mammalian brain,” *Neuron*, vol. 84, no. 1, pp. 41–54, Oct. 2014, doi: 10.1016/J.NEURON.2014.08.044.

[112] M. Li *et al.*, “PRRT2 Mutant Leads to Dysfunction of Glutamate Signaling,” *OPEN ACCESS Int. J. Mol. Sci*, vol. 16, p. 16, 2015, doi: 10.3390/ijms16059134.

[113] J. Schwenk *et al.*, “Regional Diversity and Developmental Dynamics of the AMPA-Receptor Proteome in the Mammalian Brain,” *Neuron*, vol. 84, no. 1, pp. 41–54, Oct. 2014, doi: 10.1016/J.NEURON.2014.08.044.

[114] J. Lee *et al.*, “CHARMM-GUI Input Generator for NAMD, GROMACS, AMBER, OpenMM, and CHARMM/OpenMM Simulations Using the CHARMM36 Additive Force Field,” *J Chem Theory Comput*, vol. 12, no. 1, pp. 405–413, Jan. 2016, doi: 10.1021/ACS.JCTC.5B00935/SUPPL_FILE/CT5B00935_SI_001.PDF.

[115] M. Hollmann and S. Heinemann, “Cloned Glutamate Receptors,” *http://dx.doi.org/10.1146/annurev.ne.17.030194.000335*, vol. 17, pp. 31–108, Nov. 2003, doi: 10.1146/ANNUREV.NE.17.030194.000335.

[116] P. H. Seeburg, “The TINS/TiPS Lecture. The molecular biology of mammalian glutamate receptor channels,” *Trends Neurosci*, vol. 16, no. 9, pp. 359–365, 1993, doi: 10.1016/0166-2236(93)90093-2.

[117] A. I. Sobolevsky, M. P. Rosconi, and E. Gouaux, “X-ray structure, symmetry and mechanism of an AMPA-subtype glutamate receptor,” *Nature 2009 462:7274*, vol. 462, no. 7274, pp. 745–756, Nov. 2009, doi: 10.1038/nature08624.

[118] A. D. Milstein, W. Zhou, S. Karimzadegan, D. S. Bredt, and R. A. Nicoll, “TARP subtypes differentially and dose-dependently control synaptic AMPA receptor gating,” *Neuron*, vol. 55, no. 6, pp. 905–918, Sep. 2007, doi: 10.1016/J.NEURON.2007.08.022.

[119] S. Tomita *et al.*, “Functional studies and distribution define a family of transmembrane AMPA receptor regulatory proteins,” *J Cell Biol*, vol. 161, no. 4, p. 805, May 2003, doi: 10.1083/JCB.200212116.

[120] R. Holm, M. S. Toustrup-Jensen, A. P. Einholm, V. R. Schack, J. P. Andersen, and B. Vilsen, “Neurological disease mutations of α3 Na+,K+-ATPase: Structural and functional perspectives and rescue of compromised function,” *Biochimica et Biophysica Acta (BBA) - Bioenergetics*, vol. 1857, no. 11, pp. 1807–1828, Nov. 2016, doi: 10.1016/J.BBABIO.2016.08.009.

[121] L. Peng, E. Arystarkhova, and K. J. Sweadner, “Plasticity of Na,K-ATPase Isoform Expression in Cultures of Flat Astrocytes: Species Differences in Gene Expression,” *Glia*, vol. 24, pp. 257–271, 1998, doi: 10.1002/(SICI)1098-1136(199811)24:3.

[122] M. V. Clausen, F. Hilbers, and H. Poulsen, “The structure and function of the Na,K-ATPase isoforms in health and disease,” *Front Physiol*, vol. 8, no. JUN, p. 371, Jun. 2017, doi: 10.3389/FPHYS.2017.00371/BIBTEX.

[123] A. N. Shrivastava, A. Triller, and R. Melki, “Cell biology and dynamics of Neuronal Na+/K+-ATPase in health and diseases,” *Neuropharmacology*, vol. 169, p. 107461, Jun. 2020, doi: 10.1016/J.NEUROPHARM.2018.12.008.

[124] R. Zahler, Z. T. Zhang, M. Manor, and W. F. Boron, “Sodium Kinetics of Na,K-ATPase α Isoforms in Intact Transfected HeLa Cells,” *Journal of General Physiology*, vol. 110, no. 2, pp. 201–213, Aug. 1997, doi: 10.1085/JGP.110.2.201.

[125] B. R. Larsen, A. Stoica, and N. MacAulay, “Managing Brain Extracellular K+ during Neuronal Activity: The Physiological Role of the Na+/K+-ATPase Subunit Isoforms,” *Front Physiol*, vol. 7, no. APR, p. 141, Apr. 2016, doi: 10.3389/FPHYS.2016.00141.

[126] K. P. Schlingmann *et al.*, “Germline De Novo Mutations in ATP1A1 Cause Renal Hypomagnesemia, Refractory Seizures, and Intellectual Disability,” *Am J Hum Genet*, vol. 103, no. 5, p. 808, Nov. 2018, doi: 10.1016/J.AJHG.2018.10.004.

[127] B. Sterlini *et al.*, “An interaction between PRRT2 and Na+/K+ ATPase contributes to the control of neuronal excitability,” *Cell Death Dis*, vol. 12, no. 4, Apr. 2021, doi: 10.1038/S41419-021-03569-Z.

[128] W. A. Catterall, E. Perez-Reyes, T. P. Snutch, and J. Striessnig, “International Union of Pharmacology. XLVIII. Nomenclature and Structure-Function Relationships of Voltage-Gated Calcium Channels,” *Pharmacol Rev*, vol. 57, no. 4, pp. 411–425, Dec. 2005, doi: 10.1124/PR.57.4.5.

[129] F. H. Yu and W. A. Catterall, “Overview of the voltage-gated sodium channel family,” *Genome Biol*, vol. 4, p. 207, 2003, Accessed: Jan. 09, 2023. [Online]. Available: http://genomebiology.com/2003/4/3/207

[130] E. Nanou and W. A. Catterall, “Calcium Channels, Synaptic Plasticity, and Neuropsychiatric Disease,” *Neuron*, vol. 98, no. 3, pp. 466–481, May 2018, doi: 10.1016/J.NEURON.2018.03.017.

[131] F. Hofmann, M. Biel, and V. Flockerzi, “Molecular Basis for CA2+ Channel Diversity,” *http://dx.doi.org/10.1146/annurev.ne.17.030194.002151*, vol. 17, pp. 399–418, Nov. 2003, doi: 10.1146/ANNUREV.NE.17.030194.002151.

[132] F. Fruscione *et al.*, “PRRT2 controls neuronal excitability by negatively modulating Na+ channel 1.2/1.6 activity,” *Brain*, vol. 141, no. 4, p. 1000, Apr. 2018, doi: 10.1093/BRAIN/AWY051.

[133] K. Dunlap, J. I. Luebke, and T. J. Turner, “Exocytotic Ca2+ channels in mammalian central neurons,” *Trends Neurosci*, vol. 18, no. 2, pp. 89–98, Feb. 1995, doi: 10.1016/0166-2236(95)80030-6.

[134] D. B. Wheeler, A. Randall, and R. W. Tsien, “Roles of N-Type and Q-Type Ca2+ Channels in Supporting Hippocampal Synaptic Transmission,” *Science (1979)*, vol. 264, no. 5155, pp. 107–111, 1994, doi: 10.1126/SCIENCE.7832825.

[135] R. Llinás, M. Sugimori, D. E. Hillman, and B. Cherksey, “Distribution and functional significance of the P-type, voltage-dependent Ca2+ channels in the mammalian central nervous system,” *Trends Neurosci*, vol. 15, no. 9, pp. 351–355, Sep. 1992, doi: 10.1016/0166-2236(92)90053-B.

[136] E. F. Stanley and R. R. Mirotznik, “Cleavage of syntaxin prevents G-protein regulation of presynaptic calcium channels,” *Nature 1997 385:6614*, vol. 385, no. 6614, pp. 340–343, Jan. 1997, doi: 10.1038/385340a0.

[137] D. Ferrante *et al.*, “PRRT2 modulates presynaptic Ca2+ influx by interacting with P/Q-type channels,” *Cell Rep*, vol. 35, no. 11, Jun. 2021, doi: 10.1016/J.CELREP.2021.109248.

[138] H. Lerche, “Synaptic or ion channel modifier? PRRT2 is a chameleon-like regulator of neuronal excitability,” *Brain*, vol. 141, no. 4, pp. 938–941, Apr. 2018, doi: 10.1093/BRAIN/AWY073.

[139] W. A. Catterall, “Structure and Function of Voltage-Gated Sodium Channels at Atomic Resolution,” *Exp Physiol*, vol. 99, no. 1, pp. 35–51, 2014, doi: 10.1113/EXPPHYSIOL.2013.071969.

[140] M. Noda *et al.*, “Expression of functional sodium channels from cloned cDNA,” *Nature 1986 322:6082*, vol. 322, no. 6082, pp. 826–828, 1986, doi: 10.1038/322826a0.

[141] M. De Lera Ruiz and R. L. Kraus, “Voltage-Gated Sodium Channels: Structure, Function, Pharmacology, and Clinical Indications,” *J Med Chem*, vol. 58, no. 18, pp. 7093–7118, Sep. 2015, doi: 10.1021/JM501981G/ASSET/IMAGES/LARGE/JM-2014-01981G_0013.JPEG.

[142] D. Dolivo *et al.*, “The Nax (SCN7A) channel: an atypical regulator of tissue homeostasis and disease,” *Cellular and Molecular Life Sciences*, vol. 78, no. 14, pp. 5469–5488, Jul. 2021, doi: 10.1007/S00018-021-03854-2/FIGURES/2.

[143] S. G. Waxman, “Sodium channels, the electrogenisome and the electrogenistat: lessons and questions from the clinic,” *J Physiol*, vol. 590, no. Pt 11, p. 2601, Jun. 2012, doi: 10.1113/JPHYSIOL.2012.228460.

[144] D. Gordon *et al.*, “Tissue-specific expression of the RI and RII sodium channel subtypes.,” *Proc Natl Acad Sci U S A*, vol. 84, no. 23, p. 8682, 1987, doi: 10.1073/PNAS.84.23.8682.

[145] E. Watanabe *et al.*, “Nav2/NaG Channel Is Involved in Control of Salt-Intake Behavior in the CNS,” *The Journal of Neuroscience*, vol. 20, no. 20, p. 7743, Oct. 2000, doi: 10.1523/JNEUROSCI.20-20-07743.2000.

[146] W. E. Crill, “Persistent Sodium Current in Mammalian Central Neurons,” *https://doi.org/10.1146/annurev.ph.58.030196.002025*, vol. 58, pp. 349–362, Nov. 2003, doi: 10.1146/ANNUREV.PH.58.030196.002025.

[147] I. M. Raman and B. P. Bean, “Resurgent Sodium Current and Action Potential Formation in Dissociated Cerebellar Purkinje Neurons,” *Journal of Neuroscience*, vol. 17, no. 12, pp. 4517–4526, Jun. 1997, doi: 10.1523/JNEUROSCI.17-12-04517.1997.

[148] F. S. Afshari *et al.*, “Resurgent Na currents in four classes of neurons of the cerebellum,” *J Neurophysiol*, vol. 92, no. 5, pp. 2831–2843, Nov. 2004, doi: 10.1152/JN.00261.2004/ASSET/IMAGES/LARGE/Z9K0110441910009.JPEG.

[149] C. E. Stafstrom, P. E. Schwindt, and W. E. Crill, “Repetitive firing in layer V neurons from cat neocortex in vitro,” *https://doi.org/10.1152/jn.1984.52.2.264*, vol. 52, no. 2, pp. 264–277, 1984, doi: 10.1152/JN.1984.52.2.264.

[150] Z. M. Khaliq, N. W. Gouwens, and I. M. Raman, “The Contribution of Resurgent Sodium Current to High-Frequency Firing in Purkinje Neurons: An Experimental and Modeling Study,” *Journal of Neuroscience*, vol. 23, no. 12, pp. 4899–4912, Jun. 2003, doi: 10.1523/JNEUROSCI.23-12-04899.2003.

[151] I. M. Raman and B. P. Bean, “Resurgent Sodium Current and Action Potential Formation in Dissociated Cerebellar Purkinje Neurons,” *Journal of Neuroscience*, vol. 17, no. 12, pp. 4517–4526, Jun. 1997, doi: 10.1523/JNEUROSCI.17-12-04517.1997.

[152] J. S. Bant and I. M. Raman, “Control of transient, resurgent, and persistent current by open-channel block by Na channel β4 in cultured cerebellar granule neurons,” *Proc Natl Acad Sci U S A*, vol. 107, no. 27, p. 12357, Jul. 2010, doi: 10.1073/PNAS.1005633107.

[153] Y. Chen, F. H. Yu, E. M. Sharp, D. Beacham, T. Scheuer, and W. A. Catterall, “Functional Properties and Differential Neuromodulation of Nav1.6 Channels,” *Mol Cell Neurosci*, vol. 38, no. 4, p. 607, Aug. 2008, doi: 10.1016/J.MCN.2008.05.009.

[154] P. M. Casillas-Espinosa, K. L. Powell, and T. J. O’Brien, “Regulators of synaptic transmission: Roles in the pathogenesis and treatment of epilepsy,” *Epilepsia*, vol. 53, pp. 41–58, 2012, doi: 10.1111/EPI.12034.

[155] K. Staley, “Molecular mechanisms of epilepsy”, doi: 10.1038/nn.3947.

[156] B. Zhou *et al.*, “Hyperactive putamen in patients with paroxysmal kinesigenic choreoathetosis: A resting-state functional magnetic resonance imaging study,” *Movement Disorders*, vol. 25, no. 9, pp. 1226–1231, Jul. 2010, doi: 10.1002/MDS.22967.

[157] C. Luo, Y. Chen, W. Song, Q. Chen, Q. Gong, and H. F. Shang, “Altered intrinsic brain activity in patients with paroxysmal kinesigenic dyskinesia by PRRT2 mutation: Altered brain activity by PRRT2 mutation,” *Neurological Sciences*, vol. 34, no. 11, pp. 1925–1931, Nov. 2013, doi: 10.1007/S10072-013-1408-7/TABLES/2.

[158] M. S. Grubb and J. Burrone, “Activity-dependent relocation of the axon initial segment fine-tunes neuronal excitability,” *Nature*, vol. 465, no. 7301, p. 1070, Jun. 2010, doi: 10.1038/NATURE09160.

[159] M. Mantegazza, S. Cestèle, and W. A. Catterall, “Sodium channelopathies of skeletal muscle and brain,” *Physiol Rev*, vol. 101, no. 4, p. 1633, Oct. 2021, doi: 10.1152/PHYSREV.00025.2020.

[160] M. Mantegazza, G. Curia, G. Biagini, D. S. Ragsdale, and M. Avoli, “Voltage-gated sodium channels as therapeutic targets in epilepsy and other neurological disorders,” *Lancet Neurol*, vol. 9, no. 4, pp. 413–424, Apr. 2010, doi: 10.1016/S1474-4422(10)70059-4.

[161] R. Guerrini, C. Marini, and M. Mantegazza, “Genetic epilepsy syndromes without structural brain abnormalities: clinical features and experimental models,” *Neurotherapeutics*, vol. 11, no. 2, pp. 269–285, Apr. 2014, doi: 10.1007/S13311-014-0267-0.

[162] A. Brunklaus *et al.*, “Biological concepts in human sodium channel epilepsies and their relevance in clinical practice,” *Epilepsia*, vol. 61, no. 3, pp. 387–399, Mar. 2020, doi: 10.1111/EPI.16438.

[163] M. H. Meisler, J. E. O’Brien, and L. M. Sharkey, “Sodium channel gene family: epilepsy mutations, gene interactions and modifier effects,” *J Physiol*, vol. 588, no. Pt 11, p. 1841, Jun. 2010, doi: 10.1113/JPHYSIOL.2010.188482.

[164] I. E. Scheffer *et al.*, “ILAE Classification of the Epilepsies Position Paper of the ILAE Commission for Classification and Terminology,” *Epilepsia*, vol. 58, no. 4, p. 512, Apr. 2017, doi: 10.1111/EPI.13709.

[165] W. A. Catterall, A. L. Goldin, and S. G. Waxman, “International Union of Pharmacology. XLVII. Nomenclature and Structure-Function Relationships of Voltage-Gated Sodium Channels,” *Pharmacol Rev*, vol. 57, no. 4, pp. 397–409, Dec. 2005, doi: 10.1124/PR.57.4.4.

[166] T. Sugawara *et al.*, “A missense mutation of the Na+ channel αII subunit gene Nav1.2 in a patient with febrile and afebrile seizures causes channel dysfunction,” *Proc Natl Acad Sci U S A*, vol. 98, no. 11, p. 6384, May 2001, doi: 10.1073/PNAS.111065098.

[167] S. F. Berkovic *et al.*, “Benign familial neonatal-infantile seizures: Characterization of a new sodium channelopathy,” *Ann Neurol*, vol. 55, no. 4, pp. 550–557, Apr. 2004, doi: 10.1002/ANA.20029.

[168] S. E. Heron *et al.*, “Sodium-channel defects in benign familial neonatal-infantile seizures,” *Lancet*, vol. 360, no. 9336, pp. 851–852, Sep. 2002, doi: 10.1016/S0140-6736(02)09968-3.

[169] S. J. Sanders *et al.*, “Progress in understanding and treating SCN2A-mediated disorders,” *Trends Neurosci*, vol. 41, no. 7, p. 442, Jul. 2018, doi: 10.1016/J.TINS.2018.03.011.

[170] R. Guerrini, V. Conti, M. Mantegazza, S. Balestrini, A. S. Galanopoulou, and F. Benfenati, “Developmental and epileptic encephalopathies: from genetic heterogeneity to phenotypic continuum,” *Physiol Rev*, vol. 103, no. 1, pp. 433–513, Jan. 2023, doi: 10.1152/PHYSREV.00063.2021.

[171] M. Wolff *et al.*, “Genetic and phenotypic heterogeneity suggest therapeutic implications in SCN2A-related disorders,” *Brain*, vol. 140, no. 5, pp. 1316–1336, May 2017, doi: 10.1093/BRAIN/AWX054.

[172] M. M. Trudeau, J. C. Dalton, J. W. Day, L. P. W. Ranum, and M. H. Meisler, “Heterozygosity for a protein truncation mutation of sodium channel SCN8A in a

patient with cerebellar atrophy, ataxia, and mental retardation," *J Med Genet*, vol. 43, no. 6, p. 527, Jun. 2006, doi: 10.1136/JMG.2005.035667.

[173] E. Gardella *et al.*, "The phenotype of SCN8A developmental and epileptic encephalopathy," *Neurology*, vol. 91, no. 12, pp. 1112–1124, Sep. 2018, doi: 10.1212/WNL.0000000000006199.

[174] E. Gardella *et al.*, "Benign infantile seizures and paroxysmal dyskinesia caused by an SCN8A mutation," *Ann Neurol*, vol. 79, no. 3, pp. 428–436, Mar. 2016, doi: 10.1002/ANA.24580.

[175] K. M. Johannesen *et al.*, "The spectrum of intermediate SCN8A-related epilepsy," *Epilepsia*, vol. 60, no. 5, pp. 830–844, May 2019, doi: 10.1111/EPI.14705.

[176] J. D. Calhoun and L. L. Isom, "The role of non-pore-forming b subunits in physiology and pathophysiology of voltage-gated sodium channels," *Handb Exp Pharmacol*, vol. 221, pp. 51–89, 2014, doi: 10.1007/978-3-642-41588-3_4/FIGURES/5.

[177] L. L. Isom *et al.*, "Primary structure and functional expression of the β1 subunit of the rat brain sodium channel," *Science (1979)*, vol. 256, no. 5058, pp. 839–842, 1992, doi: 10.1126/SCIENCE.1375395.

[178] K. Morgan *et al.*, "β3: An additional auxiliary subunit of the voltage-sensitive sodium channel that modulates channel gating with distinct kinetics," *Proc Natl Acad Sci U S A*, vol. 97, no. 5, p. 2308, Feb. 2000, doi: 10.1073/PNAS.030362197.

[179] S. K. G. Maier, R. E. Westenbroek, K. A. McCormick, R. Curtis, T. Scheuer, and W. A. Catterall, "Distinct Subcellular Localization of Different Sodium Channel α and β Subunits in Single Ventricular Myocytes From Mouse Heart," *Circulation*, vol. 109, no. 11, pp. 1421–1427, Mar. 2004, doi: 10.1161/01.CIR.0000121421.61896.24.

[180] W. J. Brackenbury *et al.*, "Functional reciprocity between Na+ channel Nav1.6 and β1 subunits in the coordinated regulation of excitability and neurite outgrowth," *Proc Natl Acad Sci U S A*, vol. 107, no. 5, p. 2283, Feb. 2010, doi: 10.1073/PNAS.0909434107.

[181] E. Aronica *et al.*, "Expression and regulation of voltage-gated sodium channel β1 subunit protein in human gliosis-associated pathologies," *Acta Neuropathol*, vol. 105, no. 5, pp. 515–523, May 2003, doi: 10.1007/S00401-003-0677-2/FIGURES/3.

[182] A. J. Fein, M. A. Wright, E. A. Slat, A. B. Ribera, and L. L. Isom, "scn1bb, a Zebrafish Ortholog of SCN1B Expressed in Excitable and Nonexcitable Cells, Affects Motor Neuron Axon Morphology and Touch Sensitivity," *The Journal of Neuroscience*, vol. 28, no. 47, p. 12510, Nov. 2008, doi: 10.1523/JNEUROSCI.4329-08.2008.

[183] W. J. Brackenbury and L. L. Isom, "Na+ Channel β Subunits: Overachievers of the Ion Channel Family," *Front Pharmacol*, vol. 2, 2011, doi: 10.3389/FPHAR.2011.00053.

[184] K. A. Kazen-Gillespie, D. S. Ragsdale, M. R. D'Andreall, L. N. Mattei, K. E. Rogers, and L. L. Isom, "Cloning, localization, and functional expression of sodium channel β1A subunits," *Journal of Biological Chemistry*, vol. 275, no. 2, pp. 1079–1088, Jan. 2000, doi: 10.1074/jbc.275.2.1079.

[185] G. A. Patino *et al.*, "Voltage-Gated Na+ Channel β1B: A Secreted Cell Adhesion Molecule Involved in Human Epilepsy," *The Journal of Neuroscience*, vol. 31, no. 41, p. 14577, Oct. 2011, doi: 10.1523/JNEUROSCI.0361-11.2011.

[186] B. S. Shah, E. B. Stevens, R. D. Pinnock, A. K. Dixon, and K. Lee, "Developmental expression of the novel voltage-gated sodium channel auxiliary subunit β3, in rat CNS," *J Physiol*, vol. 534, no. Pt 3, p. 763, Aug. 2001, doi: 10.1111/J.1469-7793.2001.T01-1-00763.X.

[187] J. W. Theile and T. R. Cummins, "Inhibition of Navβ4 Peptide-Mediated Resurgent Sodium Currents in Nav1.7 Channels by Carbamazepine, Riluzole, and Anandamide," *Mol Pharmacol*, vol. 80, no. 4, p. 724, Oct. 2011, doi: 10.1124/MOL.111.072751.

[188] U. K. Laemmli, "Cleavage of Structural Proteins during the Assembly of the Head of Bacteriophage T4," *Nature 1970 227:5259*, vol. 227, no. 5259, pp. 680–685, 1970, doi: 10.1038/227680a0.

[189] J. C. Phillips *et al.*, "Scalable molecular dynamics on CPU and GPU architectures with NAMD," *J Chem Phys*, vol. 153, no. 4, p. 44130, Jul. 2020, doi: 10.1063/5.0014475.

[190] B. R. Brooks *et al.*, "CHARMM: the biomolecular simulation program," *J Comput Chem*, vol. 30, no. 10, pp. 1545–1614, Jul. 2009, doi: 10.1002/JCC.21287.

[191] J. Huang *et al.*, "CHARMM36m: an improved force field for folded and intrinsically disordered proteins," *Nat Methods*, vol. 14, no. 1, pp. 71–73, Dec. 2017, doi: 10.1038/NMETH.4067.

[192] S. Jo, T. Kim, V. G. Iyer, and W. Im, "CHARMM-GUI: a web-based graphical user interface for CHARMM," *J Comput Chem*, vol. 29, no. 11, pp. 1859–1865, Aug. 2008, doi: 10.1002/JCC.20945.

[193] M. A. Lomize, I. D. Pogozheva, H. Joo, H. I. Mosberg, and A. L. Lomize, "OPM database and PPM web server: resources for positioning of proteins in membranes," *Nucleic Acids Res*, vol. 40, no. Database issue, p. D370, Jan. 2012, doi: 10.1093/NAR/GKR703.

[194] E. Neria, S. Fischer, and M. Karplus, "Simulation of activation free energies in molecular systems," *Journal of Chemical Physics*, vol. 105, no. 5, pp. 1902–1921, Aug. 1996, doi: 10.1063/1.472061.

[195] T. Darden, D. York, and L. Pedersen, "Particle mesh Ewald: An N·log(N) method for Ewald sums in large systems," *J Chem Phys*, vol. 98, no. 12, p. 10089, Aug. 1998, doi: 10.1063/1.464397.

[196] H. C. Andersen, “Rattle: A ‘Velocity’ Version of the Shake Algorithm for Molecular Dynamics Calculations”.

[197] S. E. Feller, Y. Zhang, R. W. Pastor, and B. R. Brooks, “Constant pressure molecular dynamics simulation: The Langevin piston method,” *J Chem Phys*, vol. 103, no. 11, p. 4613, Jun. 1998, doi: 10.1063/1.470648.

[198] C. W. Hopkins, S. Le Grand, R. C. Walker, and A. E. Roitberg, “Long-time-step molecular dynamics through hydrogen mass repartitioning,” *J Chem Theory Comput*, vol. 11, no. 4, pp. 1864–1874, Apr. 2015, doi: 10.1021/CT5010406/ASSET/IMAGES/MEDIUM/CT-2014-010406_0018.GIF.

[199] C. Balusek *et al.*, “Accelerating membrane simulations with Hydrogen Mass Repartitioning HHS Public Access,” *J Chem Theory Comput*, vol. 15, no. 8, pp. 4673–4686, 2019, doi: 10.1021/acs.jctc.9b00160.

[200] W. Humphrey, A. Dalke, and K. Schulten, “VMD: Visual molecular dynamics,” *J Mol Graph*, vol. 14, no. 1, pp. 33–38, Feb. 1996, doi: 10.1016/0263-7855(96)00018-5.

[201] G. H. Tan *et al.*, “PRRT2 deficiency induces paroxysmal kinesigenic dyskinesia by regulating synaptic transmission in cerebellum,” *Cell Res*, vol. 28, no. 1, p. 90, Jan. 2018, doi: 10.1038/CR.2017.128.

[202] B. P. Bean, “The molecular machinery of resurgent sodium current revealed,” *Neuron*, vol. 45, no. 2, pp. 185–187, Jan. 2005, doi: 10.1016/j.neuron.2005.01.006.

[203] T. K. Aman *et al.*, “Regulation of Persistent Na Current by Interactions between β Subunits of Voltage-Gated Na Channels,” *The Journal of Neuroscience*, vol. 29, no. 7, p. 2027, Feb. 2009, doi: 10.1523/JNEUROSCI.4531-08.2009.

[204] F. H. Yu *et al.*, “Sodium Channel β4, a New Disulfide-Linked Auxiliary Subunit with Similarity to β2,” *The Journal of Neuroscience*, vol. 23, no. 20, p. 7577, Aug. 2003, doi: 10.1523/JNEUROSCI.23-20-07577.2003.

[205] T. Kiss, “Persistent Na-channels: Origin and function: A review János Salánki memory lecture,” *Acta Biol Hung*, vol. 59, no. Issue Supplement-2, pp. 1–12, Jun. 2008, doi: 10.1556/ABIOL.59.2008.SUPPL.1.

[206] B. P. Bean, “The molecular machinery of resurgent sodium current revealed,” *Neuron*, vol. 45, no. 2, pp. 185–187, Jan. 2005, doi: 10.1016/j.neuron.2005.01.006.

[207] Y. Chen, F. H. Yu, E. M. Sharp, D. Beacham, T. Scheuer, and W. A. Catterall, “Functional Properties and Differential Neuromodulation of Nav1.6 Channels,” *Mol Cell Neurosci*, vol. 38, no. 4, p. 607, Aug. 2008, doi: 10.1016/J.MCN.2008.05.009.

[208] S. Weston, S. Czieso, I. J. White, S. E. Smith, P. Kellam, and M. Marsh, “A Membrane Topology Model for Human Interferon Inducible Transmembrane Protein 1,” *PLoS One*, vol. 9, no. 8, p. 104341, Aug. 2014, doi: 10.1371/JOURNAL.PONE.0104341.

[209] B. Lu *et al.*, “Cerebellar spreading depolarization mediates paroxysmal movement disorder,” *Cell Rep*, vol. 36, no. 12, Sep. 2021, doi: 10.1016/j.celrep.2021.109743.

[210] E. C. Merrick *et al.*, “The importance of serine 161 in the sodium channel β3 subunit for modulation of Na v 1.2 gating,” *Pflugers Arch*, vol. 460, no. 4, pp. 743–753, 2010, doi: 10.1007/s00424-009-0739-y.

[211] C. C. Kuo, R. S. Chen, L. Lu, and R. C. Chen, “Carbamazepine Inhibition of Neuronal Na+ Currents: Quantitative Distinction from Phenytoin and Possible Therapeutic Implications,” *Mol Pharmacol*, vol. 51, no. 6, pp. 1077–1083, Jun. 1997, doi: 10.1124/MOL.51.6.1077.

[212] G. H. Tan *et al.*, “PRRT2 deficiency induces paroxysmal kinesigenic dyskinesia by regulating synaptic transmission in cerebellum,” *Cell Res*, vol. 28, no. 1, p. 90, Jan. 2018, doi: 10.1038/CR.2017.128.

[213] S. Das, J. Gilchrist, F. Bosmans, and F. Van Petegem, “Binary architecture of the Nav 1.2-β2 signaling complex,” *Elife*, vol. 5, no. FEBRUARY2016, Feb. 2016, doi: 10.7554/ELIFE.10960.

[214] T. Zimmer and K. Benndorf, “The Intracellular Domain of the β2 Subunit Modulates the Gating of Cardiac Nav1.5 Channels,” *Biophys J*, vol. 92, no. 11, p. 3885, Jun. 2007, doi: 10.1529/BIOPHYSJ.106.098889.

[215] T. M. Grieco, J. D. Malhotra, C. Chen, L. L. Isom, and I. M. Raman, “Open-channel block by the cytoplasmic tail of sodium channel β4 as a mechanism for resurgent sodium current,” *Neuron*, vol. 45, no. 2, pp. 233–244, Jan. 2005, doi: 10.1016/j.neuron.2004.12.035.

[216] Y. Y. Vilin and P. C. Ruben, “Slow inactivation in voltage-gated sodium channels: molecular substrates and contributions to channelopathies,” *Cell Biochem Biophys*, vol. 35, no. 2, pp. 171–190, 2001, doi: 10.1385/CBB:35:2:171.

[217] W. Ulbricht, “Sodium channel inactivation: Molecular determinants and modulation,” *Physiol Rev*, vol. 85, no. 4, pp. 1271–1301, Oct. 2005, doi: 10.1152/PHYSREV.00024.2004/ASSET/IMAGES/LARGE/Z9J004050385S003.JPEG.

[218] F. Binda, P. Valente, A. Marte, P. Baldelli, and F. Benfenati, “Increased responsiveness at the cerebellar input stage in the PRRT2 knockout model of paroxysmal kinesigenic dyskinesia,” *Neurobiol Dis*, vol. 152, p. 105275, May 2021, doi: 10.1016/J.NBD.2021.105275.

[219] J. Schmidt, S. Rossie, and W. A. Catterall, “A large intracellular pool of inactive Na channel a subunits in developing rat brain (ion transport/neurons/cell culture/posttranslational processing/anti-Nat channel antibodies),” *Neurobiology*, vol. 82, pp. 4847–4851, 1985.

[220] C. J. Waecht Er #&!, J. W. Schmidtl, and W. A. Catteralll, “Glycosylation Is Required for Maintenance of Functional Sodium Channels in Neuroblastoma Cells*,” *Journal of Biological Chemistry*, vol. 258, no. 8, pp. 5117–5123, 1983, doi: 10.1016/S0021-9258(18)32546-8.

[221] H. A. O'Malley and L. L. Isom, "Sodium channel β subunits: emerging targets in channelopathies," *Annu Rev Physiol*, vol. 77, p. 481, Feb. 2015, doi: 10.1146/ANNUREV-PHYSIOL-021014-071846.

[222] S. Molinarolo *et al.*, "Cross-kingdom auxiliary subunit modulation of a voltage-gated sodium channel," *J Biol Chem*, vol. 293, no. 14, p. 4981, Apr. 2018, doi: 10.1074/JBC.RA117.000852.

[223] C. J. Laedermann, N. Syam, M. Pertin, I. Decosterd, and H. Abriel, "β1- and β3-voltage-gated sodium channel subunits modulate cell surface expression and glycosylation of Nav1.7 in HEK293 cells," *Front Cell Neurosci*, vol. 7, no. AUG, Aug. 2013, doi: 10.3389/FNCEL.2013.00137/ABSTRACT.

[224] E. Cortada, R. Brugada, and M. Verges, "N-Glycosylation of the voltage-gated sodium channel β2 subunit is required for efficient trafficking of NaV1.5/β2 to the plasma membrane," *J Biol Chem*, vol. 294, no. 44, p. 16123, Nov. 2019, doi: 10.1074/JBC.RA119.007903.

[225] K. Kazarinova-Noyes *et al.*, "Contactin Associates with Na+ Channels and Increases Their Functional Expression," *The Journal of Neuroscience*, vol. 21, no. 19, p. 7517, Oct. 2001, doi: 10.1523/JNEUROSCI.21-19-07517.2001.

[226] J. Coleman *et al.*, "PRRT2 Regulates Synaptic Fusion by Directly Modulating SNARE Complex Assembly," *Cell Rep*, vol. 22, no. 3, p. 820, Jan. 2018, doi: 10.1016/J.CELREP.2017.12.056.

[227] E. Savino *et al.*, "Proline-rich transmembrane protein 2 (PRRT2) regulates the actin cytoskeleton during synaptogenesis," *Cell Death Dis*, vol. 11, no. 10, Oct. 2020, doi: 10.1038/S41419-020-03073-W.

[228] E. Savino, F. C. Guarnieri, J. W. Tsai, A. Corradi, F. Benfenati, and F. Valtorta, "An Emerging Role of PRRT2 in Regulating Growth Cone Morphology," *Cells*, vol. 10, no. 10, Oct. 2021, doi: 10.3390/CELLS10102666.

[229] C. Michetti, A. Corradi, and F. Benfenati, "PRRT2, a network stability gene," *Oncotarget*, vol. 8, no. 34, p. 55770, Aug. 2017, doi: 10.18632/ONCOTARGET.19506.

[230] J. H. Döring *et al.*, "Efficacy, Tolerability, and Retention of Antiseizure Medications in PRRT2-Associated Infantile Epilepsy," 2022, doi: 10.1212/NXG.0000000000200020.

[231] I. C. Chou *et al.*, "Successful control with carbamazepine of family with paroxysmal kinesigenic dyskinesia of PRRT2 mutation," *Biomedicine (Taipei)*, vol. 4, no. 2, pp. 51–53, Jun. 2014, doi: 10.7603/S40681-014-0015-0.

[232] J. M. DeKeyser, C. H. Thompson, and A. L. George, "Cryptic prokaryotic promoters explain instability of recombinant neuronal sodium channels in bacteria," *Journal of Biological Chemistry*, vol. 296, p. 100298, Jan. 2021, doi: 10.1016/j.jbc.2021.100298.

[233] J. Jumper *et al.*, “Highly accurate protein structure prediction with AlphaFold,” *Nature 2021 596:7873*, vol. 596, no. 7873, pp. 583–589, Jul. 2021, doi: 10.1038/s41586-021-03819-2.

[234] R. E. Ithuralde, A. E. Roitberg, and A. G. Turjanski, “Structured and Unstructured Binding of an Intrinsically Disordered Protein as Revealed by Atomistic Simulations,” *J Am Chem Soc*, vol. 138, no. 28, pp. 8742–8751, Jul. 2016, doi: 10.1021/JACS.6B02016/SUPPL_FILE/JA6B02016_SI_001.PDF.

[235] E. Savino *et al.*, “An Emerging Role of PRRT2 in Regulating Growth Cone Morphology,” *Cells 2021, Vol. 10, Page 2666*, vol. 10, no. 10, p. 2666, Oct. 2021, doi: 10.3390/CELLS10102666.

[236] J. G. Lu *et al.*, “A novel PRRT2 pathogenic variant in a family with paroxysmal kinesigenic dyskinesia and benign familial infantile seizures,” *Cold Spring Harb Mol Case Stud*, vol. 4, no. 1, Feb. 2018, doi: 10.1101/MCS.A002287/-/DC1.

[237] P. Valente *et al.*, “Constitutive Inactivation of the PRRT2 Gene Alters Short-Term Synaptic Plasticity and Promotes Network Hyperexcitability in Hippocampal Neurons,” *Cerebral Cortex*, vol. 29, no. 5, pp. 2010–2033, May 2019, doi: 10.1093/CERCOR/BHY079.

[238] F. Binda, P. Valente, A. Marte, P. Baldelli, and F. Benfenati, “Increased responsiveness at the cerebellar input stage in the PRRT2 knockout model of paroxysmal kinesigenic dyskinesia,” *Neurobiol Dis*, vol. 152, May 2021, doi: 10.1016/J.NBD.2021.105275.

[239] M. P. Forrest *et al.*, “Rescue of neuropsychiatric phenotypes in a mouse model of 16p11.2 duplication syndrome by genetic correction of an epilepsy network hub,” *Nat Commun*, vol. 14, no. 1, p. 825, Feb. 2023, doi: 10.1038/S41467-023-36087-X.

# LIST OF ABBREVIATIONS

AED: antiepileptic drug

AIS: axon initial segment

AMPARs: AMPA-type glutamate receptor complex

BAP: bacterial alkaline phosphatase

BFIE: benign familial infantile epilepsy

CAE: childhood-absence epilepsy

CBZ: especially carbamazepine

CNS: central nervous system

CNS: Central Nervous System

EA: episodic ataxia

eEPSCs: evoked excitatory postsynaptic currents

FS: febrile seizures

G/Gmax: Normalized conductance-voltage curve

G: conductance

GLUT1: Glucose Transporter 1

Gmax: maximal conductance

GRIA: GluA1 subunit

HAGH: hydroxyacylglutathione hydrolase

HM: hemiplegic migraine

I: current

IC: infantile convulsions

ICCA: infantile convulsions with choreoathetosis syndrome

ICCO: infantile convulsions and choreoathetosis

IFITM: Interferon induced transmembrane proteins

IFITM1: Induced Transmembrane Protein 1

Ig: immunoglobulin

J: current density

KO: knock-out

LRRT4: Leucine-Rich Repeat Transmembrane Neuronal Protein 4

MAGUK: membrane-associated guanylate kinase

MR-1: myofibrillogenesis regulator 1

Nav: voltage-gated $Na^+$ channels

NKA: $Na^+/K^+$ ATPase

PBS: phosphate-buffered saline

PD: paroxysmal disorder

PED: paroxysmal exercise-induced dyskinesias

PFA: paraformaldehyde

PHD: paroxysmal hypnogenic dyskinesia

PKD: paroxysmal kinesigenic diskinesia

PNKD: paroxysmal non-kinesigenic dyskinesia

PNS: peripheral nervous system

PRRT1: proline-rich transmembrane protein 1

PRRT2: proline-rich transmembrane protein 2

$R_s$: Series resistance

SLC2A1: solute carrier family 2 facilitated glucose transporter member 1

SNAP-25: synaptosomal-associated protein 25 kDa

SNARE: Soluble N-ethylmaleimide-sensitive factor attachment proteins receptor

SNARE: soluble n-ethylmaleimide-sensitive factor attachment proteins receptor

*SynDIG1*: synapse differentiation-induced gene 1

Syt1/2: synaptotagmins 1/2

V: voltage

$V_{0.5\ act}$: voltage of half-maximal activation

$V_{0.5\ inact}$: voltage of half-maximal inactivation

VAMP2: vesicle-associated membrane protein 2

VGCCs: The voltage-gated $Ca^{2+}$ channels

Vh: holding potential

β4 ptd: β4 C-terminal peptide

β-gal: β-galactosidase

# PAPERS

The data discussed in this thesis is subject of the following publications:

- P. Valente, A. Marte, **F. Franchi**, B. Sterlini, S. Casagrande, A. Corradi, P. Baldelli, Fabio B., “A push-pull mechanism between PRRT2 and β4 differentially regulates membrane exposure and biophysical properties of Nav1.2 sodium channels”, Mol Neurobiol 2022, Nov 28. doi: 10.1007/s12035-022-03112-x.

- **F. Franchi**, A. Marte, B. Corradi, B. Sterlini, G. Alberini, A. De Fusco, A. Vogel, L. Maragliano, P. Baldelli, A. Corradi, P. Valente, F. Benfenati, “The intramembrane COOH-terminal domain of PRRT2 regulates voltage-dependent Na+ channels”, J Biol Chem. Accepted for publication.

- B. Sterlini, **F. Franchi**, L. Morinelli, B. Corradi, C. Parodi, M. Albini, A. Bianchi, A. Marte, P. Baldelli, G. Alberini, L. Maragliano, P. Valente, F. Benfenati, A. Corradi, “Missense mutations in the membrane domain of PRRT2 affect its interactions with Nav1.2 voltage-gated sodium channels”. In preparation.

# ACKNOWLEDGEMENT

First of all, I would like to thank my supervisor, prof. Fabio Benfenati for his valuable supervision, dedicated support and guidance.

I would like to express my sincere gratitude to my supervisor, prof. Pierluigi Valente, that was really influential in shaping my experiment methods and for his consistent support during the running of this project.

I would like to thank Prof. Anna Corradi, Prof. Antonella Marte, Prof. Bruno Sterlini, Dr. Lisastella Morinelli and Dr. Martina Albini of the Department of Experimental Medicine (DIMES) of University of Genova for the biochemical experiments and their crucial contribution to this project.

I would like to express my gratitude to Prof. Luca Maragliano, Dr. Beatrice Corradi and Dr. Giulio Alberini of the Italian Institute of Technology (IIT) for molecular dynamics investigation, which was fundamental to this project.

I would also like to thank Prof. Maurizio Taglialatela and Dr. Massimo Mantegazza for their insightful comments and suggestions about my PhD thesis.

I am also thankful to Dr. Caterina Michetti for her advice, support, and patience especially during the critical first steps of my PhD study.

I would like to extend my sincere thanks to the NSYN technicians, Dr. Arta Mehilli, Dr. Rossana Ciancio, Dr. Diego Moruzzo and Dr. Ilaria Dallorto for their kind help and support.

I would like to thank all the members of the NSYN lab. Guys, it was a long journey, I could not have undertaken it without all of you. Your friendship, encouragements, moral support, and technical advice really made the difference. Thank you for the cherished time spent in the lab.

I am also grateful to my wonderful roommates and friends Matilde, Eleonora, and Beatrice. Girls, you, more than anyone else, know how much intense this experience was. I deeply thank you for the closeness, the laughter and the fondness you have shown me.

I am also thankful to my family, my mother Marina and Anya the dog. Thank you for your sweetness and for your standing always at my side.

Last but not least, I would like to thank my love, Flavio. Thank you for your willingness to help me, to encourage me, to question me, to believe in my ability.